ÉCOLE CENTRALE DE NANTES UNIVERSITÀ DEGLI STUDI DI GENOVA

MASTER ERASMUS MUNDUS
EMARO+ "European Master in Advanced Robotics"

2019 / 2020

Master Thesis Report

Presented by

Durgesh Haribhau Salunkhe

On August 27, 2020

Optimal kinematic design of a robot mechanism for otological surgery

Jury

President:	Philippe Wenger	Research Director, LS2N, Nantes
Evaluators:	Philippe Wenger	Research Director, LS2N, Nantes
	Marcello Sanguineti	Associate Professor, University of Genova
	Olivier Kermorgant	Associate Professor, École Centrale de Nantes
Supervisors:	Damien Chablat	Research Director, LS2N, Nantes
(EMARO)	Marcello Sanguineti	Associate Professor, University of Genova
	Guillaume Michel	Surgeon, CHU Nantes
	Shivesh Kumar	Senior Researcher, DFKI-RIC, Bremen

Laboratory: Laboratoire des Sciences du Numérique de Nantes LS2N

Abstract

The use of endoscope in otological surgery provides many benefits in terms of visibility and access to the operating region but needs to be handled by the surgeon at all time making such surgeries cumbersome. A mechanism that can act as an assistant to the surgeon for manipulating endoscope can have a huge positive impact on the efficiency of the surgeon and the surgeries.

This thesis explains the technical requirements, constraints and optimization process for proposing a mechanism for such application. The importance of analysis and synthesis of the kinematic properties of the structure for an optimized output is highlighted in the study. The author presents a novel implementation of an optimization algorithm for the design optimization. Various approaches researched in the past for the optimization are presented and their advantages and disadvantages are pointed out too. The effect of parametrization, different constraints as well as rewarding strategies are discussed to stress the complexities in the optimization of closed loop kinematic chains. The thesis also presents approaches used to consider the constraints for the passive joint limits as well as avoiding internal collision in the mechanism. A novel methodology is used for a faster and efficient global search of the optimization space. The work concludes by presenting the optimised result as well as by discussing open questions regarding the future of mechanism design.

Acknowledgements

Many people have played an important role during my journey of completing the presented work and I am indebted to each and everyone for the same. Having said that, I may not be able to do justice to all of them through the following words and I ask for forgiveness from those whom I may miss to mention.

I am deeply grateful to *Prof. Damien Chablat*, who has been a constant guide and a companion during my Master thesis from the very beginning. The knowledge gained as well as the experience of working under his guidance has had a great impact on me and my decisions for the future. I extend the same intensity of gratitude towards *Prof. Marcello Sanguineti* who has continuously motivated me and guided me in the unknown territory of the optimization theory. The progress achieved in the thesis would have been simply impossible without the enthusiasm he showed at every stage of the thesis. I thank *Dr. Guillaume Michel*, for his strong support and friendly attitude because of which it was quite easy for me to involve in the thesis with better understanding. Thanks for all the free trips to the operation room. It will be unfair to thank *Dr. Shivesh Kumar* only for the thesis work. He has been a great guide and a friend for more than 3 years and I am indebted by the confidence he has shown in my work throughout these years. I am thankful to *Elise Olivier* for her insights with an alternative perspective on the thesis. Her guidance has helped improve the work to be more practical and she has been the perfect link between robotics theory and the user experience. Also, thanks for the history of Nantes and your help with French language. Thanks to *Prof. Philippe Bordure, François Pasquier* and *Sarah Normant* for the extraordinary hospitality in the operating room at the CHU. Your efforts to go at lengths to demonstrate the different scenarios while using endoscope have been very helpful in highlighting the importance of the presented work.

The people I will mention next are the most special ones. ***Aai***, ***Baba*** and ***Didi***. I find the art of expressing oneself through words very inadequate to tell you how grateful, indebted and humbled I am to have you in my life. Starting from the journey of life to taking small steps of my own in different fields of life, you have only supported me. Thanks to *Baba*, who introduced me to the world of Mathematics and I was saved from mundane learning at the school. Because of you, Mathematics was never a subject for me, it became a topic of curiosity and appreciation and I am very proud of that.

I wish to express my special thanks to *Sanket* with whom I have shared so many thoughts and have pondered upon ideas that ended up shaping my overall personality. The exchange of ideas and skills have helped me improve my experience of life. Thank you, *Yuri*, for without you none of the experiences would be the same. Your disciplined way of living has motivated me to transform myself and has given enough strength to persevere. Thanks to my friends back in India, *Vipul* and *Ankit*, whom none can replace. We have shared each other's pain and sorrows while rejoiced each others success and I'll be there for you like I've been there before. Thanks to *Anirvan*, who has been inspirational with his undeterred focus on research and with whom I had the good fortune to work with. Thanks to *Francesco* for the times spent together, we have shared so much over this 2 years and I stay grateful for everything. I know that you will reach greater heights learning your way to the top. Thanks to *Pablo*, with whom I have debated on various topics and have pondered over different aspects of life. Thanks to my Italian friends in

France, *Angie, Nic, Mario, Klav, Erri* and *Andrea*, and also *Sunny* for the fun we had in Nantes, I wish we had more time to celebrate. Thanks to *Mbarre, Orianna, Francesca* and *Ricardo* for an amazing time in Sicilia and Nantes, you guys will never be forgotten. Thanks to *Judith* and *Esra*, my friends from Erasmus, for your cheerful company. Thanks to *Rohit*, your friendship has played an important role in reassessing my perspective of life. These people have helped me during various stages of my thesis and life in overall, and I hope that I had at least some if not equal influence on their life.

THANK YOU

Notations

κ conditioning number

κ^{-1} quality index

κ_g^{-1} global quality index

$\mathbf{J}$ Jacobian matrix

$\mathbf{q_i}$ input vector

$\mathbf{x}$ generalized output vector

$\mathcal{D}$ configuration space

$\mathcal{F}$ feasible set

$\mathcal{K}$ output space

$\mathcal{O}$ optimisation space

v_e manipulability ellipsoid volume

$\boldsymbol{SE(3)}$ special Euclidean group of dimension 3

$\boldsymbol{SO(3)}$ special orthogonal group of dimension 3

CHU Centre Hospitalier Universitaire

COR centre of rotation

DE Differential Evolution

DGS direct geometric solution

DH Denavit Hartenberg

dof degrees of freedom

EE end-effector

GA Genetic Algorithm

IGS inverse geometric solution

MOEA/D Multi-Objective Evolutionary Algorithm based on Decomposition

MOO Multi Objective Optimization

NM Nelder-Mead

NSGA-II Non-dominated Sorting Genetic Algorithm

OR Operating Room

PKM Parallel Kinematic Manipulator

PSO Particle Swarm Optimization

RDW Regular Dextrous Workspace

RDW$_d$ desired Regular Dextrous Workspace

RR Revolute-Revolute

SPM Spherical Parallel Mechanism

SS Spherical-Spherical

US Universal-Spherical

Abbreviations

κ conditioning number

κ^{-1} quality index

κ_g^{-1} global quality index

$\mathbf{J}$ Jacobian matrix

$\mathbf{q_i}$ input vector

$\mathbf{x}$ generalized output vector

$\mathcal{D}$ configuration space

$\mathcal{F}$ feasible set

$\mathcal{K}$ output space

$\mathcal{O}$ optimisation space

v_e manipulability ellipsoid volume

$\boldsymbol{SE(3)}$ special Euclidean group of dimension 3

$\boldsymbol{SO(3)}$ special orthogonal group of dimension 3

CHU Centre Hospitalier Universitaire

COR centre of rotation

DE Differential Evolution

DGS direct geometric solution

DH Denavit Hartenberg

dof degrees of freedom

EE end-effector

GA Genetic Algorithm

IGS inverse geometric solution

MOEA/D Multi-Objective Evolutionary Algorithm based on Decomposition

MOO Multi Objective Optimization

NM Nelder-Mead

NSGA-II Non-dominated Sorting Genetic Algorithm

OR Operating Room

PKM Parallel Kinematic Manipulator

PSO Particle Swarm Optimization

RDW Regular Dextrous Workspace

RDW$_d$ desired Regular Dextrous Workspace

RR Revolute-Revolute

SPM Spherical Parallel Mechanism

SS Spherical-Spherical

US Universal-Spherical

List of Figures

Contents

Chapter 1

Introduction

The recent health crisis of 2020 due to the Covid-19 virus made us realise the high importance of our health system. The situation took all the humanity by surprise and the soldiers in this crisis, our doctors, were completely exhausted and found themselves inadequately equipped. Many important lessons were learnt at the various stages of the crisis and the following report mainly addresses about the need of an efficient state of art in every possible area of healthcare system. The medical field has made enormous progress in the past century leading to a higher life expectancy. The growing age of the population also resulted in the rise of medical emergencies and surgeries. It is estimated that by 2030, 5000 surgeries will be conducted per 100,000 population [4]. In order to cope up with the rise of surgeries, it is important that we explore different technologies that can be combined to make surgeries faster yet safer and more reliable. Surgical robots play an important role in revolutionizing the conventional surgery procedures and is researched for more than three decades. The first Food and Drug Administration (FDA) approved endoscopic robotic surgery system was commissioned in 1990 by the AESOP system [5]. Several works have been reported earlier for minimally invasive surgeries by robots [6, 7, 8] with great success.

The concept of human robot collaboration to improve the efficiency of a task by combining the accuracy of a robot and intuition of a human has become popular in recent years. The implementation of robots in inner ear surgery [9] and middle ear surgery [10, 11] were discussed in detail in [12]. Some of them provide a complete solution for robotic surgery, while some can be used as an assistant for the surgeon. The robots in surgery can be used to replace tasks of the surgeon that are mandatory but demand no human expertise. One of the applications in this area is the use of endoscope in otological surgeries.

There are many advantages of using an endoscope instead of the conventionally used microscope in otological surgeries [13]. Some of them include better view with easy access to the operating area and proximity to the patient while operating (Fig. 1.1). Endoscopic surgeries lead to less bone sacrifice and thus improves the recovery period of the patient. Though agile in application, endoscopic surgeries pose different challenges to the surgeon. The confrontation interviews conducted by Elise Olivier under this project suggests that due to certain limitations of endoscope, surgeons prefer to operate with microscope which is comfortable to use. Currently, the surgeon can only use one tool at a time in endoscopic surgeries in contrast to two tools with the use of a microscope as illustrated in Fig. 1.2. This makes the endoscopic surgeries cumbersome as the

(a) Surgeon observing ∼25 cm away from the ear

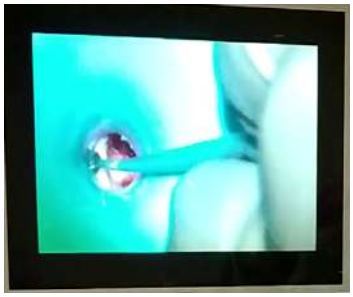

(b) View of the operating area in a microscope

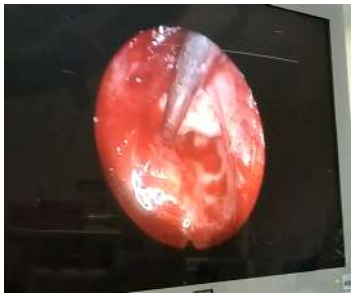

(c) View of the operating area in an endoscope

Figure 1.1: The comparison of the view and proximity to operation while using an endoscope and a microscope.. Courtesy: Dr. Guillaume Michel, CHU Nantes

(a) The use of 1 hand to hold endoscope limits the number of instruments

(b) The surgeon can use 2 instruments while using a microscope

Figure 1.2: The comparison of the number of instruments possible to use simultaneously while using an endoscope and a microscope.. Courtesy: Dr. Guillaume Michel, CHU Nantes

surgeon has to switch between tools to operate and manage bleeding in the ear. The incapability of using both hands for the surgery leads to frustration and fatigue of the surgeon. The use of a robot arm to manipulate the endoscope as needed can improve the performance of the otological surgeries remarkably. Using assistive systems can result in drastic reduction in the operating time and positively affect both, the surgeon as well as the patient. Previously, robot mechanisms with a serial architecture were proposed as a solution for the endoscopic surgery [10] and one of such implementation is illustrated in Fig. 1.3. The clinical report regarding the same has been published recently [14]. The serial manipulators have larger workspace in contrast to its parallel counterpart and are relatively easier to design and analyse. That been said, parallel manipulators are generally known for their stiffer structure and are kinematically more robust. This can be attributed to the reason that the error in joints is cumulative in serial mechanisms. It is easier to have a fixed centre of rotation (COR) in a parallel mechanism by the virtue of its architecture and the joint selection. These inherent advantages of parallel mechanisms gives them a considerable edge for the application of the endoscope manipulation.

In mechanism design, the optimisation methodology plays an important role and is governed by the definition of the objective function and constraints implemented. In

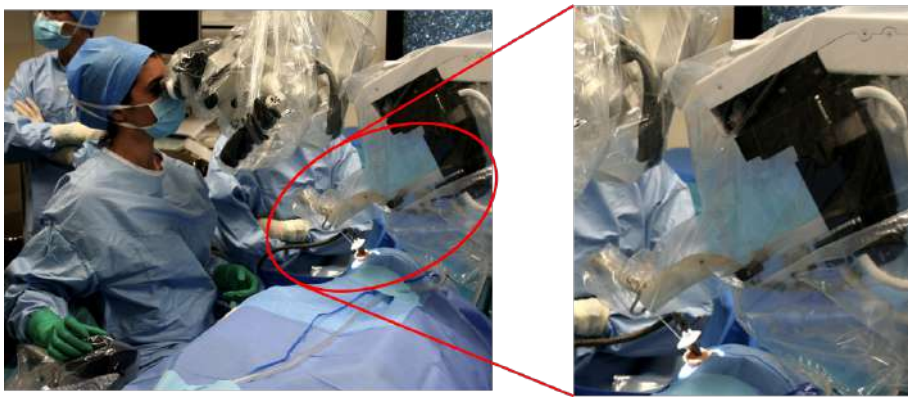

Figure 1.3: The serial architecture (Robotol) used for endoscope manipulation
Source: Collin Medical, France

the past, several design optimization methods were proposed in the field of mechanism. Some of them utilise the mathematical formulation of the objective function in order to implement gradient descent method [15]. Where such luxury is not present, numerical approaches and evolutionary algorithms are extensively implemented in the past. The most widely submitted work in this area uses the Genetic Algorithm (GA) [16, 17, 18] while there exists literature with other evolutionary algorithms [19]. A recent work implemented co-optimzation strategy which presents the efficient search of implicitly expressed optimization space [20].

In this report, we present the kinematic comparison of different parallel mechanisms that can be used to manipulate an endoscope. Works presented in [21] have been considered for comparison along with a novel 2 degrees of freedom (dof) rotational parallel mechanism [1] and its variant. One of the main objectives for the thesis is to present new design optimization methodology that can adapt to constraints involving internal collisions along with the physical joint limits and physical stroke of the actuator. We propose a fast local search algorithm, i.e. Nelder-Mead algorithm, coupled with a global search mechanism. This method allows to achieve a global optimum faster even for mechanisms that have computationally expensive objective functions. The overall output of the work is a general algorithm for design optimization that is flexible with the definition of the objective function as well as is modular and adaptive to any constraints.

The report is organised in the following way: Chapter 3 defines the task and its constraints clarifying the surgeons' requirement for the design. It also explains the choice of architecture, joint type, joint placement, and their effect on the workspace. The three Spherical Parallel Mechanism (SPM) are also detailed in this section. Chapter 4 is the most important part of the report where the authors detail upon the optimization methodology along with the choice of the objective function and constraint implementation. The results of the thesis work are presented in Chapter 5 followed by the conclusions and pointers to future work.

Chapter 2

State of the art

In this chapter, a detailed survey of the previously reported work is presented. The problem statement is discussed in more details to explain the required degrees of freedom and the nature of mobility of the mechanism. Different mechanisms of such mobility and their synthesis presented in the past are discussed in the following sections. The implementations of these mechanisms in different fields are provided to highlight the ubiquity of parallel mechanisms and therefore the importance of their design optimization. Later, we discuss the state of the art for the optimization procedures. Different evolutionary and novel algorithms that have been used successfully implemented in recent years are presented in depth. The advantages and disadvantages of these methods are discussed allowing the reader to appreciate the need of new methodology for the same.

2.1 State of the art: design choices

In otological surgeries, ossiculoplasty, stapedotomy, tympanoplasty and myringoplasty can be carried out with better efficiency if performed with endoscope. On the other hand, all the sinus surgeries make use of endoscope for its advantages. In order to operate on some parts during these surgeries, it is of prime importance that the surgeons can use both-hands simultaneously. Without a robotic manipulator, an assistant surgeon has to perform the task of manipulating endoscope which is not only unergonomic and hard to synchronize but also very less productive use of his presence in the Operating Room (OR). Fig. 2.1 is an ideal illustration from the OR of the problem statement we are trying to resolve.

2.1.1 Choice of mechanism - First things first

The final objective of the project is to have a complete robotic solution as an assistant for the surgeons to handle an endoscope. There has been an active dialogue between the surgeons of Centre Hospitalier Universitaire (CHU) Nantes and the authors in order to decouple the problem and translate it into the language of mechanisms. This allowed the authors to formalize the expectations of the proposed solution which should have:

1. A possibility to locate the system in the appropriate location in OR.

2. The ability to manipulate the endoscope with a fixed center of rotation (cor)

3. The ability to have a translation along the direction of the endoscope.

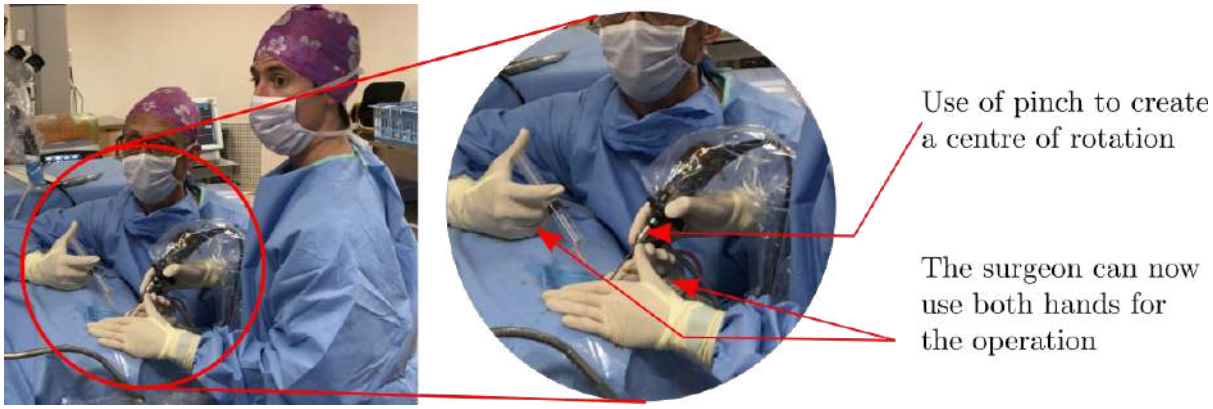

Figure 2.1: The issue in current scenario.The assistant surgeon needs to hold the endoscope to operate on certain part. Courtesy: Dr. Guillaume Michel, CHU Nantes

As the importance of rotational movement is higher than the translational movement, it is a wise choice to decouple them. This allows us to use actuators of different size, speed and accuracy according to the need of the movement. Such ideology has been implemented in the past and is known as the macro/micro manipulators [22]. It is also useful to have decoupled rotation and translation motion for analyzing the kinematic properties of the mechanism and we can dare to use several tools without fearing the entanglement of the dimensions of the Jacobian matrix. The rotation of an endoscope about its own axis is not very useful and thus the essential dof of the mechanism used to manipulate an endoscope are 2-rotations and 1-translation. The foundational study and analysis of a suitable mechanism was performed prior to the start of the presented work by Dr. Guillaume Michel, Prof. Philippe Bordure and Prof. Damien Chablat. As the translational movement is considered to be decoupled, the presented work focuses on choosing a 2-dof orientation mechanism. The spherical parallel mechanisms have been extensively researched in the past [23, 24, 25] and remain a topic of interest to current researchers too [26]. A lot of theory and research is available from the previous decade regarding parallel mechanisms with 2 orientation dof. The following subsections present different implementations of the same.

2.1.2 The Orthoglide wrist

The Orthoglide wrist shown in fig. 2.2b is a mechanism similar to a 2 dof agile eye [27] mechanism. The wrist was introduced as the decoupled orientation mechanism for the translational Orthoglide [28] mechanism. The center of rotation of the wrist is at the intersection of the two motors as shown in the fig. 2.2b. The detailed geometric and kinematic analysis of this manipulator has been mentioned in [25] and [27]. The number of inverse geometric solution (IGS) depends on the architecture of the mechanism. For example, the 2 dof agile eye mechanism proposed by [27] has 4 IGS while the [25] has only one IGS. This result is attributed to the joint arrangements of the mechanisms as well as the joint limits of the actuators and collision avoidance between the components. The number of direct geometric solution (DGS)s for [27] are 2 while the [25] has a unique DGS.

The DGS and IGS were analyzed by using Denavit Hartenberg (DH) parameterization. The type I and type II singularities of these mechanisms are elaborated by detailing the conditions in which the Jacobian matrix, **A** and **B** matrix mentioned in [29], loses a rank.

The advantage of this system is the robust construction and the kinematic precision due to the closed loop. One of the drawbacks of this system is that the end-effector (EE) has to be mounted in such a way that the point of interest of the EE coincides with the COR.

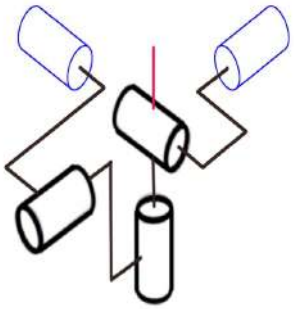

(a) The schematic of orthoglide wrist

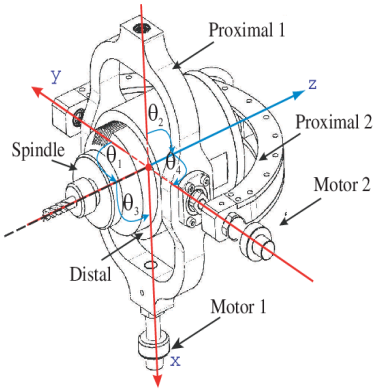

(b) Orthoglide wrist as proposed in [25]

2.1.3 2 dof agile eye with an offset

The 2 dof agile eye mechanism with an offset was discussed in [24]. This mechanism is same in construction as the 2 dof agile eye but the COR is displaced by using a parallelogram joint as shown in fig. 2.3. The maximum joint displacement of the actuators is 60 degrees as shown in fig. 2.3b. The number of geometric solutions of this mecha-

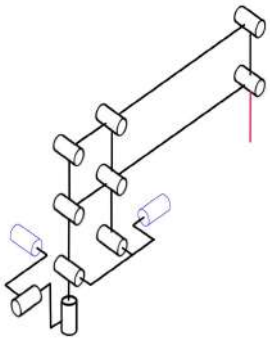

(a) The schematic of the mechanism

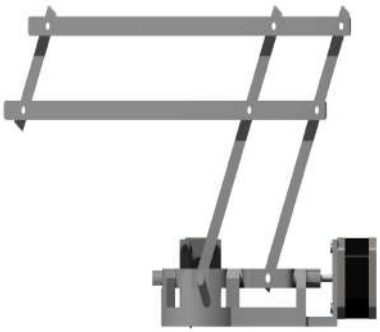

(b) The mechanism in 60^0 pitch

Figure 2.3: The details of the 2 dof agile eye with an offset. Courtesy: Prof. Damien Chablat, LS2N

nism changes once the constraints related to the joint limits and internal collisions are added. The advantage of this mechanism is that the COR can be displaced according to the requirement. This helps in locating the actuators on ground and manipulating the endoscope remotely. This leverage also leads to a more complex kinematic analysis as the properties of the parallelogram structure also affect the overall performance. The mechanical design of such mechanisms is of prime importance as they have long cantilever beams and the load (weight of the endoscope) is applied at the extreme end which can lead to bending issues.

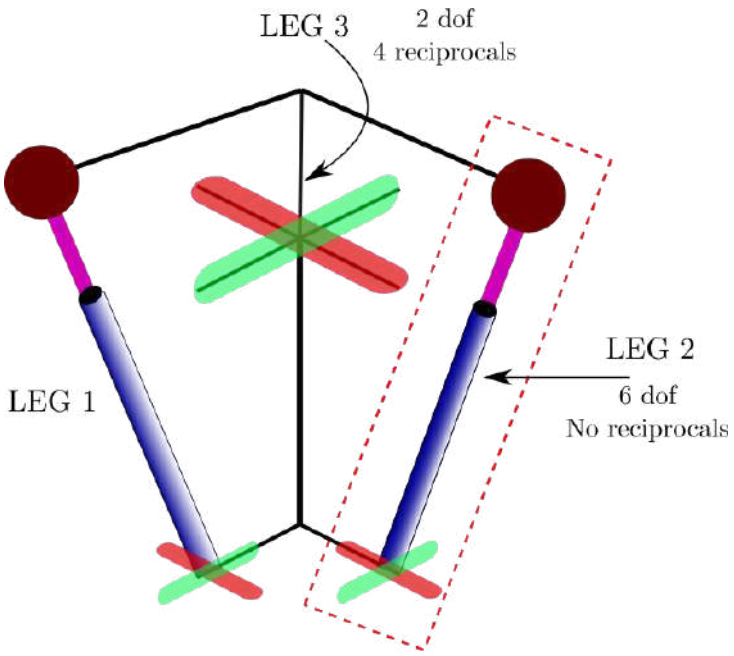

Figure 2.4: The architecture with redundant passive leg

2.1.4 2 dof orientation mechanism with passive leg

Another implementation is done by introducing a motion constraint leg to achieve the necessary degrees of freedom. In such architectures (with 2-dof), 2 legs with 6 degrees of freedom are used and a passive redundant leg is introduced which governs the degrees of freedom as well as the nature of mobility of the overall mechanism. The idea is illustrated in Fig. 2.4. The passive leg with the universal joint, i.e. leg 3 in Fig. 2.4 defines the center of rotation as there are no constraint wrenches applicable in the 6-dof legs, leg1 and leg2. The mechanism is actuated with a prismatic joint present in each active leg. The type synthesis of such class of mechanism was first presented in [30]. A procedure regarding the choice of joints while designing mechanisms with such architectures is also detailed in the same.

A parallel mechanism with architecture 2U$\underline{\text{P}}$S-1U is previously proposed for bone milling operations [31]. This work presents the workspace analysis with some assumptions in the architecture. This architecture has been widely proposed in past research for various applications [32, 33, 34, 35, 36]. Other variant of the architecture is the 2$\underline{\text{P}}$US-1U which has been implemented in the Valkyrie humanoid [37]. A recent variation of the 2U$\underline{\text{P}}$S-1U is the 2S$\underline{\text{P}}$RR-1U [21] which highlights the advantage of using a Revolute-Revolute joint as a replacement of the Universal joint in the active legs.

2.2 State of the art: optimization

Different algorithms have been suggested previously to optimize the mechanism design. In problems where the objective function and the constraints are well formulated, algorithms that exploit the derivative of the objective functions are most successful [15]. Unfortunately, in mechanism design, it is common to encounter a non-smooth objective function with non-linear constraints. In such cases, the derivative-free algorithms are

implemented. We are particularly interested in this type of optimization and the reasons for the same will be discussed in Chapter 4.

The search for global optimum in the mechanism design is a challenging topic and different nature-inspired evolutionary algorithms are implemented during such endeavors. The algorithms used for single objective are Differential Evolution (DE) [38] and Genetic Algorithms (GA) [39] while most widely used algorithm for the Multi Objective Optimization (MOO) is the Non-dominated Sorting Genetic Algorithm (NSGA-II) [16, 18, 40, 41] in which the theory of genetic evolution is implemented. It treats a point in optimisation space ($\mathcal{O}$) as a chromosome and evaluates the fitness value (reward strategy) of the population (several chromosomes spread in $\mathcal{O}$) in one iteration. Then the operations such as selection, crossover and mutation take place to generate a set of new population and the process continues. The advantage of this methodology is that it performs a global search of the optimization space. Other evolutionary algorithms that have been implemented are the Particle Swarm Optimization (PSO) [19] and Multi-Objective Evolutionary Algorithm based on Decomposition (MOEA/D) and are claimed to be superior than NSGA-II in [42]. Nonetheless, all the above mechanisms are computationally expensive as the efficiency of the algorithm highly depends on the population size. Also, only a guess of the required chromosomes is provided for an efficient global search of the optimization space. This dependency makes them vulnerable in case of demanding objective functions and also limits the quantity and nature of the constraints that can be implemented.

A recent work in mechanism design optimization is the co-optimization with the motion trajectories [20]. In this work, the design parameters and the motion equations are represented implicitly and efficient algorithms are used to traverse the implicitly defined manifold. This type of methodology can provide better insights on the global optimum of the optimization space. The work also highlights the importance of joint placement of prismatic actuators in the optimization process. Keeping in focus the computational cost of optimizing a mechanism, different local search methods can be implemented. To avoid the solution converging in local area, different methodologies can be used to combine local optimization methodologies with global searches [43, 44, 45, 46]. Such algorithms have been proved to be utilizing the advantages of the individual methods.

Most of the literature presented above focuses primarily upon the problem formulation and use the existing methodology as an optimization tool. The author believes that diving deeper into the implementation of the optimization algorithm can provide better flexibility and capability to handle different constraints efficiently.

Chapter 3

Design choices

In this chapter, the authors discusses in detail the mechanisms used for comparison along with the motivation behind choosing them. The initial sections present different variations, their geometric solutions as well as the nature of their singularity curves. In next sections, the type of joints chosen and the changes occurring in passive limits because of them is discussed. Later, the importance of workspace representation is highlighted. The chapter concludes by detailing the procedure used to decide on the important parameters of the design optimization. The aim of this chapter is to familiarise the reader with the background behind the mechanism chosen and subsequently the components for the same.

3.1 Proposed mechanism and its variations

Based on the requirements and cross-functional discussions, a novel mechanism was introduced to cater to the current scenario. A 2-dof parallel mechanism with a passive leg was used to achieve the 2 rotational degrees of freedom while a parallelogram joint was introduced for a remote center of rotation [1]. The required linear motion in endoscope is achieved by a rack and pinion arrangement as shown in Fig. 3.1c.

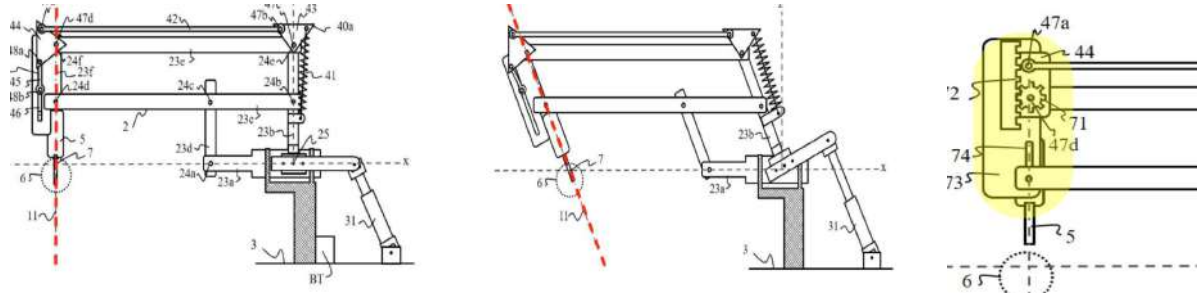

(a) Side view of the mechanism in home position

(b) Mechanism with the remoter center of rotation

(c) Decoupled linear motion

Figure 3.1: The patented proposed mechanism for the presented work [1]

The proposed architecture can be implemented in several ways. Depending on the choice of the actuators, rotary or linear, the kinematic properties such as singularities, number of inverse geometric solutions and joint limits change dramatically. The presented work limits the scope to only prismatic joint as actuators to keep the analysis comparatively simple. Even while using a prismatic joint, a designer has to choose between the

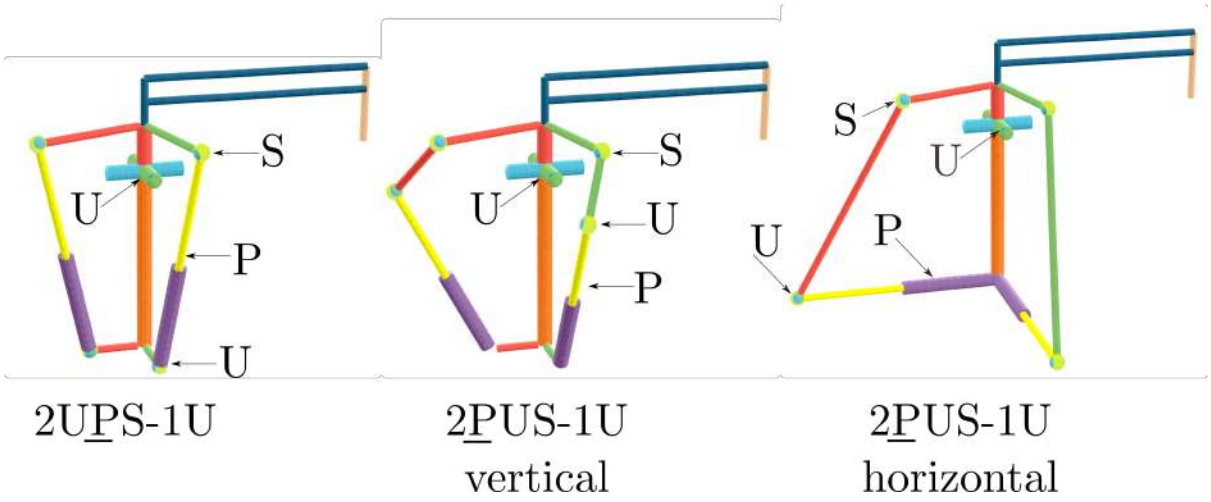

Figure 3.2: The 3 variations of the proposed architecture

different joint orders, type of joints and their placements. For example, the three variations occurring from different order and placement of joints for the patented idea using prismatic joint actuator are shown in Fig. 3.2. The 2UPS-1U variation has a prismatic joint linking the passive universal and spherical joint of a leg while the 2PUS-1U variation has a fixed orientation for the prismatic joint. A major consequence of this is the possibility of using bigger or heavier actuators for the 2PUS-1U variation. In this case, we do not have to worry about the inertia of the prismatic joint as well as the collision between the two actuators. The 2UPS-1U variation has a better kinematic performance compared to a 2PUS-1U architecture and allows us to have a larger workspace satisfying all the necessary constraints. These qualities of different variations motivates the need of a comparative analysis for a conclusive proposal of the architecture.

3.2 Inverse geometry

The general parameterization of the 2UPS-1U variation can be done with the help of 13 parameters as shown in Fig. 3.3a while the 2PUS-1U variation also requires 13 parameters, it considers the orientation of the prismatic joint and assumes that the z-coordinate of the base of the actuator as zero. If we use the Euler angles (α, β) to represent the output space as detailed further in Section 3.5.1, the orientation of the end-effector can be given as:

$$\mathbf{R} = \mathbf{R}_\alpha \, \mathbf{R}_\beta = \begin{bmatrix} cos(\beta) & 0 & sin(\beta) \\ sin(\alpha)\, sin(\beta) & cos(\alpha) & -cos(\beta)\, sin(\alpha) \\ -cos(\alpha)\, sin(\beta) & sin(\alpha) & cos(\alpha)\, cos(\beta) \end{bmatrix} \tag{3.1}$$

3.2.1 Inverse geometry: 2UPS-1U variation

If the base frame of the manipulator is considered to be at the bottom point where all the three legs meet as shown in Fig. 3.3a, then the coordinates of the 2 universal joints

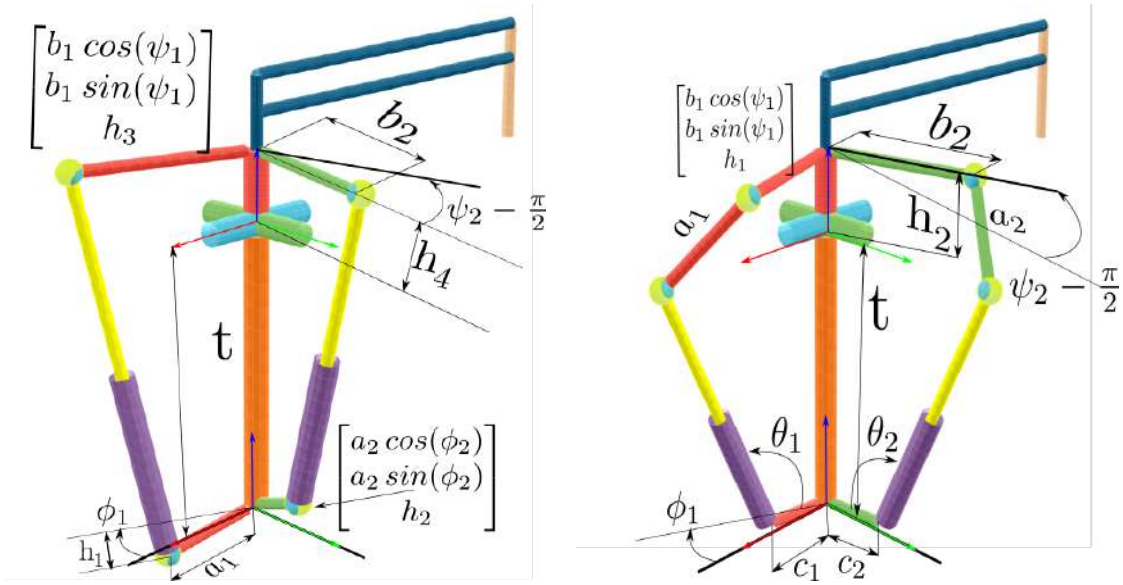

(a) Parameters in 2UPS-1U (b) Parameters in 2PUS-1U

Figure 3.3: The general parameterization of the 2UPS-1U and 2PUS-1U variation

with respect to the origin are represented as:

$$\mathbf{u}_{11} = \begin{bmatrix} a_1\,cos(\phi_1) \\ a_1\,sin(\phi_1) \\ h_1 \end{bmatrix}, \mathbf{u}_{21} = \begin{bmatrix} a_2\,cos(\phi_2) \\ a_2\,sin(\phi_2) \\ h_2 \end{bmatrix} \tag{3.2}$$

The universal joint of the third passive leg, $\mathbf{u}_3$, is given by $[0, 0, t]^T$ and the spherical joints of the mechanisms are represented in the frame of the universal joint $\mathbf{u}_3$ as:

$$\mathbf{s}_{12} = \begin{bmatrix} b_1\,cos(\psi_1) \\ b_1\,sin(\psi_1) \\ h_3 \end{bmatrix}, \mathbf{s}_{22} = \begin{bmatrix} b_2\,cos(\psi_2) \\ b_2\,sin(\psi_2) \\ h_4 \end{bmatrix} \tag{3.3}$$

Here, a_1 and a_2 are the lengths of the links that join the base with the universal joints and b_1, b_2 are the lengths of the links joining the end-effector with the spherical joint as shown in Fig. 3.3a. $\phi_{1,2}$ are the angles deciding the orientation of the universal joints with respect to the x-axis while $\psi_{1,2}$ are the angles deciding the placement of the spherical joints with the respect to the x-axis of the chosen end-effector frame. The transformation matrix corresponding to the end-effector frame at a certain pose (α, β) is:

$${}^0\mathbf{T}_e = \begin{bmatrix} \mathbf{R} & \mathbf{t} \\ \mathbf{0} & 1 \end{bmatrix}, \mathbf{t} = [0, 0, t]^T \tag{3.4}$$

$$\begin{aligned} {}^0\mathbf{s}_{12} &= {}^0\,\mathbf{T}_e\,\mathbf{s}_{12} \\ {}^0\mathbf{s}_{22} &= {}^0\,\mathbf{T}_e\,\mathbf{s}_{22} \end{aligned} \tag{3.5}$$

As we have all the joints in the origin frame, the distance between the universal joint as well as the spherical joint will give us the required actuator length.

$$\rho_1 = \left\| {}^0\mathbf{s}_{12} - \mathbf{u}_{11} \right\| = f(\alpha,\, \beta) \tag{3.6}$$

$$\rho_2 = \left\| {}^0\mathbf{s}_{22} - \mathbf{u}_{21} \right\| = g(\alpha,\, \beta) \tag{3.7}$$

differentiating (3.6) and (3.7) with respect to time gives us:

$$\begin{bmatrix} \dot{\rho}_1 \\ \dot{\rho}_2 \end{bmatrix} = \begin{bmatrix} \dfrac{\partial f}{\partial \alpha} & \dfrac{\partial f}{\partial \beta} \\ \dfrac{\partial g}{\partial \alpha} & \dfrac{\partial g}{\partial \beta} \end{bmatrix} \begin{bmatrix} \dot{\alpha} \\ \dot{\beta} \end{bmatrix} \tag{3.8}$$

We define the Jacobian matrix ($\mathbf{J}$) as the mapping between the output velocities of the mechanism, ($\dot{\mathbf{x}}$), and the input joint velocities, ($\dot{\mathbf{q}}$), and is given by:

$$\begin{aligned} \mathbf{J}_x \dot{\mathbf{x}} &= \mathbf{J}_q \, \dot{\mathbf{q}} \\ \dot{\mathbf{x}} &= \mathbf{J}_x^{-1} \mathbf{J}_q \, \dot{\mathbf{q}} \\ \mathbf{J} &= \mathbf{J}_x^{-1} \, \mathbf{J}_q \end{aligned} \tag{3.9}$$

The matrix in (3.8), is the inverse mapping of the Jacobian matrix and is denoted as $\mathbf{J}^{-1}$. This matrix is of particular importance for singularity analysis as well as the evaluation of the quality of motion and will be presented in next sections. The joint orientations

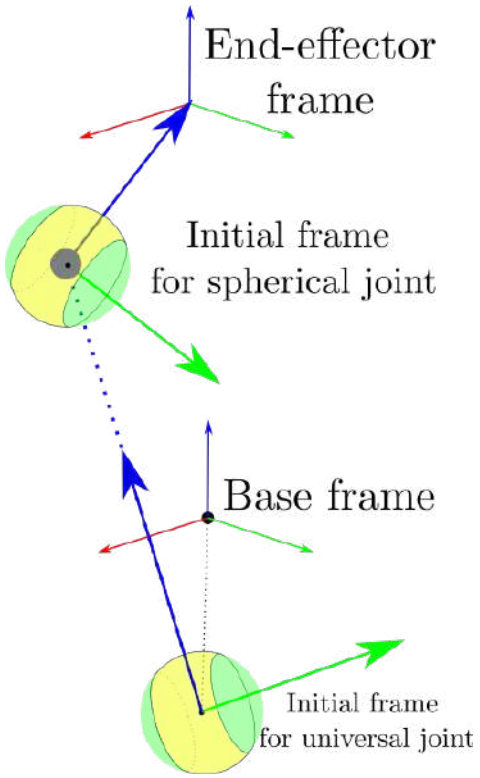

Figure 3.4: The initial frames for the joints in a leg

are the next important thing to consider as the joint limits are one of the important constraint in the optimization. We choose the tilt-torsion representation for calculating the passive joint values and the motivation for the same has been discussed in Section 3.4.1. The spherical joints were aligned such that in the initial position all the joints are in their default position with no rotation as shown in Fig. 3.4. The initial frame for the universal joint can be calculated by:

$$\mathbf{z}_{u11} = \frac{{}^0\mathbf{s}_{12} - \mathbf{u}_{11}}{\|{}^0\mathbf{s}_{12} - \mathbf{u}_{11}\|}, \mathbf{y}_{u11} = \frac{-\mathbf{u}_{11} \times \mathbf{z}_{u11}}{\|\mathbf{u}_{11}\|}, \mathbf{x}_{u11} = \mathbf{y}_{u11} \times \mathbf{z}_{u11} \tag{3.10}$$

While the initial frame for the spherical joint can be calculated by:

$$\mathbf{z}_{s12} = \frac{-\mathbf{s}_{12}}{\|-\mathbf{s}_{12}\|}, \mathbf{y}_{s12} = \frac{-\mathbf{t} \times \mathbf{z}_{s12}}{\|\mathbf{t}\|}, \mathbf{x}_{s12} = \mathbf{y}_{s12} \times \mathbf{z}_{s12} \tag{3.11}$$

The azimuth angle and the tilt angle for the universal joint is calculated by equivalent axis representation for the z-axis of current and initial frame of the universal joint. θ_{au} is the azimuth angle while θ_{tu} is the tilt angle for the universal joint.

$$\begin{aligned} \omega &= {}^{u11}\mathbf{z}_{initial} \times {}^{u11}\mathbf{z}_{current} \\ \theta_{au} &= atan2(\omega(2), \omega(1)) \\ \theta_{tu} &= acos({}^{u11}\mathbf{z}_{current} \cdot {}^{u11}\mathbf{z}_{initial}) \end{aligned} \tag{3.12}$$

The rotation matrix after the tilt operation for the universal joint can be given by Euler-Rodrigues' formula. $\tilde{\omega}$ is the anti-symmetric matrix notation of the vector ω

$$\begin{aligned} \mathbf{R}_{tu} &= \mathbf{e}^{\tilde{\omega}\,\theta_{tu}} \\ &= \mathbf{I} + \tilde{\omega}\, sin(\theta_{tu}) + \tilde{\omega}^2 (1 - cos(\theta_{tu})) \end{aligned} \tag{3.13}$$

$$\mathbf{R}_{ts} = \begin{bmatrix} cos(\theta_{tu}) + \omega_x^2 (1 - cos(\theta_{tu})) & \omega_x \omega_y (1 - cos(\theta_{tu})) - \omega_z\, sin(\theta_{tu}) & \omega_y\, sin(\theta_{tu}) + \omega_x \omega_z (1 - cos(\theta_{tu})) \\ \omega_z\, sin(\theta_{tu}) + \omega_x \omega_y (1 - cos(\theta_{tu})) & cos(\theta_{tu}) + \omega_y^2 (1 - cos(\theta_{tu})) & \omega_z \omega_y (1 - cos(\theta_{tu})) - \omega_x\, sin(\theta_{tu}) \\ \omega_x \omega_z (1 - cos(\theta_{tu})) - \omega_y\, sin(\theta_{tu}) & \omega_x\, sin(\theta_{tu}) + \omega_y \omega_z (1 - cos(\theta_{tu})) & cos(\theta_{tu}) + \omega_z^2 (1 - cos(\theta_{tu})) \end{bmatrix} \tag{3.14}$$

The same method is used to calculate the azimuth and the tilt angles for the spherical joint. The torsion angle is calculated by using the $\mathbf{R}_{ts}$ (refer (3.14)) matrix and comparing the initial y-axis of the spherical joint's frame with the current orientation.

$${}^{s12}\mathbf{y}_{current} = \mathbf{R}_{ts}\, \mathbf{R}(z, \theta_{torsion})\, {}^{s12}\mathbf{y}_{initial}$$

3.2.2 Inverse geometry: 2PUS-1U variation

The 2PUS-1U variation can be defined with 13 parameters as shown in Fig. 3.3b. The origin frame is considered be at the junction point of all three legs. The base of the actuators in the origin frame is given by:

$$\mathbf{c}_1 = [c_1\, cos(\phi_1), c_1\, sin(\phi_1), 0], \mathbf{c}_2 = [c_2\, cos(\phi_2), c_2\, sin(\phi_2), 0] \tag{3.15}$$

The line of actuator, $\mathbf{l}_1$ and $\mathbf{l}_2$, along which the prismatic joint will act can be given as:

$$\begin{aligned} \mathbf{l}_1 &= \mathbf{c}_1 + \lambda_1\, \mathbf{v}_1 \\ where, \mathbf{v}_1 &= [(c_1 - cos(\theta_1))\, cos(\phi_1), (c_1 - cos(\theta_1))\, sin(\phi_1), sin(\theta_1)]^T \\ \lambda_1 &: constant \end{aligned} \tag{3.16}$$

$$\begin{aligned} \mathbf{l}_2 &= \mathbf{c}_2 + \lambda_2\, \mathbf{v}_2 \\ where, \mathbf{v}_2 &= [(c_2 - cos(\theta_2))\, cos(\phi_2), (c_2 - cos(\theta_2))\, sin(\phi_2), sin(\theta_2)]^T \\ \lambda_2 &: constant \end{aligned} \tag{3.17}$$

The co-ordinates of the spherical joint of the leg in the end-effectors frame is represented as:

$$\mathbf{s}_{12} = \begin{bmatrix} b_1\, cos(\psi_1) \\ b_1\, sin(\psi_1) \\ h_1 \end{bmatrix}, \mathbf{s}_{22} = \begin{bmatrix} b_2\, cos(\psi_2) \\ b_2\, sin(\psi_2) \\ h_2 \end{bmatrix} \tag{3.18}$$

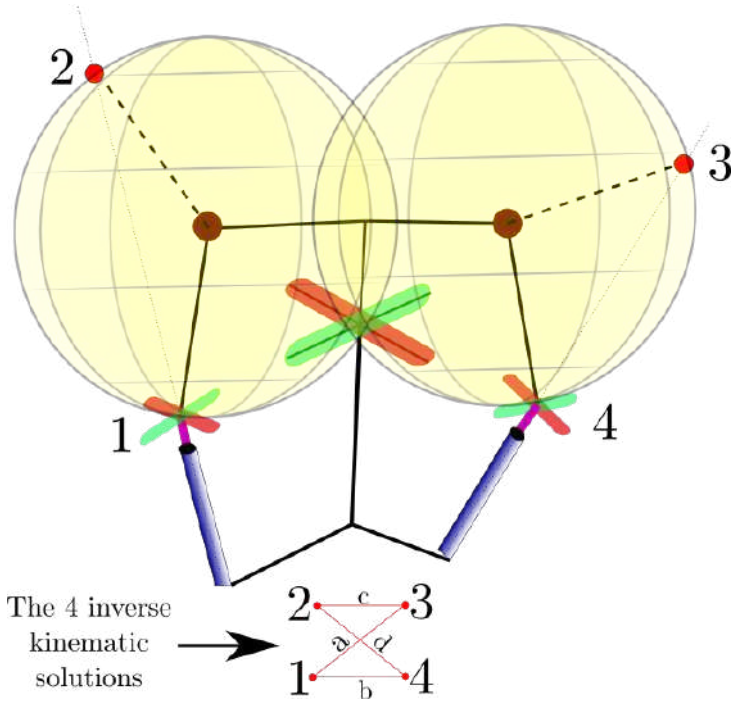

Figure 3.5: The 4 intersection points for showing the possible inverse geometic solutions

The universal joint lies at one of the intersection points between the sphere centered at $\mathbf{s}_{12}$ and $\mathbf{s}_{22}$ and the actuators line of action, $\mathbf{l}_1$ and $\mathbf{l}_2$. We have 4 Inverse geometic solution as shown in Fig. 3.5 and we always check for the 1-4 solution's feasibility. Once we have the universal joint's position in the origin's frame, we can calculate the actuator lengths, ρ_1 and ρ_2 as:

$$\rho_1 = \|\mathbf{u11} - \mathbf{c}_1\| = f(\alpha, \beta) \tag{3.19}$$

$$\rho_2 = \|\mathbf{u21} - \mathbf{c}_2\| = g(\alpha, \beta) \tag{3.20}$$

The Jacobian matrix is derived by differentiating (3.19) and (3.20) with respect to time similar to (3.8).

3.3 Singularity analysis

The singularity curves were analyzed for all the three variations shown in Fig. 3.2. The condition for input-output singularity in the proposed mechanism is calculated from the following condition:

$$\det(\mathbf{J}) = 0 \tag{3.21}$$

As we are using a motion constraint generator, we do not have a case of constraint singularities. The passive universal joint will always have 4 reciprocals and so the mechanism will never have an instantaneous dof greater than 2. The redundancy added with passive leg avoids cases of actuation singularity in the 2U<u>P</u>S-1U variation with basic care in modeling. But the 2<u>P</u>US-1U is susceptible to the actuation singularity if not modeled correctly and the parameters have to be chosen carefully. One such condition is shown in Fig. 3.6. In this case, the actuation wrench for the active legs degenerate thus losing the control of actuators on the end-effector. In the case shown below, the end-effector will

have 2 dof, rotation about the axes in the plane of the reciprocal screws shown in red in Fig. 3.6.

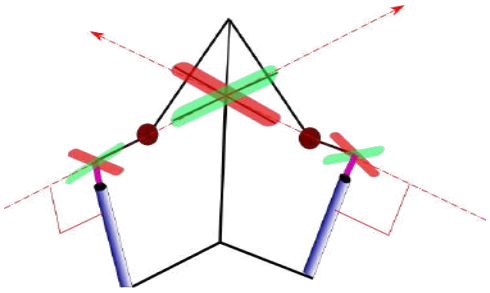

Figure 3.6: Actuation singularity in 2PUS-1U variation. The reciprocals to the passive joints are also reciprocal to the actuator

The singularity curve divides the workspace into aspects which are defined as t-connected regions or the singularity free areas of the output space. It is therefore inferred that we can have a feasible trajectory between two points in the output space if they belong to the same aspect. The Fig. 3.7 shows a case for 2UPS-1U variation where the singularity curve divides the workspace in 4 different singularity-free regions. The optimization problem is related to choosing the parameters such that the singularity curves lead to a large enough desired aspect.

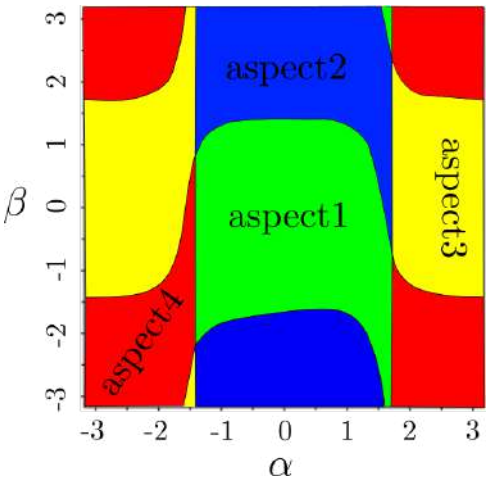

Figure 3.7: The workspace divided by 4 apsects. We can use only one of the aspects for a t-connected feasible workspace.

3.4 Choosing joints

As discussed in previous sections, the revolute joints or prismatic joints can be used as an actuator. Apart from the active joints, the passive joints in the mechanism can be chosen in various ways too. In the presented mechanism, we have one universal joint and one spherical joint in a leg. Interestingly, a Spherical-Spherical (SS) joint pair can be used to replace the Universal-Spherical (US) joint pair. This adds redundancy in the leg without affecting the resultant dof of the mechanism and has been implemented in various previous researches [47]. Also, the universal joint can be replaced with a Revolute-Revolute

(RR) joint and has been reported to have better kinematic performance [21].

This creates several challenges, especially while calculating the passive joint limits. The question that needs to be addressed is, 'How can I define passive limits if there is no order in the rotation?' For example, if we use 3 revolute joints as a spherical joint,

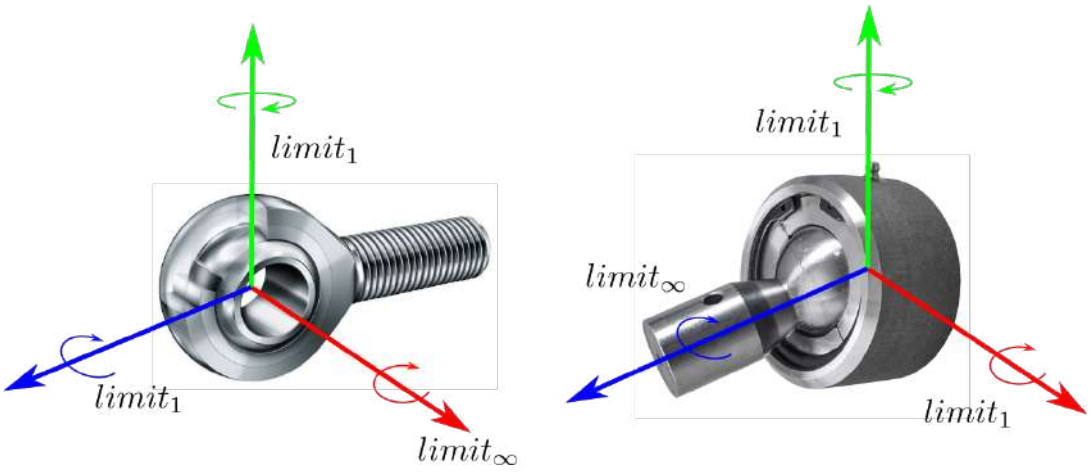

Figure 3.8: The implemented spherical joint as well as the ball-socket joint

then we know the exact order of rotation as well as the limit on the individual axis. The assumption of order fails while implementing a ball-socket joint but we do not have to worry as we have a constant limit in any direction. But, it is not straightforward to implement limits when we have spherical joints that are not in the ball-socket arrangement. The spherical joints in both the arrangements are shown in Fig. 3.8. In the joint shown in left, the joint limits depends on the axis about which the joint is being rotated. In other words, if we represent the orientation of the joint with tilt-torsion [48], then the passive joint limits is a function expressed in terms of the azimuth angle. Because of this reason, the orientation of the spherical joint is also an important parameter to consider, but more importantly, 'What do we mean by passive joint limits?'

3.4.1 Spherical joint limits

The special orthogonal group of dimension 3 ($SO(3)$) is a non-euclidean space defining all the orientations in the 3d-space and is the subspace of the special Euclidean group of dimension 3 ($SE(3)$). In translational space ($SE(3)\backslash SO(3)$), we have established a single definition of distance, path and the shortest distance between two points but it is quite hard to define the same uniquely in the $SO(3)$. The shortest distance between two orientations is solely dependent on the representation chosen. So, the shortest distance between two orientations will differ with the XZX convention and the YZY convention. It is not only Euler angles but also the tilt-torsion representation and the quaternions which have their own definition of shortest distance and the path travelled to reach from one orientation to another. So, if the path is representation-dependent, then aren't the limits dependent on the representation too?

For example, in Fig. 3.8, if we represent the orientation in XZX-convention and a particular orientation is $\{25^0, 32^0, 45^0\}$. The very same orientation will have different values in XYX-orientation and thus it is not valid to implement limits on individual axis.

In tilt-torsion representation, this can be countered in case of zero torsion. The reason being, we know the azimuth angle and the tilt-angle and they are unique for an orientation. So, we can still implement the joint limits while using the spherical joint as a replacement for the universal joint. When we have non-zero torsion angle, there are more challenges. The path assumed to be travelled in the zero-torsion case is shown in Fig. 3.9a. It can be seen that the limit is dependent on the orientation of the azimuth axis, so there is a range of directions that have no limits and can rotate continuously. As shown

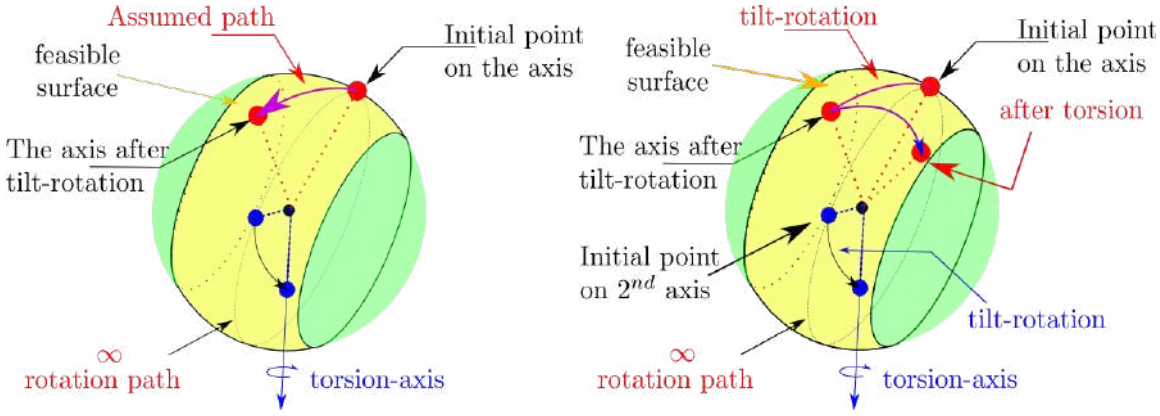

(a) Spherical rotation without torsion (b) Spherical rotation with torsion

Figure 3.9: The different travel paths of an axis in tilt-torsion representation.

in Fig. 3.9b, we have reached the final path by a combination of two different paths that represent the tilt-rotation and the torsion-rotation. It is important to note that this occurs solely because of the representation in the tilt-torsion convention. We would have 3 individual paths if we would have used the Euler angles. So, the natural question to be asked is : 'Can we use this path followed by the axis to reach from an initial point to a final orientation for implementing joint limits?'

A solution can be to use tilt-torsion representation in the zero-torsion case as we have an unique path connecting two orientations. In case of torsion, we can check limits for the final orientation as well as the intermediate point as shown in Fig. 3.9a. In this case, we will have to consider two axis as we are rotating about an axis in a plane, for example the **xy**-plane, for tilt-angle and later rotate about the axis perpendicular to the plane, the **z**-axis, for the torsion angle. So, if the path respects the joint limits, we know that there is at least one way to reach the final orientation but if the path does not respect the passive limits, in such case we can not tell the truth for sure. Thus, the limits by tilt-torsion representation only implies the truth about the passive joint limits.

3.5 Workspace representation

In this section, the discussion from the above section has been continued but for a different application. The representation of the workspace is crucial while considering optimization variables and also to visualize the feasible workspace. The different possibilities to represent the workspace and their pros and cons are discussed in this section.

3.5.1 Euler angles

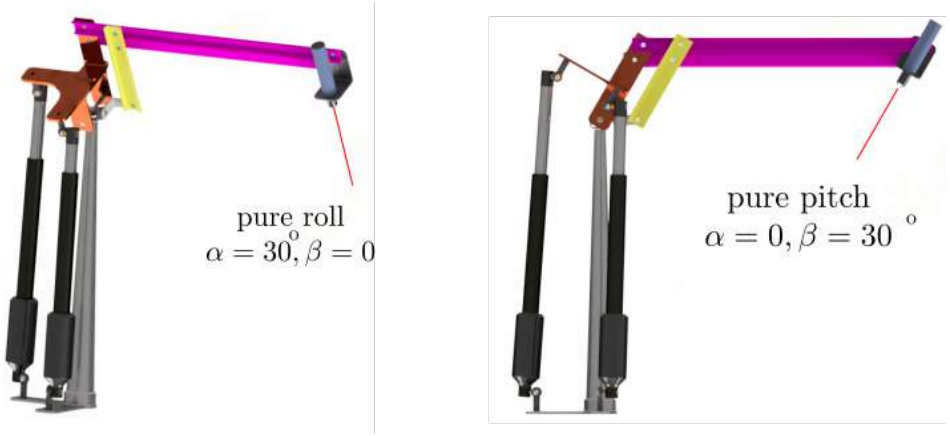

Figure 3.10: The different poses of the mechanism in Euler representation

As we are proposing a 2-dof orientation mechanism, we can use Euler angles without the issue of gimbal lock. The workspace is represented in two angles, α and β, that represent an ordered rotation about x-axis and y-axis respectively. The value of α can be directly linked with the roll motion of the mechanism but β is the pitch movement in the rolled-orientation. The feasible workspace can be represented as a rectangle with independent limits on α and β. In fig.3.10, different end-effector poses are shown to highlight the interpretation of individual angles in the Euler-angle representation. In this representation a point in the output space can be represented as the combination of the ordered rotation by α and β respectively.

$$\mathbf{R}(\alpha,\beta) = \mathbf{R}_{\alpha}\,\mathbf{R}_{\beta} = \begin{bmatrix} cos(\beta) & 0 & sin(\beta) \\ sin(\alpha)\,sin(\beta) & cos(\alpha) & -cos(\beta)\,sin(\alpha) \\ -cos(\alpha)\,sin(\beta) & sin(\alpha) & cos(\alpha)\,cos(\beta) \end{bmatrix} \tag{3.22}$$

3.5.2 Azimuth-tilt angles

We can use the the tilt-torsion representation and treat the workspace as a zero-torsion case [48]. The advantage of such representation is an easier visualization of the feasible workspace and thus the the desired workspace can be easily analyzed as shown in Fig. 3.12. A big disadvantage that was found while analyzing the mechanism with this representation is that we encounter a singularity at the default position ($\alpha = 0$, $\beta = 0$) of the manipulator. This can be attributed to a reason that when the tilt-angle is zero, the azimuth angle has infinite solutions for the same representation. A further study into this will be carried out to investigate the root of the issue and mitigate the same. The azimuth angle in the tilt-torsion representation gives the direction in which the endoscope is going to tilt and the tilt-angle gives the measure of amount of the inclination of the endoscope. In this representation a point in the output space can be represented as the rotation of a vector about axis ω by θ_t as stated in (3.23)

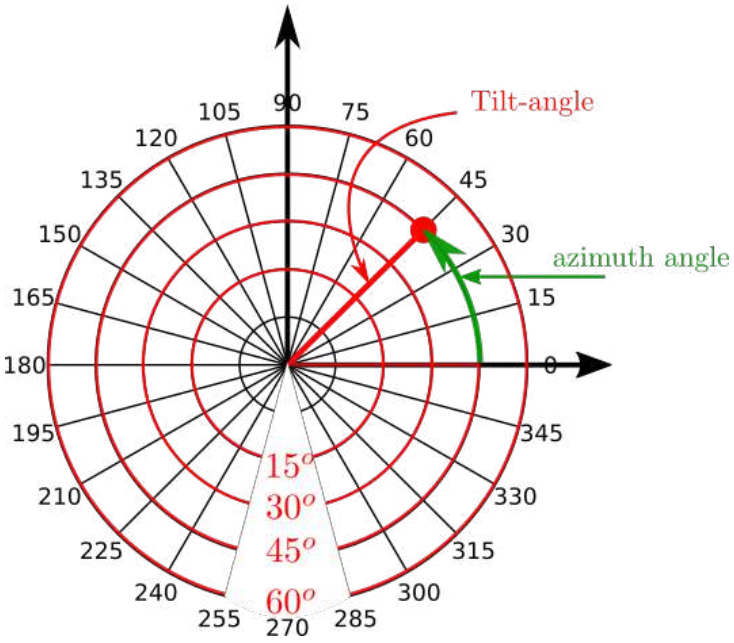

Figure 3.11: The polar representation of the azimuth-tilt angles

$$\begin{aligned} \mathbf{R}_t &= \mathbf{e}^{\tilde{\omega}\,\theta_t} \\ &= \mathbf{I} + \tilde{\omega}\, sin(\theta_t) + \tilde{\omega}^2\,(1 - cos(\theta_t)) \end{aligned} \tag{3.23}$$

The expansion of the same is given in (3.14). The azimuth angle is solely derived from the components of vector ω and is given as:

$$\theta_a = atan2(\omega_y, \omega_x) \tag{3.24}$$

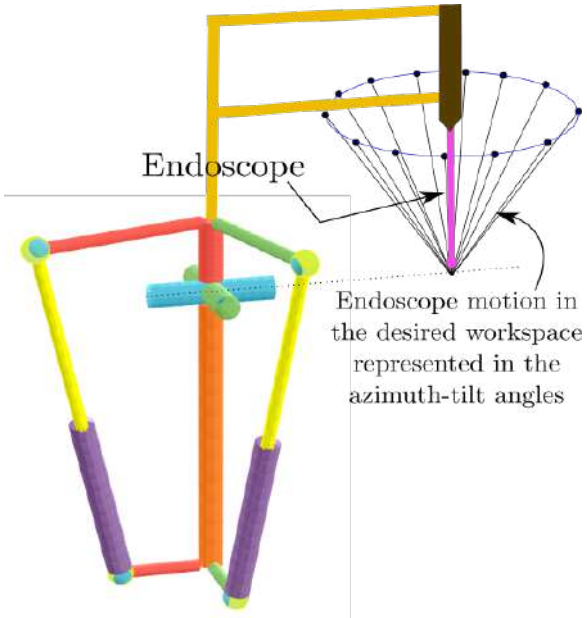

Figure 3.12: The visualization for endoscope motion in azimuth-tilt representation

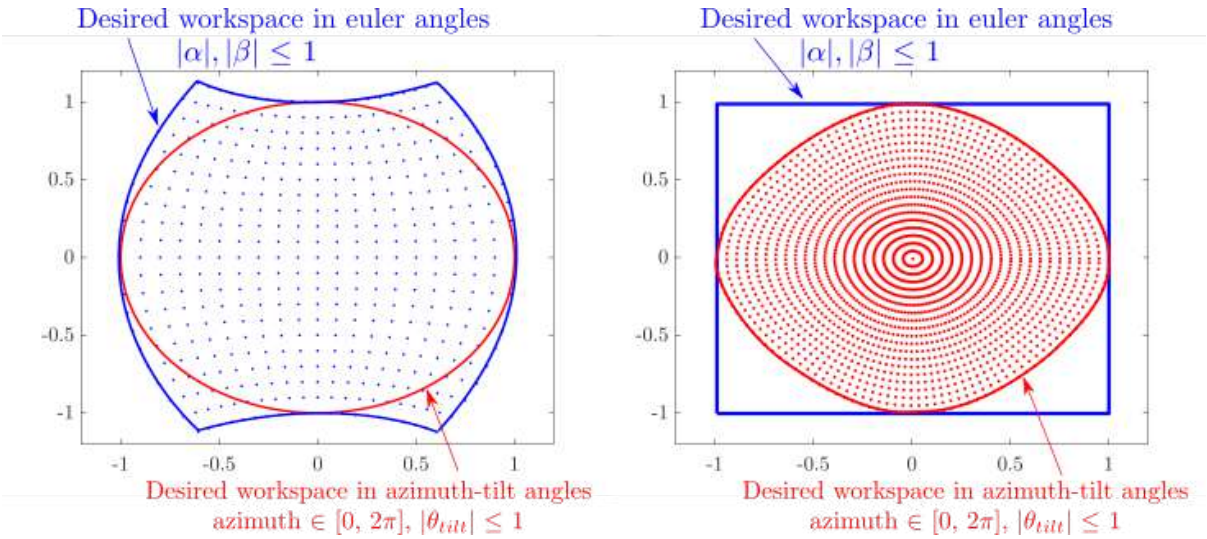

Figure 3.13: The comparison of the desired workspace in Euler-angles (blue) representation and the azimuth-tilt (red) representation.

In Fig. 3.11, the workspace has been presented in polar co-ordinates. It is very easy to visualize and understand the workspace in this representation. Fig. 3.12 shows the motion of the endoscope when the workspace is represented in the azimuth-tilt representation. The area covered in Fig. 3.11 is nothing but the base of the cone in Fig. 3.12. The height of the cone is just a representation of the length of endoscope but it has no meaning in the orientation workspace.

3.6 User-centric choices

In this section, we discuss the different choices considered while proposing an optimum design. Taking into account the application in our case, it is of prime importance that the feedback from surgeons is analyzed in order to tweak the requirements and solutions related to them.

We created a questionnaire in order to understand the requirements and expectations from the mechanism by the surgeons. The questionnaire was designed in two stages. In the first stage, few preliminary questions were asked that could relate the answers to a desired speed of the actuator as well as their accuracy. A 3D CAD-model was designed in order to compare the size of the mechanism with respect to the workspace of the ear as well as the sinus as shown in Fig. 3.14. To familiarise the surgeons with the speed of the mechanism, we prepared simulations of the movement and asked the surgeons to rate them as fast, slow or adequate. The questionnaire also presented an option to prioritize between four requirements; (i) speed of the mechanism, (ii) size of the mechanism, (iii) ease of operation and (iv) multiple operation capacity. We were able to elicit interesting conclusions and the results have been presented in Fig. 5.2.

It was helpful to get a rough idea of what surgeons perceived when they were presented with the idea of a robotic assistance. In the first phase, the number of participants were 9 and no information regarding their level of expertise was taken into account.

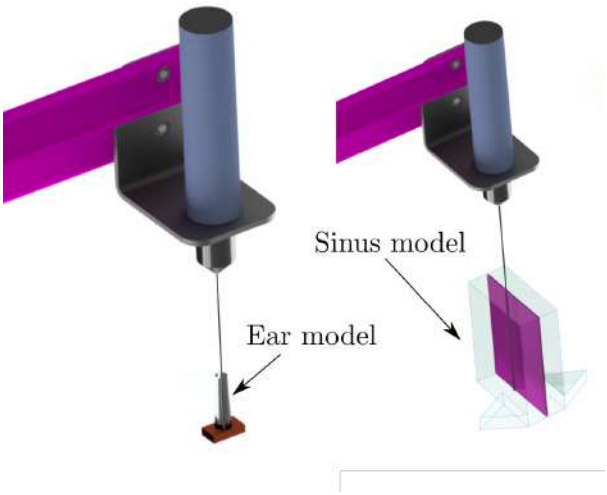

Figure 3.14: The renderings used for size comparison in the phase 1 questionnaire

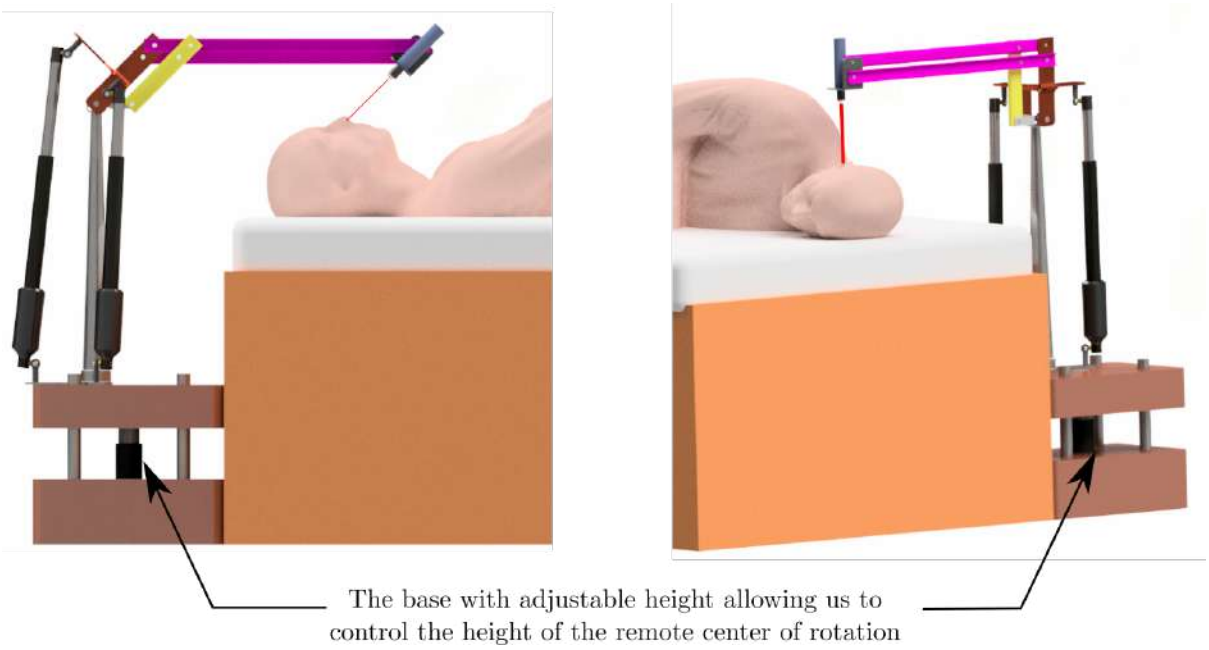

Figure 3.15: The renderings used for size comparison in the phase 2 questionnaire

To get better insights, we designed a questionnaire with better understanding of the surgeons perspective. As we learned that the surgeons prioritized the ease of use over other parameters, we implemented the System Usability Scale (SUS), the most widely used standardized questionnaire for the assessment of perceived usability and learnability [49]. The information regarding the expertise and years of practise with and without endoscope was also collected. This was important as for a technology to be accepted in the environment, it is important to measure the comfort of adapting to such mechanisms. It also allowed us to have weighted feedback in order to design a mechanism for future operations. The complete environment was created on the CAD model for better perception of the size of the mechanism. The rendered image for the same has been shown in Fig. 3.15

This questionnaire was also shared with a larger group of surgeons from various regions of France in order to get a conclusive idea on the speed, size and accuracy required for proposing a solution. The feedbacks from these questions provides a strong foundation for the optimization problem where the optimized solution completely depends on the constraints which are governed by the requirements from the surgeons.

Chapter 4

Mechanism optimization

Before we plunge into the core essence of the optimization methodology, it is important that we understand the motivation behind it. In mechanism design the various choices that have to be made are:

1. The architecture of the manipulator: the variants shown in Chapter 3
2. Type of joints: different combinations of joints to achieve the same dof
3. Pose of the joints: where to place and how to place a particular joint's frame?

Making a particular choice is non-trivial, especially because of its effect on the workspace, kinematic solutions and size of the mechanism. Another interesting challenge is that the same architecture can be used to perform different tasks with either kinematic or dynamic constraints and thus have to be optimized accordingly. This chapter presents the optimization methodology adapted for the parallel mechanisms to be used for the otological surgery.

4.1 Elements of the optimization

To solve any optimization problem, we should ask ourselves the following questions:

- What is the goal?
- What are the constraints?
- What can we change to reach the goal?

The answer to the above questions form the elements of the optimization problem. The importance of each element is that they affect the final goal, the computational cost as well as the algorithm suitable for the problem. The following sections elaborate on these elements allowing us to further understand the choice of the algorithm.

4.2 Objective function

The choice of the objective function of a mechanism completely depends on the application of the manipulator. Some use cases require a good kinematic behaviour, for e.g: camera manipulation, while some may demand a good dynamic characteristic, for e.g:

machining tasks. In this thesis, we are primarily concerned about the kinematic characteristics of the manipulator as our application is similar to that of a camera manipulation.

The most important property of a manipulator is its feasible workspace and so maximizing workspace is a natural choice of the objective function. A detailed analysis of the volume available for endoscope manipulation in otological as well as sinus surgery is presented in [2]. The work presents the study of the petrous bone and the paranasal sinuses of several patients of different age (2 to 95 years) and sex. This establishes a firm ground for the requirement of the orientation ranges in the endoscope manipulator. Fig.

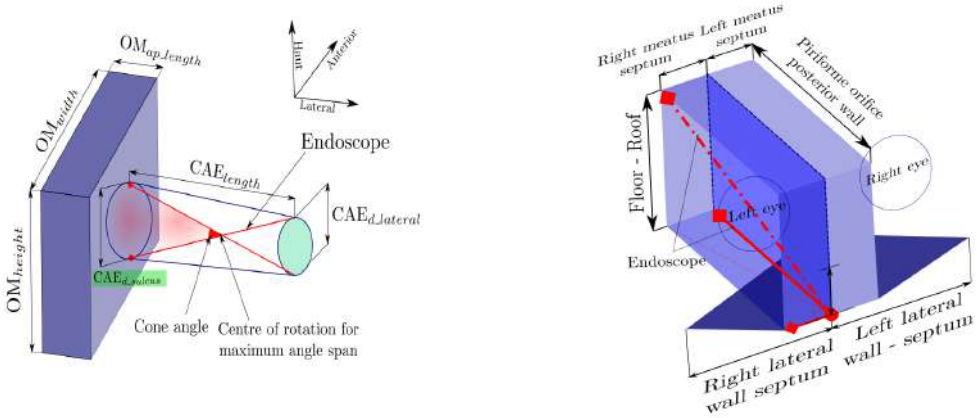

(a) Different measurements of the ear (b) Different measurements of the sinus

Figure 4.1: The models of the ear and the sinus presented in [2].. The sinus model suggests that we need a 90 degree travel of the endoscope (± 45 deg)

4.1 illustrates the models of the ear and sinus and the endoscope manipulation in the same. It was observed that the otological surgery has a small workspace and the range required is low. In the case of sinus surgery, the workspace is larger as the partition in the nose is sometimes removed. Also, as the centre of rotation of the manipulator can be changed, there are positions where the endoscope has an orientation travel of $\pi/2$ radians.

4.2.1 Multiple objectives

When we are designing a manipulator with kinematic characteristics in mind, it is important that we evaluate the quality of the motion performed. There are several quality indices presented in the past and a brief comparison between widely used indices is presented in this section. Apart from the quality of the motion, we also concentrate on the passive joint limits of the mechanism. This is the reason that the presented work also considered implementing a reward strategy related to keeping the joints as far as possible from their limits. The feasible workspace and the global quality of the manipulator are directly related in our case and thus can be implemented together with appropriate weights. The two objective functions, the quality index and the passive joint norm, appear to be contrasting in their nature and thus a compromise has to be made in order to choose a mechanism performing well in both the objective functions.

4.2.2 Multiple objectives : Workspace of the manipulator

The presented work considers a Regular Dextrous Workspace (RDW) that is a square in output space represented by the Euler angles. It is thus implied that the roll and pitch movements of the manipulator are of equal importance for the endoscope manipulation. As we were interested in exploring the possibility of implementing the mechanism for multi-purpose surgeries, the required workspace is not treated as a constraint rather it tries to achieve a workspace larger than required ($\pm$ 1 radian). This allowed us to also observe the effect of different constraints if the manipulator is to be used in different application.

The concept of safe working zone for parallel manipulators has been introduced in [50] where a feasible workspace is free of singularities, internal link collisions as well as respects passive joint limits. The presented work considers only the collision of actuating prismatic joints as the rest of the links can be redesigned to counter the resulting collision issues, if any. The context of feasible set ($\mathcal{F}$) in this literature relates to the set of all points in the in the discretized output spaceoutput space ($\mathcal{K}$) that are:

1. Non-singular
2. Respect passive joint limits
3. There is no collision between the actuators at this configuration

The desired Regular Dextrous Workspace (RDW_d) in the context of the report is:

$$RDW_d : span\{(\alpha, \beta) \mid \alpha, \beta \in [-1, 1]\}$$

4.2.3 Multiple objectives : Quality of the manipulator

Different quality indices such as the manipulability ellipsoid volume (v_e) [51] and the conditioning number (κ) [52] were used previously for quantifying the quality of the motion of a manipulator. Later, different quality indices were introduced in order to mitigate the shortcomings of these indices. One such parameter is the velocity amplification factor [53]. This parameter has a physical interpretation and directly represents the efficiency of motion amplification in the actuators to that of the end-effectors.

4.2.4 Measuring quality via the manipulability ellipsoid

The manipulability ellipsoid measures the volume of the reachable workspace at a particular configuration of a manipulator when the l_2-norm of the input vector ($\mathbf{q_i}$) is less than 1 and is calculated as shown in (4.2). This ellipsoid gives the idea of the reachable workspace but provides no information on the ease of direction of travel. In some cases, the ellipsoid is a sphere and thus the manipulator can travel in every direction with equal agility. This configuration is called the *isotropic configuration* and is highly desirable for uniform performance of the manipulator. The manipulability ellipsoid quantifies a sphere and an ellipsoid of same volume as equally good but we know that the *isotropic configuration* is preferable. The linear mapping between the $\mathbf{q_i}$ and generalized output vector ($\mathbf{x}$) is given by the $\mathbf{J}$ as:

$$\dot{\mathbf{x}} = \mathbf{J}\dot{\mathbf{q}}_\mathbf{i} \tag{4.1}$$

$$v_e = \sqrt{det(\mathbf{J}\mathbf{J}^{\mathbf{T}})} \tag{4.2}$$

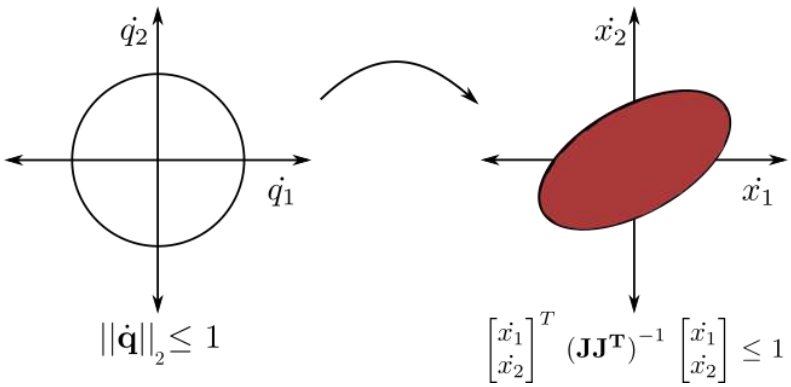

Figure 4.2: The change in plot while expressing the same constraint in different spaces

4.2.5 Measuring quality via the conditioning number

To counter the shortcomings of the manipulability ellipsoid, the conditioning number (κ) was introduced in [52] to quantify the quality of motion. The condition number is defined as the value of the asymptotic worst-case relative change in output for a relative change in input and is used to measure how sensitive a function is to changes in the input. It is geometrically interpreted as the eccentricity of the ellipsoid giving information about the ease of travel in a direction relative to the others. When the κ is equal to 1, we have a sphere and it is the *isotropic configuration*. The conditioning number (κ) can also be interpreted as an index that tells us how far the current configuration is from the *isotropic configuration*. The value of κ ranges from 1 to ∞ and so its inverse is used as a quality index (κ^{-1}) for bounded values and is calculated in (4.3), where σ is the singular value of the jacobian matrix, $\mathbf{J}$.

$$\kappa^{-1} = \frac{\sigma_{min}}{\sigma_{max}}, \quad \kappa^{-1} \in [0, 1] \tag{4.3}$$

Both the quality indices, the manipulability ellipsoid and the conditioning number, suffer from dimensional inhomogeneity of the Jacobian matrix and are not suitable for manipulators with both translational and rotational movements [54]. This is an important issue to consider while implementing the proposed optimization methodology for a general manipulator. The thesis was focused more on the optimization algorithm and its implementation to a specific application. As the manipulator proposed in this work has only 2 rotational dof, we decided to use the inverse of conditioning number as the quality index. As we wanted a global quality index (κ_g^{-1}), the mean of summation of the values of κ^{-1} over the discretized workspace point was used.

$$\kappa_g^{-1} := \frac{\sum_{1}^{W} \kappa^{-1}}{W}, \quad W : \text{total workspace points} \tag{4.4}$$

4.2.6 Measuring quality via the velocity amplification factor

The velocity amplification factor (vaf) was introduced in [53] and has been used in measuring the quality of motion in the past [55, 28]. The vaf allows us to analyze the relation between the actuator speeds with the velocities of end-effector at a certain configuration. The vaf can be bounded within desirable range according to the chosen actuators. One of the main advantages of vaf over the previously mention quality indices is that the bounds are very practical in nature and the performance of the manipulator can be analyzed with physical interpretation. As we plan to use off the shelf actuators, it is very important to have realistic bounds on the velocity of the actuators. Velocity amplification factor helps us to measure the quality of the end-effector motion with respect to the speeds of individual actuators.

In previous works, the vaf is calculated by assuming the l_2-norm of the $\mathbf{q_i}$ to be less than 1. It allows us to get a square matrix $\mathbf{JJ}^T$ and we can further analyse this matrix with different mathematical tools. This choice of input vector is strange as we make the input velocity of a particular joint dependent on the other input joints [56]. A better condition would be to implement an independent constraints on the actuated joint velocities and thus implementing the ∞-norm.

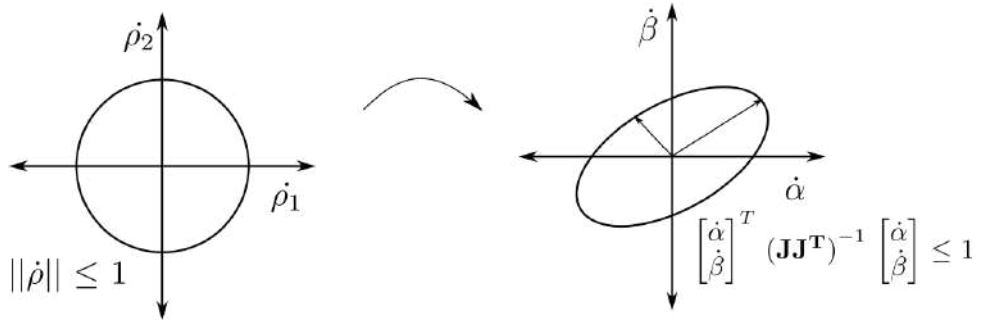

Figure 4.3: The geometric interpretation with the assumption of $\|\dot{q}\| \leq 1$

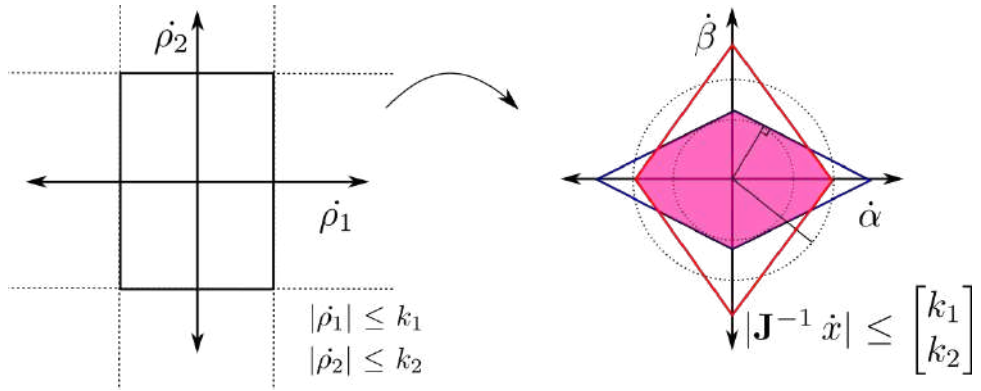

Figure 4.4: The geometric interpretation with the independent constraints

Let k_1 and k_2 be the maximum velocity of the individual actuators. The formulation

of the vaf is given as:

$$|\dot{\rho}| \leq \begin{bmatrix} k_1 \\ k_2 \end{bmatrix}$$
$$|\mathbf{J}^{-1}\,\dot{\mathbf{x}}| \leq \begin{bmatrix} k_1 \\ k_2 \end{bmatrix} \tag{4.5}$$

$$|J_{11}\dot{\alpha} + J_{12}\dot{\beta}| \leq k_1 \tag{4.6}$$
$$|J_{21}\dot{\alpha} + J_{22}\dot{\beta}| \leq k_2 \tag{4.7}$$

We obtain four lines from (4.6, 4.7) which form two origin-centered rectangles as shown in Fig. 4.4. The intersection of these two rectangles (the pink area in Fig. 4.4) is the valid region in the output space that respects the limits of the actuator velocities. We calculate the radius of the incircle as well as the circumcircle of this area to obtain the minimum as well as the maximum amplification of the velocities. These distances are used as bounded constraints and the quality of the manipulator is the ratio of the inradius to the circumradius.

As we are using a bounded constraint on the inradius as well as the circumradius, it is important to understand their properties. It was observed that the inradius as well as the circumradius amplifies or shrinks upon scaling of the dimensions, i.e. if the manipulator is scaled to have double size, the velocity amplification increases too. This can be a problem as neither the workspace nor the quality of motion should change upon scaling for manipulators that have pure rotational dof. This problem occurs if we use constant limits for k_1 and k_2 as the bigger actuators have more stroke length but we are limiting their maximum travel speed equal to the actuator with half of its stroke length. In our implementation, we are choosing LA22 actuators from LINAK as shown in Fig. 4.19. The maximum speed of this actuator is 37 mm/sec while the stroke length is 200 mm. We use the same ratio for our optimization problem. If the scale of the manipulator is such that the stroke of the actuator is s mm, then the limits k_1 and k_2 are assigned as:

$$k_1 = k_2 = k = s\,\frac{37}{200} \tag{4.8}$$

The comparison of the velocity amplification factor with the conditioning number is presented in Fig. 4.5. It is interesting to observe that the singular regions are not exactly reflected in vaf. This is attributed to the reason that we derive the inverse jacobian matrix, $\mathbf{J}^{-1}$, and do not synthesize and are not concerned with its eigen values or the determinant. This means that even when the matrix is not invertible, there exists a stable one way mapping between the input and output spaces.

4.2.7 Multiple objectives : Joint limits norm

After we have a good desirable workspace with acceptable quality, we can also try to keep the joints away from the limits. This objective function was implemented to explore the areas where simple joints with limited motion can be used. It is not straightforward to define the distance of a joint orientation from its limits for a spherical joint. We have proposed the projection of the rotated vector onto a plane to define the distance from its limits as shown in Fig. 4.6. It is not the accurate presentation of the distance from limits but a detailed analysis would require time and more mathematical analysis into

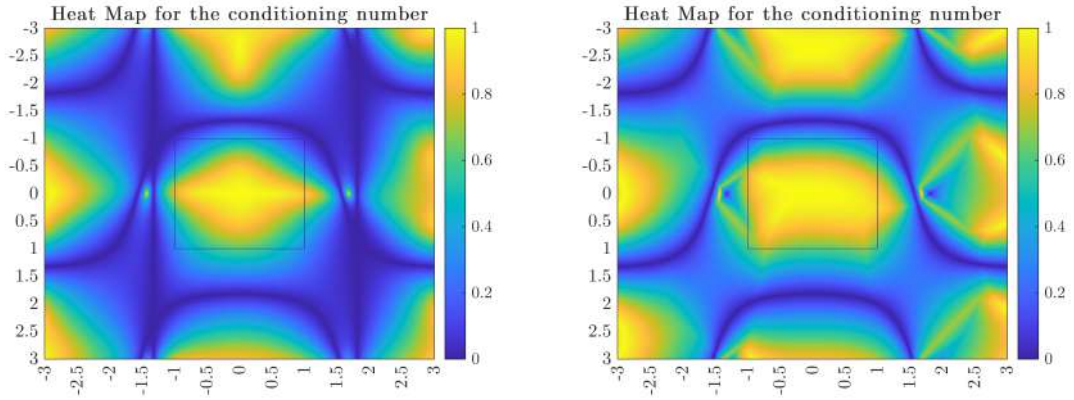

(a) Heatmap for the conditioning number of chosen parameters

(b) Heatmap for the VAF of chosen parameters

Figure 4.5: The comparison between the conditioning number and the velocity amplification factor

orientation space and defining the 'essence' of travel, distance and shortest distance in orientation. As we are implementing the same spherical joint, the distances were not weighted and summation of the distances was used as the joint limit norm at a particular configuration (q_{pi}). The summation of q_{pi} over the workspace is used as an evaluation while maximizing the distance from the joint limits.

$$\|q_{pi}\| := \sum_{n=1}^{4} (l_{limit} - l_{current})_n, \quad n : no.of joints \tag{4.9}$$

$$\|q_p\| := \sum_{i=1}^{W} \|q_{pi}\| \tag{4.10}$$

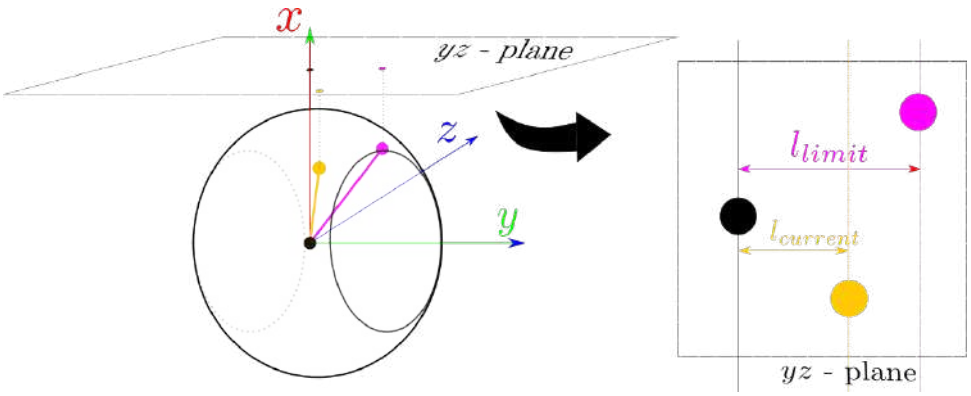

Figure 4.6: Illustration of the joint limit distance

4.2.8 Summary of the used objectives

So, to summarise the objective functions implemented in the presented methodology, we are looking to:

1. Maximize the feasible set in the desired regular dextrous workspace

2. Maximize the quality of motion in the feasible workspace.

3. Maximize the distance of the passive joints from their respective limits

Mathematically denoting,

$$\text{Objective functions} : max\left(\mathcal{F} \bigcap RDW_d\right) \tag{4.11}$$

$$max\left(\kappa_g^{-1}\right) \tag{4.12}$$

$$max\left(\|q_p\|\right) \tag{4.13}$$

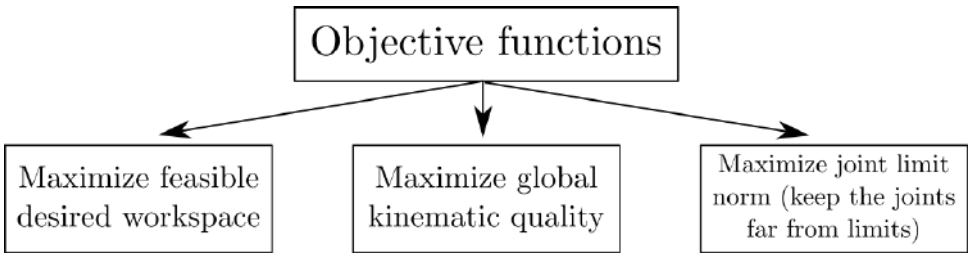

Figure 4.7: Summary for the different objective functions

4.3 Constraints

Parallel Kinematic Manipulators (PKMs) have 2 distinct features from a serial chain as they have:

1. Passive joints whose orientation can be calculated but not controlled explicitly.

2. Multiple legs - serial chains connecting the end-effector with the base.

These two points are of great importance as they affect the workspace of the manipulator. So, we take note that the passive joint limits and avoiding internal collisions among different legs of the Parallel Kinematic Manipulator (PKM) are two important constraints to be implemented in our optimization problem. The $\mathcal{K}$ space of the mechanism is separated by the singularity curves thus resulting into several connected regions also called as the *aspects* [57]. As we cannot travel from one *aspect* to another, it is important that the desired RDW (RDW_d) lies in a single *aspect*. Fig. 4.8a illustrates a valid set of parameters while Fig. 4.8b corresponds to a non-useful architecture for our application. If the box in the Fig. 4.8 consists of multiple colors, then it is evident that there are more than one *aspect* and thus we cannot travel to every configuration in the RDW.

4.3.1 Feasible actuator range

Another important constraint while designing is of the actuator which is represented as the active joint ranges. This work specifically focuses on the range of the prismatic joint to be chosen for maximizing the points in $\mathcal{F} \bigcap RDW_d$. Generally, a prismatic joint is expressed as a constraint with a certain minimum and maximum range and with a constraint on the ratio of the lengths in completely acuated state and its default length:

$$\min \leq \rho \leq \max \tag{4.14}$$

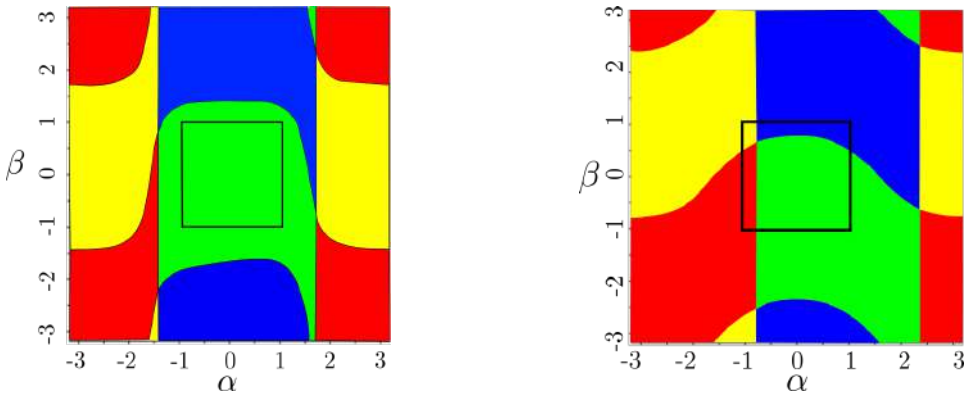

(a) RDW in one connected region (*aspect*), a valid set of parameters

(b) RDW is intersected by the singularity curves, an invalid set of parameters

Figure 4.8: The *aspects* of the $\mathcal{K}$ space in different cases

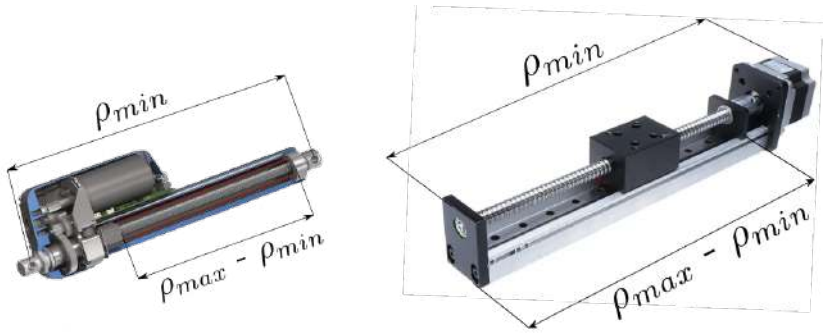

Figure 4.9: The industrial prismatic joints and the relation between ρ_{min} and ρ_{max} Source: Hanpose linear actuator HPV5 SFU1204, `www.pngegg.com/en/png-mckkp`

$$\rho_{max} \leq \text{stroke} \times \rho_{min}, \quad stroke \in [1, 2] \tag{4.15}$$

Eq. 4.15 comes from the physical build of general prismatic joints. If the unextended length of the actuator is ρ_{min}, then it is not practical for common prismatic joints to extend beyond their original length ($\rho_{max} < 2.\rho_{min}$) as explained in Fig. 4.9. The novelty in expression of the actuator range in our work is that we do not have a static value as a limit as mentioned in (4.14), i.e, we express the constraint only in terms of the stroke ratio expressed in (4.15). This allows us to choose the best actuator ranges to maximize the feasible workspace without putting any constraint on the minimum or maximum size of the prismatic joint. This is best illustrated in the Fig. 4.10 and Fig. 4.11 and the implementation is detailed further in Section 4.5.4

4.4 Optimizing variables

Optimizing variables are the parameters that are changed in order to optimize the objective function. In a mechanism, the position or the orientation or both (pose) of the joints in the kinematic chain are the design parameters that are to be optimized. The number of variables form the dimension of the optimization problem which governs the size of the search space (also denoted as $\mathcal{O}$) and so the computational capacity. In deciding the optimizing variables, we have to consider the following options:

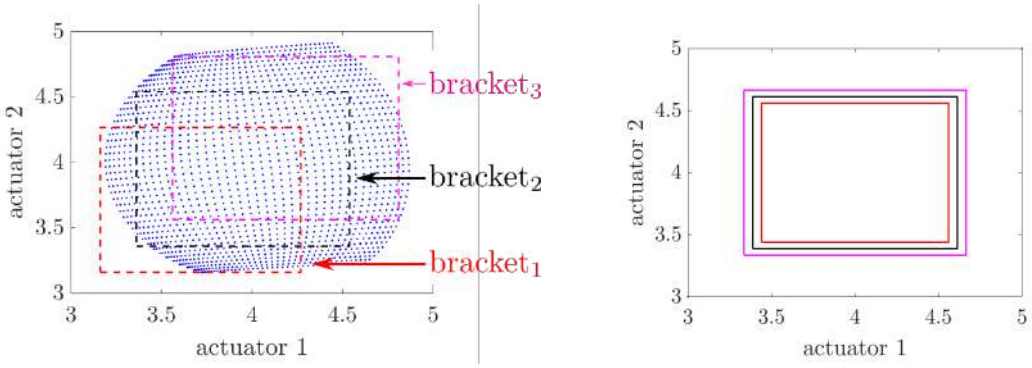

(a) Different search brackets within the actuator space (input space)

(b) Comparison of the size of the search brackets showing their variable nature

Figure 4.10: The varying search brackets for range of actuators.. The blue dots correspond to the pair of lengths of actuators for a configuration in RDW

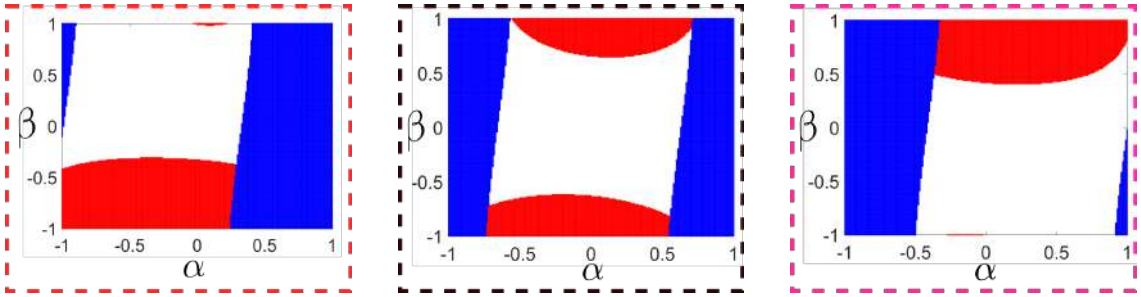

(a) Feasible workspace (white) when red bracket in Fig. 4.10a is implemented

(b) Feasible workspace (white) when black bracket in Fig. 4.10a is implemented

(c) Feasible workspace (white), magenta bracket in fig.4.10a is implemented

Figure 4.11: Comparison of feasible workspace (white space) within the RDW_d for different search brackets.. The red and blue part represent the violation due to actuator lengths of leg1 and leg2 respectively.

- Use a general approach, we have 3 variables x, y, z for each joint (Fig. 4.12a).
- Use human intuition to fix certain variables in order to reduce the search space.

Each of the above-mentioned options have some advantages and disadvantages. If we use a general approach to optimize the position of the joints, then we can produce some results that are counter-intuitive but efficient. This comes at a cost of dimensional blowup as there are many joints in a parallel mechanism. For e.g, in the mechanism architecture proposed in this work, we have two legs with 6 dof and a leg with 2 dof. In a case where we use a combination of revolute joints to form a universal joint and a spherical joint, we can have as much as 14 joints (6 dof $\times$ 2 legs + 2 dof $\times$ 1 leg). This results into an optimization space of dimension 42 which is a very large space given the nature of constraints and the time required to compute the objective function for a particular configuration. In the other option, we can seriously reduce the dimension for $\mathcal{O}$ by using human intuition and trying to bring careful symmetry (avoiding obvious singularities) in the mechanism. For example, in the 2UPS-1U variant of the proposed architecture, we can reduce the optimization space to dimension 4 as shown in Fig. 4.12b.

The choice of fixing some variables comes at a cost that we may miss some configurations that are better performing but it has several advantages. Thanks to the human intuition, we use links of same length and try to optimize the mechanism by assuming the leg1 and leg2 are identical from the manufacturing and assembling point of view. So, as every designer seeks in every project he does, we can certainly explore the possibility of a compromise between these 2 choices.

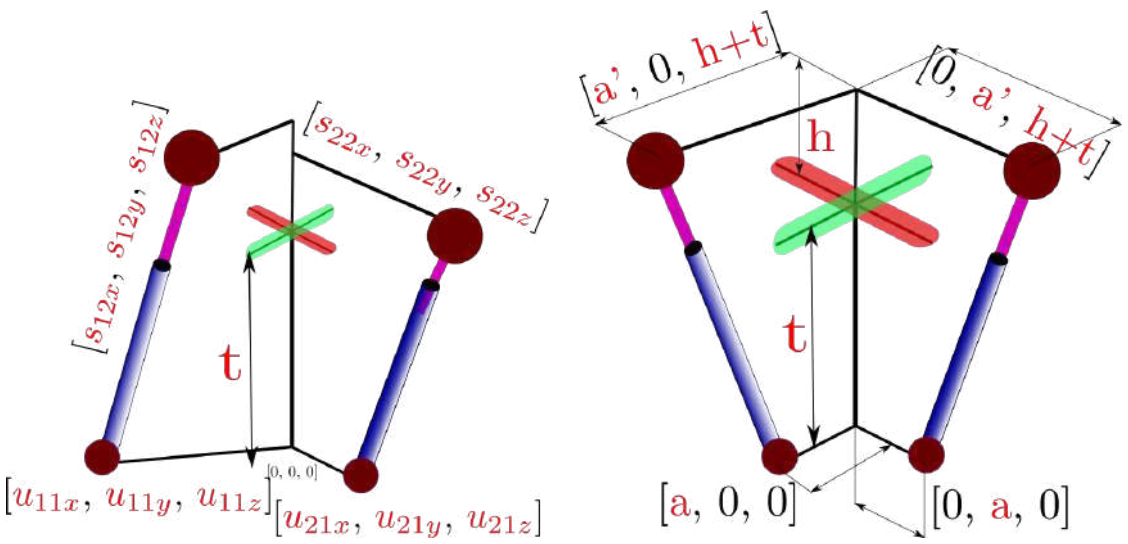

(a) Mechanism with 13 optimization variables shown in red

(b) Mechanism reduced to dimension-4 by human intuition (variables in red)

Figure 4.12: The different definitions of the same architecture . varying the number of parameters. In 13 (left) parameters, we do not fix any variable for the position of the joints while in 4 parameters (right), we assume equal lengths, symmetry and perpendicular legs.

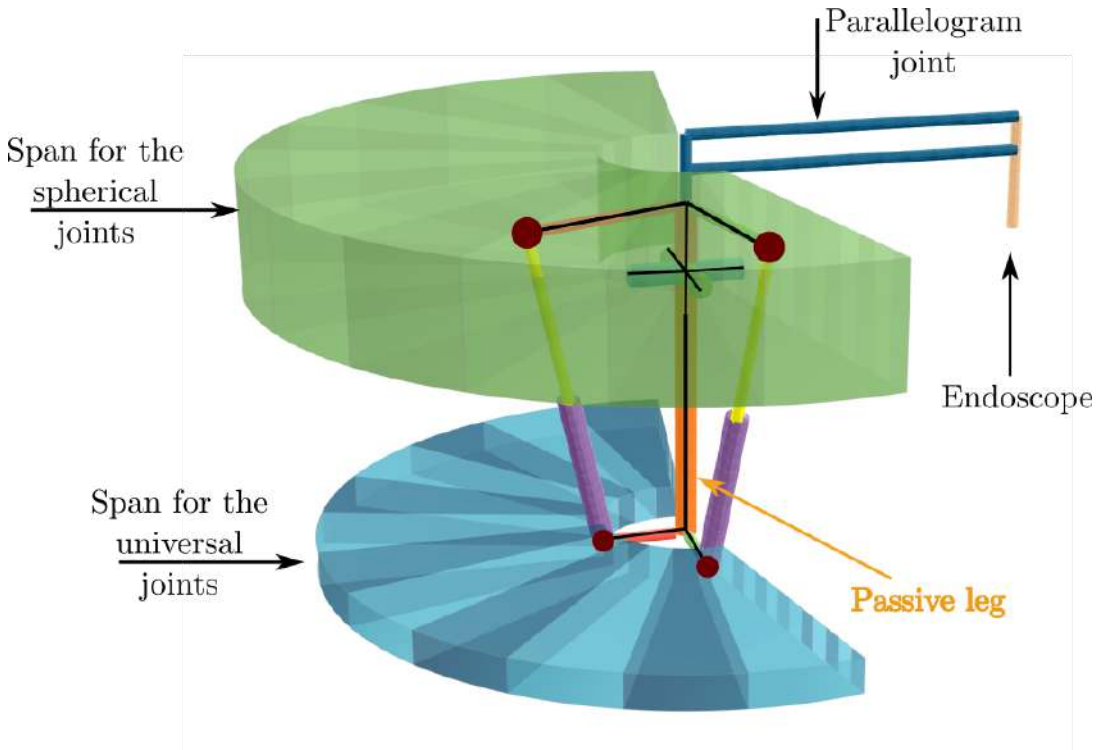

Figure 4.13: The range of optimizing variables. The lower and upper joints of each leg can be place in their respective cylindrical enclosures shown in blue and green.

Fig. 4.13 shows the space in which the universal joints and the spherical joints can lie in. The arc angle of the span is 200 degrees with a minimum and maximum range. The height of the span decides the range of the z-coordinate of the joints. It is to be noted that the blue span is with respect to the ground while the green cylindrical arc is with respect to the universal joint of the third passive leg. When the dimension is reduced to 4 as shown in Fig. 4.12b, the 2 cylindrical arc get reduced to 4 squares in 2 perpendicular planes.

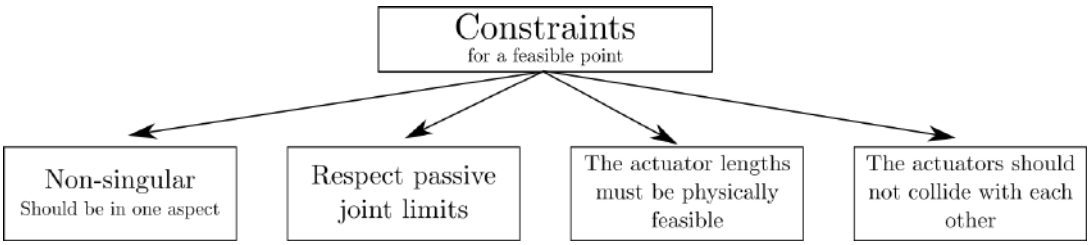

Figure 4.14: Summary for different constraints in the optimization process

4.5 Local search algorithm

The Nelder-Mead algorithm is a derivative-free optimization algorithm proposed by John Nelder and Roger Mead [58] in 1965. It is also called the *downhill-simplex algorithm* as it uses *simplexes* to search the space locally. In this section, we present the algorithm for a *single start* which searches in the local vicinity of the initial simplex. Later, we discuss the implementation of the algorithm in mechanism optimization with different rewarding

strategies and detail the method for extracting the best actuator ranges from the solution. We conclude the section with a summary of the algorithm with its implementation highlighting few strengths and weaknesses of the same.

4.5.1 The Nelder-Mead (NM) Algorithm

For a n-dimensional $\mathcal{O}$, we require a simplex of at least n+1 points in $\mathcal{O}$ to avoid *premature convergence*. This can be explained with a simple graphics for 2-dimensional $\mathcal{O}$ as show in Fig. 4.16.

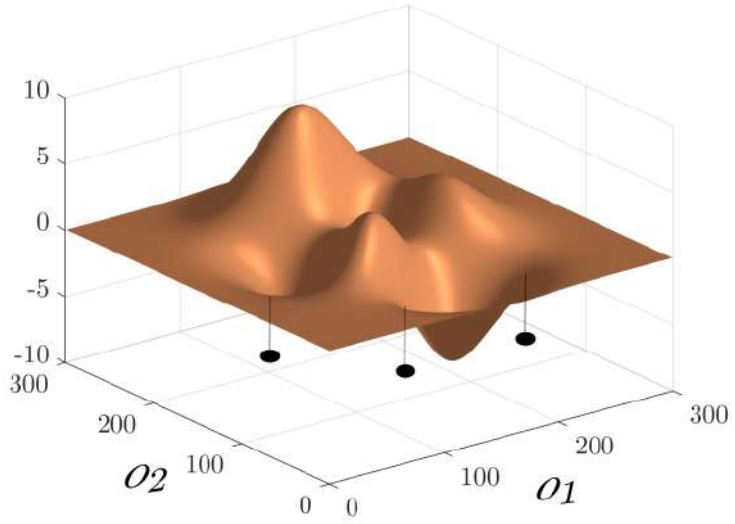

Figure 4.15: An example of mapping with 2 optimization variables

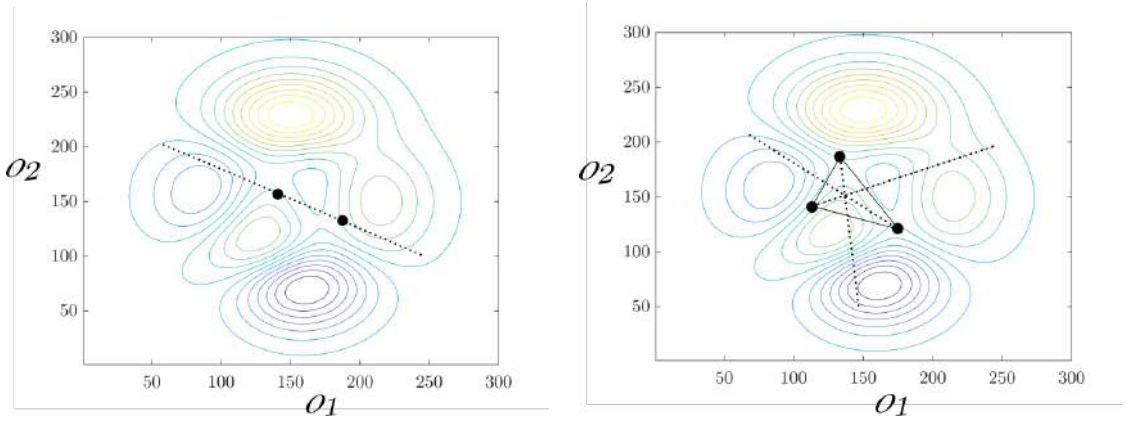

(a) The traversing in $\mathcal{O}$-space with 2 point simplex, we can explore the points on the line only

(b) The traversing in $\mathcal{O}$-space with 3 point simplex, we can travel in both directions exploring the complete space

Figure 4.16: The premature convergence while using a simplex of less than (n+1) points in n-dimensional $\mathcal{O}$-space.

In our implementation of the algorithm, we start with a sorted simplex of n+1 points $(\mathbf{v_0}, \mathbf{v_1}, ...\mathbf{v_n})$ such that the objective function evaluated of the i^{th} vertex has a value

better than or equal to that of $(i+1)^{th}$ vertex. A mean point ($\mathbf{v_m}$) is calculated by excluding the worst point.

$$\mathbf{v_m} := \frac{\sum_{i=0}^{n-1} \mathbf{v_i}}{n} \tag{4.16}$$

The optimization algorithm then compares the mean point and searches for better points by geometrical operations termed as (i) reflection, (ii) expansion, (iii) contraction and (iv) shrinkage. These operations can be explained as follows:

- Reflection:

$$\mathbf{v_{reflect}} := \mathbf{v_m} + r\,(\mathbf{v_m} - \mathbf{v_n}), \quad r := \text{reflection coefficient}\,(r > 0) \tag{4.17}$$

- Expansion:

$$\mathbf{v_{expand}} := \mathbf{v_m} + e\,(\mathbf{v_{reflect}} - \mathbf{v_m}), \quad e := \text{expansion coefficient}\,(e > 1) \tag{4.18}$$

- Outside contraction:

$$\mathbf{v_{oc}} := \mathbf{v_m} + k\,(\mathbf{v_m} - \mathbf{v_n}), \quad k := \text{contraction coefficient}\,(0 < k < r) \tag{4.19}$$

- Inside contraction:

$$\mathbf{v_{ic}} := \mathbf{v_m} - k\,(\mathbf{v_m} - \mathbf{v_n}), \quad k := \text{contraction coefficient} \tag{4.20}$$

- Shrinkage:

$$\forall\, i \in [1, n] \quad \mathbf{v_i} = s\,.\mathbf{v_i}, \quad s := \text{shrinkage factor}\,(0 < s < 1) \tag{4.21}$$

The new point ($\mathbf{v_{new}}$) introduced in the simplex depends on the evaluation of the $\mathbf{v_{reflect}}$, $\mathbf{v_{expand}}$, $\mathbf{v_{oc}}$ and $\mathbf{v_{ic}}$. The operation is continued till the stopping criteria is reached. The simplex stops if it shrinks below a certain value ϵ_1 and the evaluations of every vertex of the shrunk simplex vary by maximum threshold ϵ_2. The stopping criteria is presented in Algorithm 1 and the complete procedure for one start of the Nelder-Mead (NM)-algorithm is given in Algorithm 2. An example of the operations in a 2-dimension $\mathcal{O}$ is illustrated in Fig. 4.17 to present the geometrical nature of search of the $\mathcal{O}$ in NM-algorithm. In Fig. 4.18, an example of the points explored during an optimization process is graphically represented.

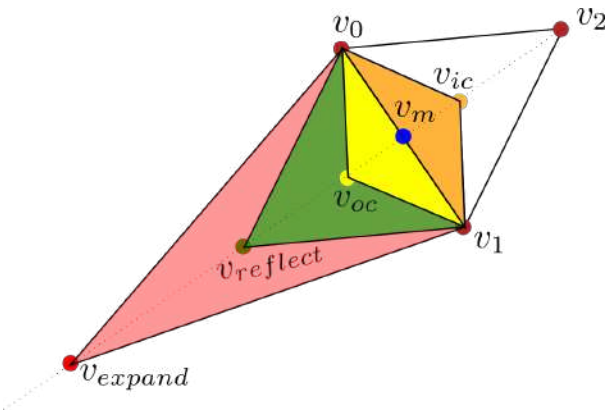

Figure 4.17: An example of an operation on a simplex in 2-dimensional $\mathcal{O}$

Algorithm 1: Stopping criteria for the NM algorithm

Result: Boolean for stopping condition

sorted simplex $\{\mathbf{v_0}, \mathbf{v_1}, \mathbf{v_2}, ..., \mathbf{v_{n-1}}, \mathbf{v_n}\}$;
evaluations $\{e_0, e_1, e_2, ..., e_{n-1}, e_n\}$;
maximum iteration *max_iter* iteration count iter;
$l_{ij} = \|\mathbf{v_j} - \mathbf{v_i}\|$;
$e_{ij} = |e_i$ - $e_j|$;
size = max(l_{ij});
eval = max(e_{ij});
if $size \leq \epsilon_1$ && $eval \leq \epsilon_2$ **then**
    stop = 1
else
    stop = 0
end
if $iter \geq max\_iter$ **then**
    stop = 1
else
    stop = 0
end

4.5.2 Implementation

We will see an example for optimization of 2UPS-1U mechanism with 4 variables to optimize as shown in Fig. 4.12b and also mention the method to optimize other mechanisms with the algorithm. As discussed in Section 4.2, we want to calculate an evaluation for a mechanism that circumpasses information related to the feasible workspace, $\mathcal{F} \bigcap RDW_d$, along with the global quality, κ_g^{-1} , or the passive joint limit norm $\|q_p\|$. As we know that the κ_g^{-1} and $\|q_p\|$ are conflicting objectives, we design different rewarding functions for each of them.

4.5.3 Rewarding strategies

Rewarding strategies refer to the different methods implemented to calculate the evaluation for a particular objective function. For example, to optimize the quality of the

Algorithm 2: Single start of the Nelder-Mead optimization algorithm

Result: Local minimum evaluation and the optimized parameters

initial sorted simplex $\{\mathbf{v_0}, \mathbf{v_1}, \mathbf{v_2}, ..., \mathbf{v_{n-1}}, \mathbf{v_n}\}$;
evaluations $\{e_0, e_1, e_2, ..., e_{n-1}, e_n\}$;
while *stop == 0* **do**
    calculate $\mathbf{v_m}, \mathbf{v_{reflect}}$ and $e_{reflect}$;
    if $(e_n < e_{reflect} < e_0)$ **then**
        $\mathbf{v_n} = \mathbf{v_{reflect}}$;
    else if $(e_0 < e_{reflect})$ **then**
        if $(e_{reflect} < e_{expand})$ **then**
            $\mathbf{v_n} = \mathbf{v_{expand}}$;
        else
            $\mathbf{v_n} = \mathbf{v_{reflect}}$;
        end
    else if $(e_n < e_{reflect} < e_{n-1})$ **then**
        if $(e_{oc} > e_{reflect})$ **then**
            $\mathbf{v_n} = \mathbf{v_{oc}}$;
        else
            $\forall\, i \in [1, n] \quad \mathbf{v_i} = s.\mathbf{v_i}$;
        end
    else if $(e_{reflect} > e_n)$ **then**
        if $(e_{ic} > e_{reflect})$ **then**
            $\mathbf{v_n} = \mathbf{v_{ic}}$;
        else
            $\forall\, i \in [1, n] \quad \mathbf{v_i} = s.\mathbf{v_i}$;
        end
    sort the simplex;
    if $\mathbf{v_{0new}} > \mathbf{v_0}$ **then**
        iter = 0
    else
        iter = iter + 1
    end
    Update stop from Algorithm 1
end
return $\mathbf{v_0}, e_0$

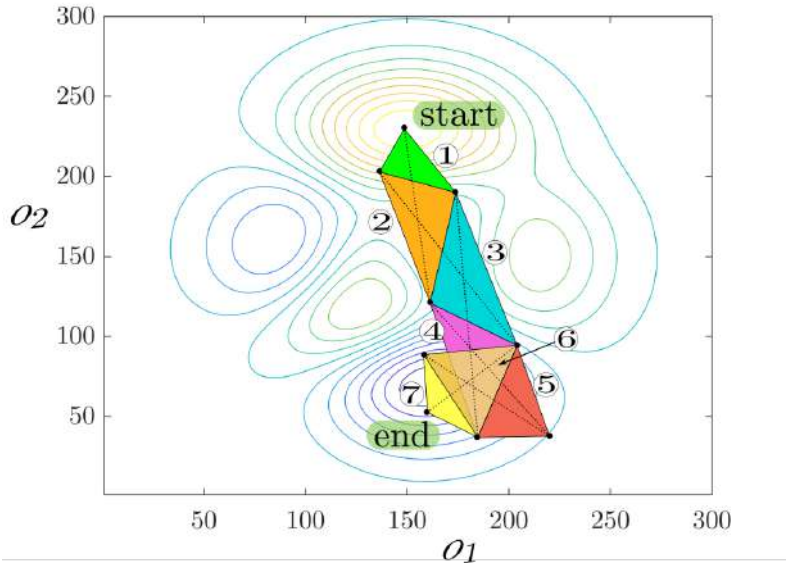

Figure 4.18: An example of the travel path of optimization in Nelder-Mead algorithm

constraint, we can bias the reward towards the center. This results in mechanisms having very good motion in and around the center of the desired Regular Dextrous Workspace (RDW_d). Different strategies can be used to evaluate the objective leading to desirable mechanism parameters. We discretize the RDW_d by dividing the range of each degree of freedom into 201 points (2/201 radians division) resulting into equispaced 40401 points to calculate the necessary evaluation at every configuration of the workspace.

For a given set of optimizing variables $[a, a', h, t]$ from Fig. 4.12b, we want to know how good is the mechanism. We solve for the IGS of the mechanism at each configuration, $(\alpha, \beta) \in \text{RDW}_d$, and get the complete configuration space ($\mathcal{D}$). This provides us with all the passive joint values and the actuated length for both legs. The same function is also used to derive $\mathbf{J}$ and its determinant. As we are also checking for collision between actuators, a function has been written to accommodate the collision check. This function is denoted as f($\mathbf{v}$) in Algorithm 3. The actuators considered for the mechanism has a wider bore diameter at the bottom and is smaller at the top as shown in Fig. 4.19.

So, the actuator was divided in 5 points and the distance between these discretized points was calculated. Knowing that the inner piston is smaller than the outer radius for the actuator, we also reduced the constraint for the distance between points that belong to the inner piston. For example, the distance used as a collision constraint for bottom 4 points in Fig. 4.19 is different than that for the 5^{th} point as it lies on the inner piston and thus is smaller in size. This adjustment in collision constraint though seemingly small, has a huge impact on the evaluation depending on how the rewarding strategies are defined.

Rewarding strategies : Only feasible workspace

As we explore the possibility of having a large workspace with the proposed mechanism, it was decided to first see the results for maximizing the feasible workspace only. This is done by the binary reward strategy. Each configuration is awarded either 1 or 0 depending

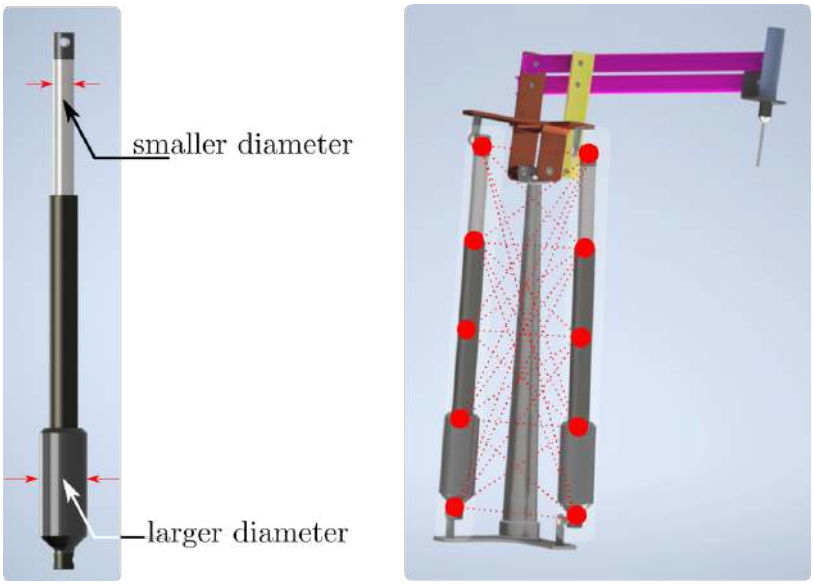

Figure 4.19: The actuator considered for the mechanism and the discretized points for collision calculation (right)

upon the point respecting the passive joint limits and the actuator limits only as shown in Fig. 4.20. The constraints for non-singular points and collision are treated more strictly. If any configuration in the RDW_d is singular or does not respect the collision constraint, then the evaluation is given a very large penalty. This makes sure that no matter how big the feasible workspace is, it is disqualified as a valid solution if it contains any singular curve or colliding configurations. We can also bias the reward to have better kinematic performances in and around the center of the feasible workspace. One of such ideas is illustrated in Fig. 4.21

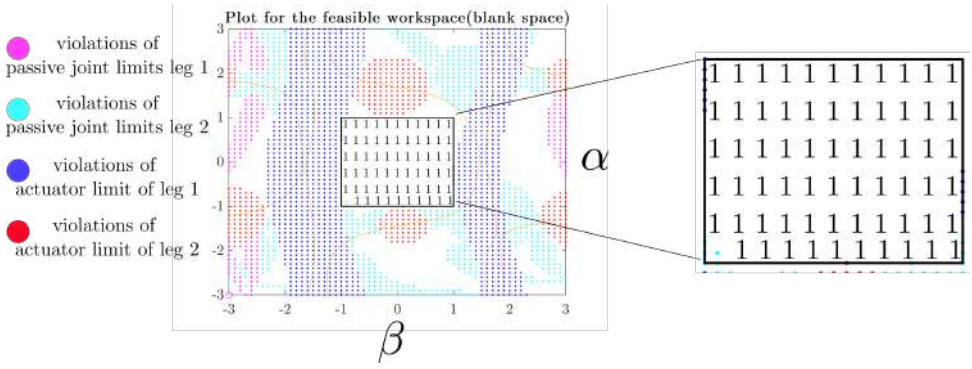

Figure 4.20: An illustration for binary reward of the feasible workspace

Rewarding strategies: minimum quality

As we are using a globality quality to quantify the ability of the manipulator to move along any direction, it is understandable that we want to maximize the same. We want to have a manipulator which has the capability to move in any direction with equal agility in any configuration of the feasible workspace. This is a goal not easy to reach, in fact, we already know that the workspace is mainly bound by the singularity curves and as we go near singular configurations, the $\mathbf{J}$ tends to lose at least one rank. As the global

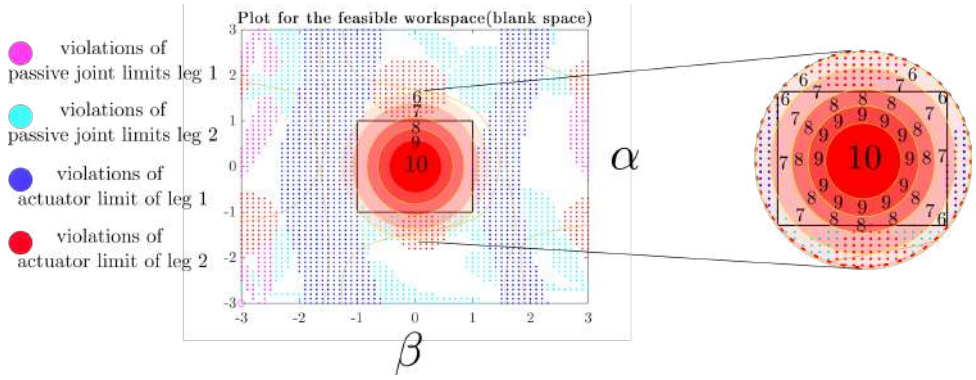

Figure 4.21: An illustration for biased reward of the feasible workspace. The feasible points near the center of the feasible workspace is given higher weightage

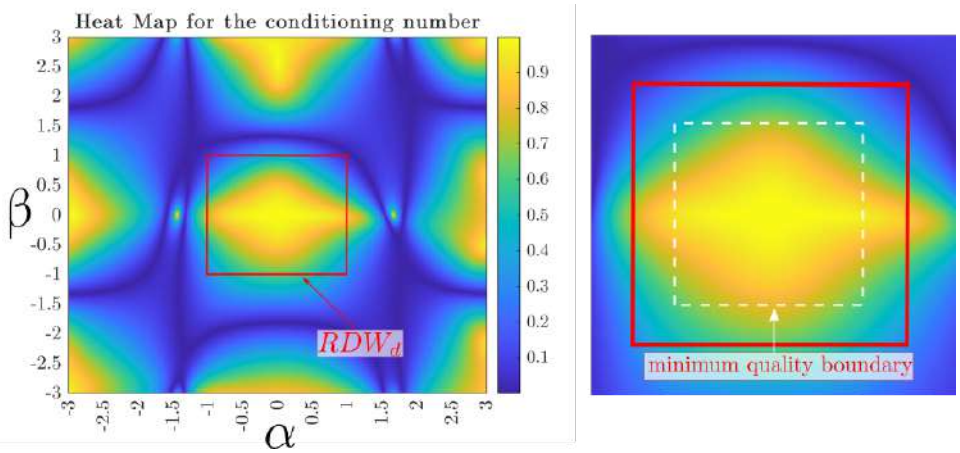

Figure 4.22: The minimum quality constraint. The left figure is the heatmap for the quality index of a particular architecture of the mechanism. The right figure is a zoomed view. The dashed white box in right image shows the area with a minimum quality constraint.

quality, κ^{-1} or the velocity amplification factor, depends on the singular values of $\mathbf{J}$, it becomes harder to have dextrous mobility near singular boundaries as shown in (4.2) and (4.3). So, a constraint is necessary to place a minimum value of the quality index in a particular workspace that will be used very often. This also allows us a buffer to controllably stop the manipulator if it shoots away from this prescribed working area. We bound the the quality with acceptable ranges in the 64% of the RDW$_d$. So, the quality of the manipulator is treated as a constraint in this box and rewarded with either binary or biased reward outside the inner box. The concept is graphically represented in Fig. 4.22.

Rewarding strategies : Maximize quality or joint limit norm

In order to combine another objective function with the feasible workspace, we propose to change the binary reward strategy to κ_g^{-1} or $\|q_p\|$. If we want to maximize the quality, then the summation of inverse of conditioning number, κ^{-1} at each configuration is treated as the reward for the mechanism with given parameters. Otherwise, the joint limit norm as detailed in Section 4.2 is used as an evaluation. In the joint limit, the weighted norm can also be implemented if joints with different limits are implemented. In our case, we

are proposing to implement the same spherical joint for all cases and thus implemented a non-weighted Manhattan (l_1) norm.

4.5.4 Implementing best actuator range

We have to choose a physically possible range of actuators to assure that the points deemed as feasible (mathematically) also respect the actuator lengths and their physical limits. The constraints for actuators are shown in (4.15) and illustrated in Fig. 4.9 and 4.10. To implement the same, we recheck the recorded valid points in the RDW_d for the different brackets of the actuator range. When we are maximizing the global quality or the joint limit norm, we also ensure that the chosen bracket (refer to Fig. 4.10a) has at least 90% of the RDW_d. For example, if a particular bracket is chosen that has higher global quality (meaning that there is a particular zone that is super good), but if that bracket does not have at least 90% of the discretized 40401 points, then we ignore the quality and choose the bracket with maximum valid points as detailed in Algorithm 4.

As the search is geometric, different rewarding functions were tested to check the efficiency of the algorithm. The choice of rewarding function affects the convergence of the algorithm. For example, the implementation in the next Algorithm 3 penalises the mechanism with negative infinite value if even one point is near singularity. It is defined as the the *infinite penalty* in the context of this report. It is hard to distinguish between how close or far we are from a region free of singularity with such rewarding function. Later, we change the penalty function to take into account this issue. If a singular point is detected in RDW_d, we count the number of points near singularity and completely deny any reward for the feasible points in this case. Both these examples are illustrated in Fig. 4.23 and Fig. 4.24.

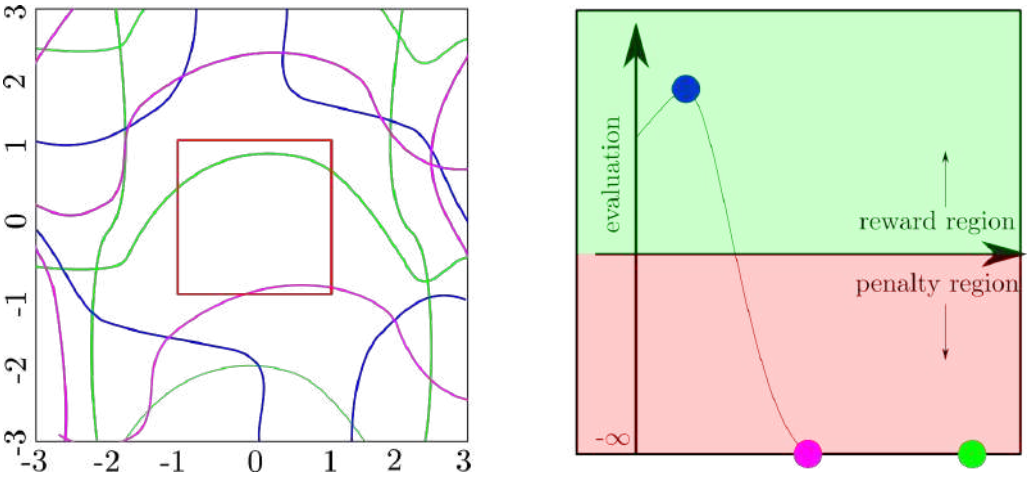

Figure 4.23: The evaluations for infinite penalty. The different colors represent singularity boundaries for different parameters. The red box is the RDW_d. The colored dot on the right side represent the evaluation corresponding to their colored singularity curve.

4.5.5 Pros and cons of the NM-algorithm

The Nelder-Mead algorithm is quite straightforward to model the optimization problem for mechanism design. This advantage allows us to have a general methodology for op-

Algorithm 3: Implemented rewarding function for workspace only

Result: evaluation e for a given parameter set **v**

input $\rightarrow$ **v**;
for $\alpha = -1 : 0.01 : 1$ **do**
  for $\beta = -1 : 0.01 : 1$ **do**
    f(**v**) := function that solves IGS, collision distance and κ^{-1};
    [det(**J**), passive_joints, ρ_1, ρ_2, κ^{-1}, collision distance] = f(**v**);
    if $|det(\mathbf{J})| \leq \epsilon_3$ **then**
      e = -∞;
      break;
    else
      $reward = 1$
    end
    if $\|q_p\| \geq limits$ **then**
      $reward = 0$
    else
      $reward = 1$
    end
    if $collision\_distance \geq limits$ **then**
      $reward = 0$
    else
      $reward = 1$
    end
    if $reward == 1$ **then**
      e = e + reward;
      valid_points[i] = [ρ_1, ρ_2, reward]
    $\rho_{\mathbf{vec}}[i]$ = [ρ_1, ρ_2];
  end
end
rho_range = [maximum($\rho_{\mathbf{vec}}$), minimum($\rho_{\mathbf{vec}}$)];
Checking for feasible set of the actuators;
if $stroke \times rho\_range[1] \geq rho\_range[2]$ **then**
  for $rho\_bracket = \rho_{min} : steps : \rho_{max}$ **do**
    for $n = 1 : length(valid\_points)$ **do**
      e = 0;
      if $\rho_1, \rho_2 \leq rho\_bracket \,||\, \rho_1, \rho_2 \geq stroke \times rho\_bracket$ **then**
        feasible_points[j] = valid_points[n];
        j = j+1;
        e = e + valid_points[n, 3];
    end
    eval_vector[k]= [e, ρ_{min}];
    k = k + 1;
  end
  e = maximum(eval_vector, 1);
  rho_range = ρ_{min}corresponding to e;
return e

Algorithm 4: Implementation for choosing best actuator range considering workspace and quality

Result: evaluation for a given parameter set $\mathbf{v}$

input $\rightarrow \mathbf{v}$;
get the matrix of valid_points from Algorithm 3 rho_range = [maximum($\rho_{\mathbf{vec}}$), minimum($\rho_{\mathbf{vec}}$)];
Checking for feasible set of the actuators;
if *stroke* $\times$ *rho_range[1]* $\geq$ *rho_range[2]* **then**
    for *rho_lower* = ρ_{min} *: steps :* ρ_{max} **do**
        for *n = 1 : length(valid_points)* **do**
            e = 0;
            if ρ_1, $\rho_2 \leq$ *rho_lower* || ρ_1, $\rho_2 \geq$ *stroke* $\times$ *rho_lower* **then**
                feasible_points[j] = valid_points[n];
                j = j+1;
                e = e + valid_points[n, 3];
        end
        eval_vector[k]= [e, ρ_{min}, j];
        k = k + 1;
    end
    [e_1, $index_1$] = maximum(eval_vector, 1);
    [e_2, $index_2$] = maximum(eval_vector, 3);
    if *eval_vector[*$index_1$*][3]* $\leq$ *0.9* $\times$ *40401* **then**
        e = $eval\_vector[index_2][1]$;
        $\rho_{min} = eval\_vector[index_2][2]$;
    else
        e = $eval\_vector[index_1][1]$;
        $\rho_{min} = eval\_vector[index_1][2]$;
    end
    rho_range = [ρ_{min}, stroke.ρ_{min}];
return e

timizing any parallel mechanism. As it is a derivative-free algorithm, we can introduce complex objective functions that are hard to formalise. An example is the quality index, κ_g^{-1}, defined in Section 4.3. Also, as NM-algorithm is a local search algorithm, it returns a stationary point (no proof for convergence) in a considerably low time compared to the currently implemented global optimization methodologies. This makes it possible for the designer to structure an objective function that is computationally expensive. Also, the constraints can be constructed modularly allowing us to experiment different constraints at any stage of the development. Another important advantage of the Nelder-Mead algorithm relevant to the mechanism design is its geometric search method. The basis of optimization space in NM-algorithm are the optimization variables themselves. It is logical to use this method as the next best design parameters are chosen as a result of the combination of parameters of previous simplex rather than using complex methods to represent a mechanism in the optimization space which may not have geometrical explanation for choosing the next best proposal, e.g: chromosomes in the GA. We can also tune the exploring parameters, the reflection, expansion, contraction and shrinkage coefficients, with human intuition and some prior knowledge about the importance of

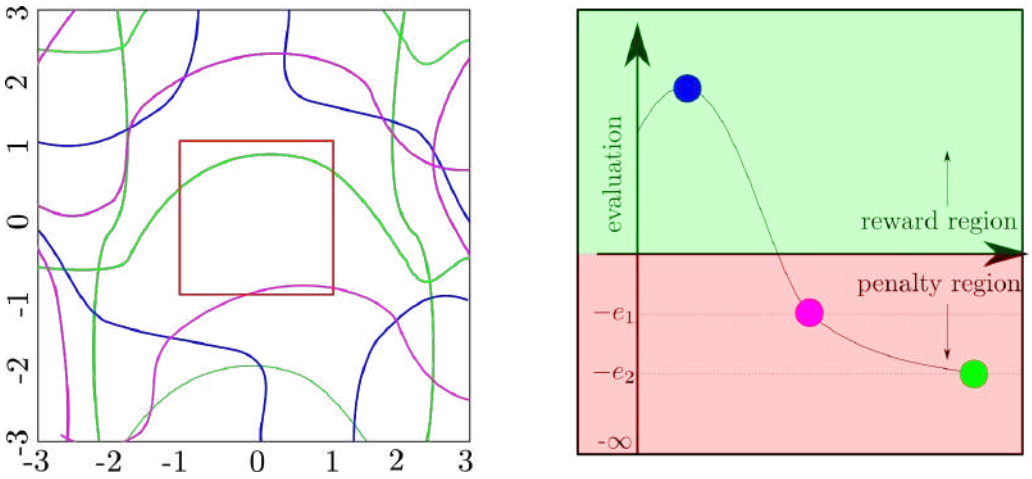

Figure 4.24: The evaluations for smooth penalty. The different colors represent singularity boundaries for different parameters. The red box is the RDW_d. The colored dot on the right side represent the evaluation corresponding to their colored singularity curve.

different parameters.

Though suitable for our application, there are certain disadvantages of using this algorithm too. Under some hypotheses, the NM algorithm has proof of convergence up to dimension 2 [59] and has no proof for convergence beyond 2-dimensional optimization. If not implemented correctly, it gets into a collapsing simplex patterns thus converging onto a non-stationary solution [60]. The convergence highly depends on the initial size of the simplex and the effect of the coefficients have been discussed in [61]. Despite these shortcomings, the NM-algorithm is useful in our case as the aim is not finding the absolute optimized design parameter but to satisfy all constraints and then get an acceptable quality of performance and has been implemented in such areas with great success [45, 46]. Different convergent variants have also been proposed to get around the premature convergence [62] allowing the algorithm to explore extra points in case of near collapse.

To get better results, we complement the local search of the NM algorithm with few variants and with a multi-start technique for a global search of the optimisation space, as discussed in the next section.

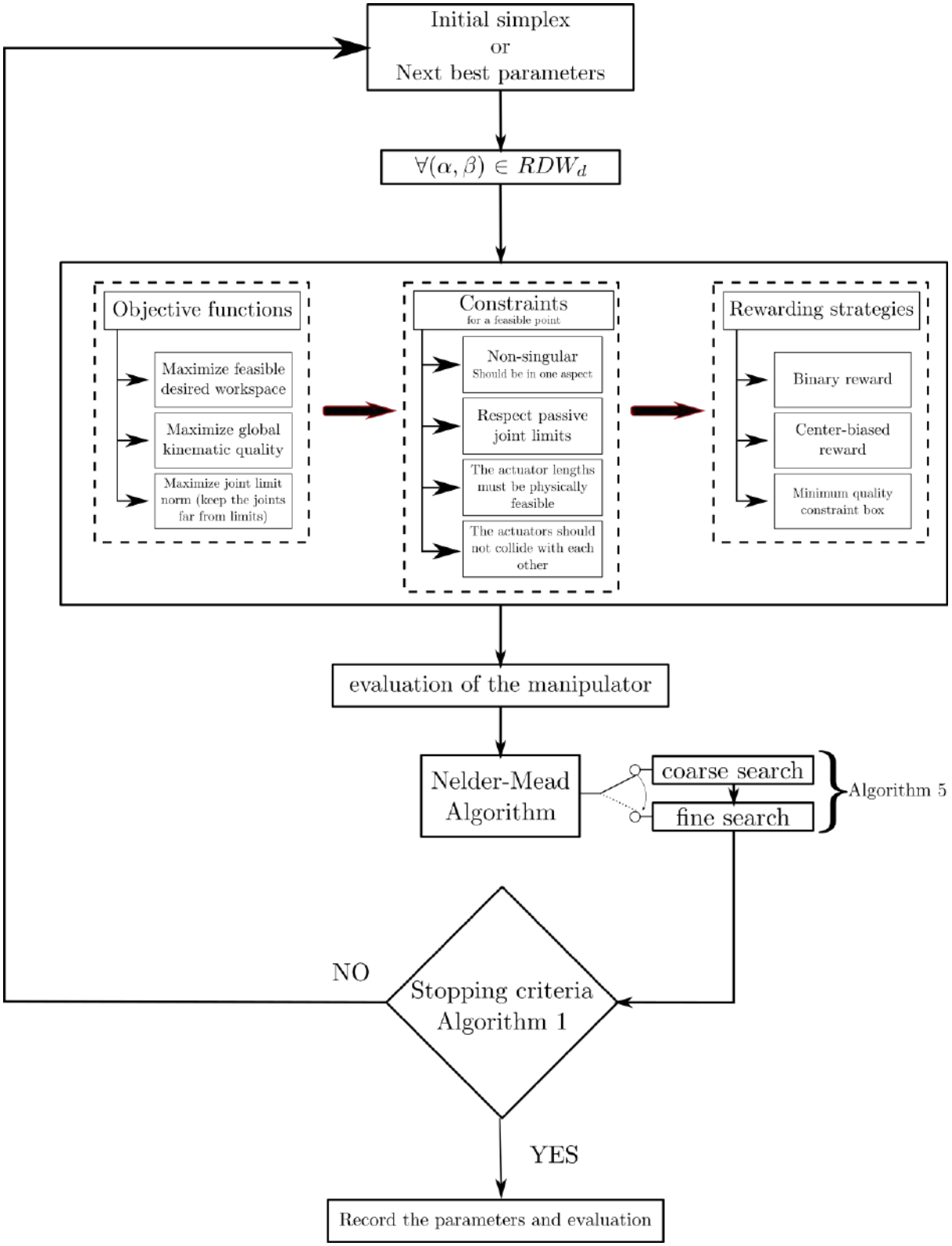

Figure 4.25: The flowchart for single start of the implemented optimization methodology

4.6 Global search algorithm

NM-algorithm combined with other global search methods such as low-discrepancy points [63], genetic algorithm [43] and Powell optimization [44] have been proposed. We imple-

mented a multi-start Nelder Mead algorithm with low discrepancy points for exploring a global optimization space. In this method, we execute the NM algorithm with different initial simplexes. It is very important that we have a uniformly distributed initial simplexes over the optimization space in order to explore the maximum area of the optimization space.

4.6.1 Initial simplexes for multi-start

An easily implementable way to obtain a sampling set $\mathcal{O}_M \subset \mathcal{O}$ is *Monte Carlo sampling* with a uniform distribution (see, e.g., [64]), i.e., *random sampling*. Unfortunately, it is known [65] that the resulting points have the tendency to form clusters, particularly in high-dimensional contexts, which undermine the uniformity of the discretization. A better choice consists in having the M points of the discretization $\mathcal{O}_M$ of $\mathcal{O}$ spread "well-uniformly". In particular, it is desirable the points to be close enough to one another, without leaving space regions undersampled. To this end, as done in [66, 3, 67, 68], one can use certain deterministic sampling techniques. The discussion of the properties of such techniques contained in the remaining of this section is from [66].

Dispersion and discrepancy

Let $O_M \subset \mathcal{O}$ be a set of M sample points $o_i,\ i = 1, \ldots, M$ and define the *dispersion* [65] of O_M as

$$\theta(O_M) := \max_{o \in \mathcal{O}} \min_{\tilde{o} \in O_M} \|o - \tilde{o}\| \tag{4.22}$$

It is clear from the definition that dispersion quantifies "how uniformly" the points are spread in the space: it is a measure of the uniformity of the distribution of the points of O_M in $\mathcal{O}$. Roughly speaking, a small value of $\theta(O_M)$ guarantees that the points of O_M are spread on $\mathcal{O}$ "in a uniform way," i.e., without leaving regions of the space "undersampled," and by letting the points "close enough" to one another. The best dispersion properties, in the sense described above, belong to special *deterministic* sequences called low-discrepancy sequence, commonly employed in the fields of number-theoretic methods, statistics, and quasi-Monte Carlo integration. To introduce them, one needs the concept of discrepancy [65, 69] to measure the uniformity of a set of points in a compact domain. In the following we discuss results that are referred to the n-dimensional unit cube $I^n := [0, 1]^n$, but other compact sets can be considered by performing suitable transformations.

Let O_M be a set of M points in I^n. Define $\mathcal{P}$ as the family of all subintervals $\mathcal{I}$ of the form $\times_{i=1}^{n}[o_{1,i}, o_{2,i}]$, where $o_{1,i}, o_{2,i} \in [0, 1],\ o_{1,i} < o_{2,i}$, and let $c(\mathcal{I}, O_M)$ be the *counting function*, which counts the number of points of O_M in $\mathcal{I}$ (i.e., $c(\mathcal{I}, O_M)$ is the number of points of O_M that belong to $\mathcal{I}$). The *discrepancy* of O_M is defined as [69]

$$D(O_M) := \sup_{\mathcal{I} \in \mathcal{P}} \left| \frac{c(\mathcal{I}, O_M)}{M} - \lambda(\mathcal{I}) \right| ,$$

where $\lambda(\mathcal{I})$ is the Lebesgue measure of $\mathcal{I}$.
Discrepancy is strictly related to dispersion. In particular, it can be shown [69] that, for any set of M points on I^n, the inequalities

$$(b_n M)^{-1/n} \leq \theta(O_M) \leq \sqrt{n} D(O_M)^{1/n}$$

hold, where b_n is the volume of the n-dimensional unit ball. Then, a "low-discrepancy set" is also a "low-dispersion set".

Low-discrepancy sequences

Sequences such that their *discrepancy* satisfies

$$D(\{O_M\}) \leq O(M^{-1}(\log M)^n) \tag{4.23}$$

are called *low-discrepancy sequences*. Their construction varies from method to method. In [69], a common framework for the construction certain sequences, called (t, n)-*sequences*, that satisfy deterministically the condition (4.23), was presented. Other examples are the *good lattice points sequence* the *Halton sequence*, and the *Hammersley sequence* [69, 65]. The use of such *low-discrepancy sequences* is at the basis of the so-called *quasi-Monte Carlo methods* [69], originally introduced as an efficient alternative to classic Monte Carlo methods for the numerical computation of integrals.

To sum up: on the basis of the discussion above, an effective procedure to generate uniformly scattered deterministic sets of points consists in taking finite portions of low-discrepancy sequences. They attain *deterministically* a rate of convergence for the dispersion of order

$$O\left(M^{-1/2n}\right) \leq \theta\left(S_M\right) \leq O\left(\sqrt{2n}M^{-1/2n}\right)$$

Fig. 4.26 shows the comparison between a sampling of the 2-dimensional unit cube by a sequence of 500 points i.i.d. according to the uniform distribution and by a sampling of the same cube obtained via a low-discrepancy sequence (in this case, the *Sobol sequence* [70]). It can be clearly seen how the space is better covered by the second sequence, as well as how the largest empty spaces among the points appear in the first sampling scheme.

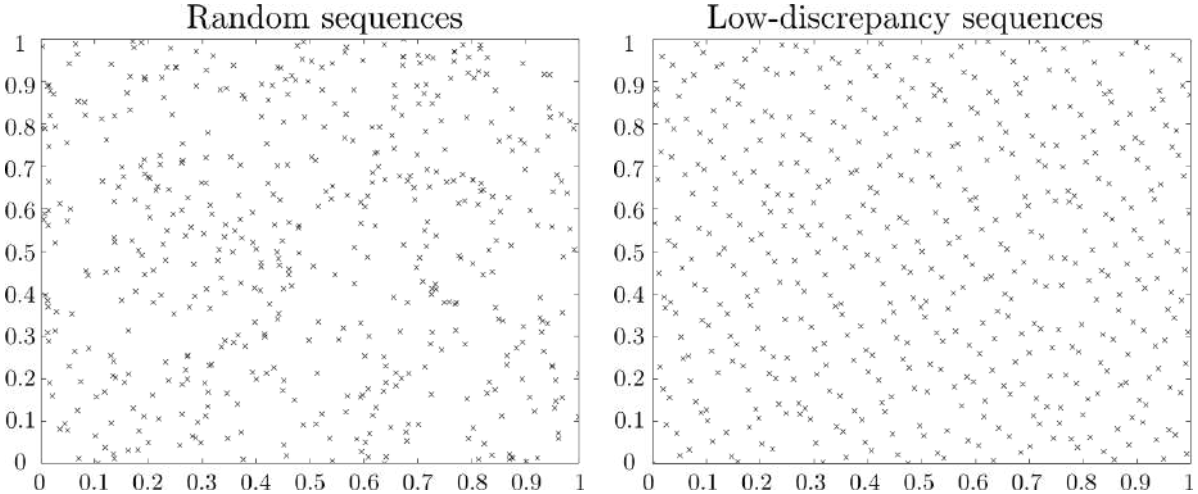

Figure 4.26: Comparison between random and low-discrepancy samplings of the 2-dimensional unit cube from [3]

4.7 Coarse and fine searches

In a normal execution of the Nelder-Mead algorithm, the iteration stops either when the simplex has shrunk to a desirable size with near to same evaluations or if we have encountered the same best point for preset allowable maximum iterations, refer to Algorithm 1. In an attempt to decrease the time for local convergence allowing us to explore more initial simplexes, we adapt a methodology inspired from the practise of rough and fine turning in lathe machines. In general, when we want to remove the excess stock from the workpiece as rapidly as possible, we increase the feed rate and do not focus on the finish of the work. Later, when we are close to desired dimensions, the feed is decreased and now the focus is shifted on the finishing of the work.

In our case, the idea is to initialise simplexes in multi-start and perform a coarse search for the local optima. Later, we collect the local optima from all the used simplexes and then implement a stricter stopping criteria on few selected local optima allowing them to converge to a stationary point with finer quality. Fundamentally, we are discarding the local optima that do not promise a good evaluation even after a longer search bringing down the implementation time considerably. Also, as we already have an optimized vertex as an initial simplex, we can build the rest of the vertices as per our choice thus controlling the size of initial simplex. One of such implementation is detailed in Algorithm 5, where the condition of incrementing the iteration is changed. We implement a condition that the new evaluation found is better than the previous only if it exceeds the previous evaluation by 1%.

Algorithm 5: An example of coarse local search criteria

Result: The iteration count, refer to Algorithm 2

input : Previous and current best evaluations $\{\mathbf{v_0}, \mathbf{v_{0new}}, \}$;
For coarse search;
max_iter = 3 n;
margin = 1.01 ... (suggesting 1% increment);
For fine search;
max_iter = 10 n, margin = 1;
if $\mathbf{v_{0new}} > margin\, \mathbf{v_0}$ **then**
    iter = 0
else
    iter = iter + 1
end
if *iter* > *max_iter* **then**
    return $\mathbf{v_{0new}}$;
    break;
return iter

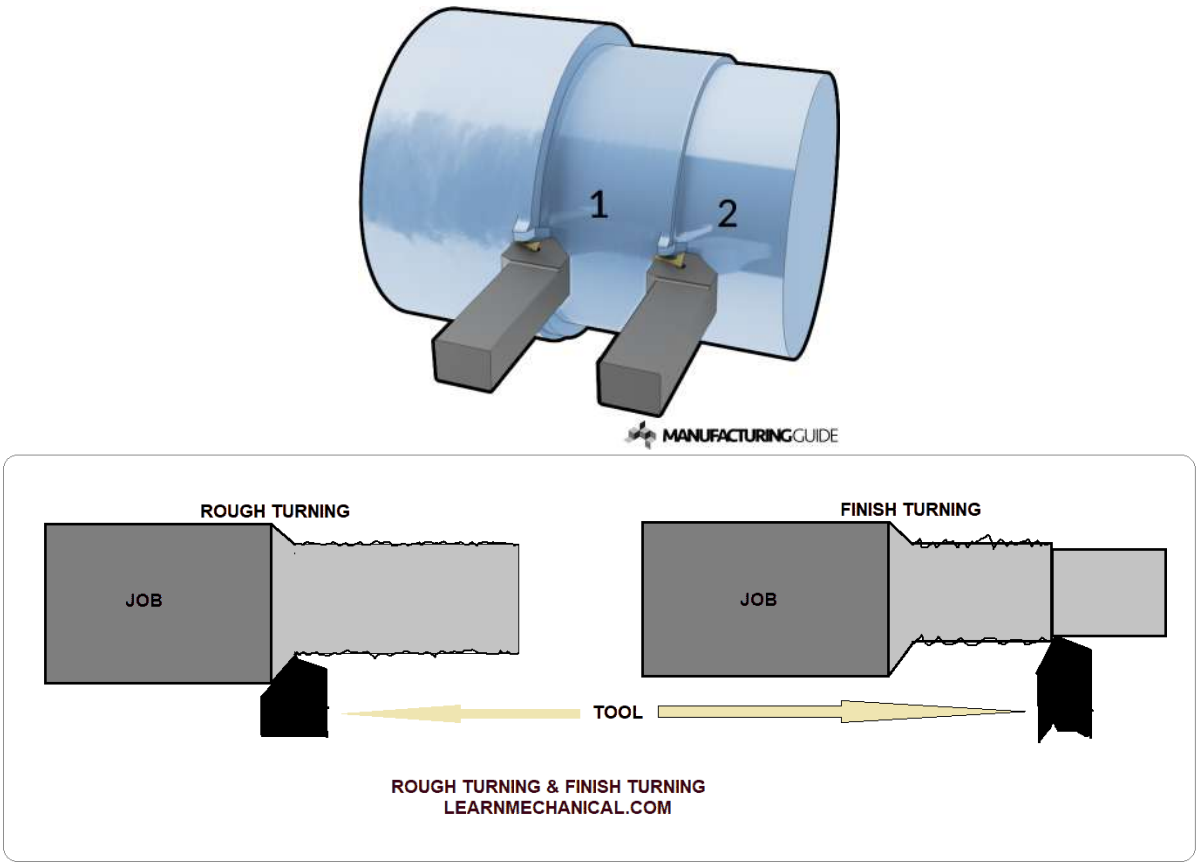

Figure 4.27: The rough and fine turning in lathes. The motivation for implementing a faster and efficient global search

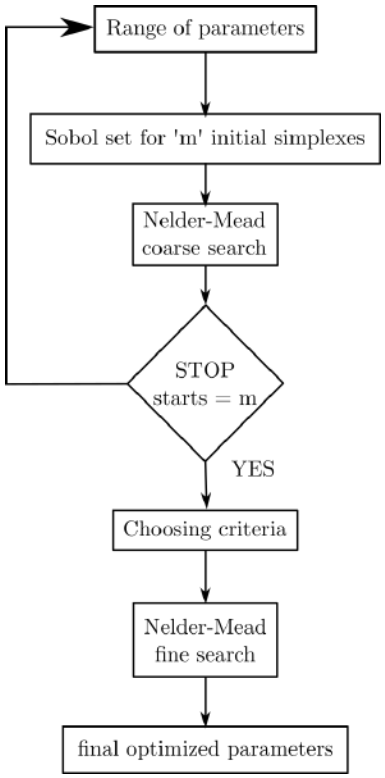

Figure 4.28: The flowchart for the complete implemented optimization methodology

Algorithm 6: An example of implemented multi-start optimization

Result: The fine optimized result of the mechanism

Assuming we have 'm' starts for a 'n' dimensional optimization problem;
We need m.(n+1) valid n-dimensional points from the sobol set generated;
later, we choose 'k' local optima for further fine search;
for *start = 1:m* **do**
    Initial simplex = $\{\mathbf{v_{(m-1).(n+1)}} \cdots \mathbf{v_{mn+m-1}}\}$;
    Implement Single start NM-algorithm from Algorithm 2 with coarse search in Algorithm 5;
    save local optima and evaluation;
end
for *fine_start = 1:k* **do**
    Generate n simplexes around the chosen local optima;
end
return Best point

4.8 Summary

In this chapter we present different objective functions that can be used for an optimized result. The consequent sections discuss the different constraints such as passive joint limits, actuator feasibility, internal collision as well as the non-singular condition. We also discuss the methodology to choose the best actuator stroke for maximizing the feasible workspace. Later, the various rewarding strategies are presented and their relevance in certain situations is also discussed.

The existing Nelder-Mead algorithm is detailed to highlight the geometric nature of search of the optimization space to motivate its relevance in the design optimization. It is followed by the algorithms with implementation for different constraints and rewarding strategies. In the last section, we present a novel implementation for changing nature of search within the Nelder-Mead algorithm for faster and efficient global search of the optimization space. Fig. 4.25 shows the flowchart for the implemented optimization methodology. The figure also illustrates the different choices available and various decisions needed to make for a complete definition of the optimization problem. In Fig. 4.28, the complete process is illustrated. In this figure, the multi-start simplexes as well as the order of coarse search and fine search in the single start Nelder-Mead algorithm for the final optimized parameter is shown.

Chapter 5

Results and discussions

In this chapter, the author presents the different results obtained during the thesis work. The results are arranged in the same manner as the topics are introduced in the report. Along with the results, few interesting facts and observations are discussed to provide the reader a clear flow of the choices made for the optimization of the mechanism design.

5.1 Results from design choices

In this section, the results regarding the design choices are presented. Different issues such as the type of joint, the orientation of joints and their effect on the workspace are analyzed. Later, we also present the important effect of orientation representation and the problems posed in their transformation from one representation to another.

5.1.1 Different joint placements

We studied 3 variations of the 2UPS-1U type as illustrated in Fig. 3.2. After different starts and kinematic analysis of the kinematic curves, it was concluded that the 2PUS-1U with the prismatic joint in horizontal direction performed the worst.

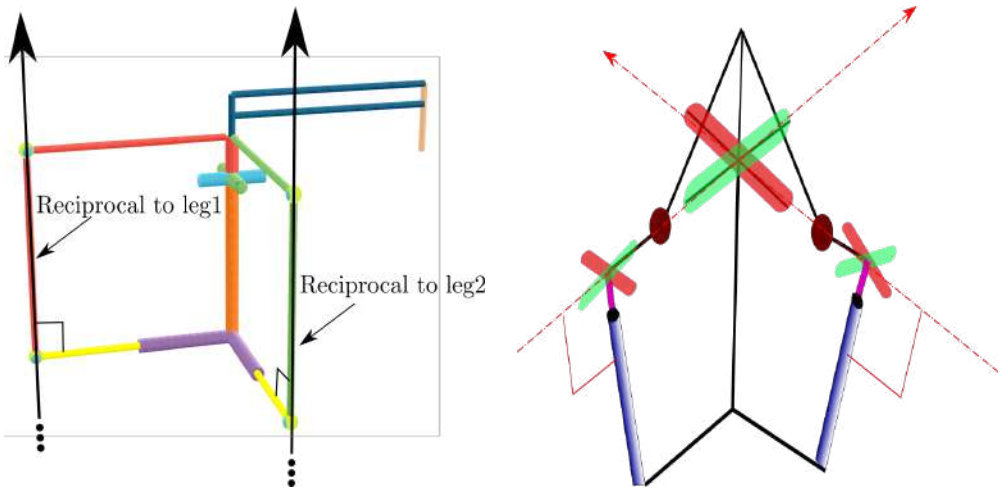

(a) The singularity in 2PUS-1U horizontal architecture

(b) The actuation singularity in 2PUS-1U vertical architecture

Figure 5.1: The singularities occurring in the 2PUS-1U variation

This can be reasoned with the reciprocal screw theory itself. The screw that is reciprocal to the universal joint as well as the spherical joint is a force passing through both the center of the joints. If this screw is also reciprocal to the actuated prismatic joints, then the manipulator loses its mobility as the constraint wrenches has dimension 6. The reason why this architecture performs poor is that there are many such instances when the above-mentioned case occurs and the manipulator is as good as a rigid structure. The condition is illustrated in the Fig. 5.1a. Fig. 5.1b is an actuation singularity of a special nature, there exists no actuation wrench in the active leg and this singularity cannot be changed by altering the actuator joints. The effect of such singularity is that the actuators cannot control the instantaneous motion of the end-effector.

5.1.2 User-centric choice

We collect the information from 9 surgeons of various expertise working on otologic as well as sinus surgery at CHU Nantes. The feedback on speed and size seemed to be coherent and everyone preferred the actuators with maximum speed. To analyze better the importance of the features, the surgeons were asked to prioritize few parameters. It was concluded that most of the surgeons expected a robotic assistant that is easy to use. The next important parameter is the size of the mechanism while speed and multiple operation capacity were not considered as high priority by the surgeons.

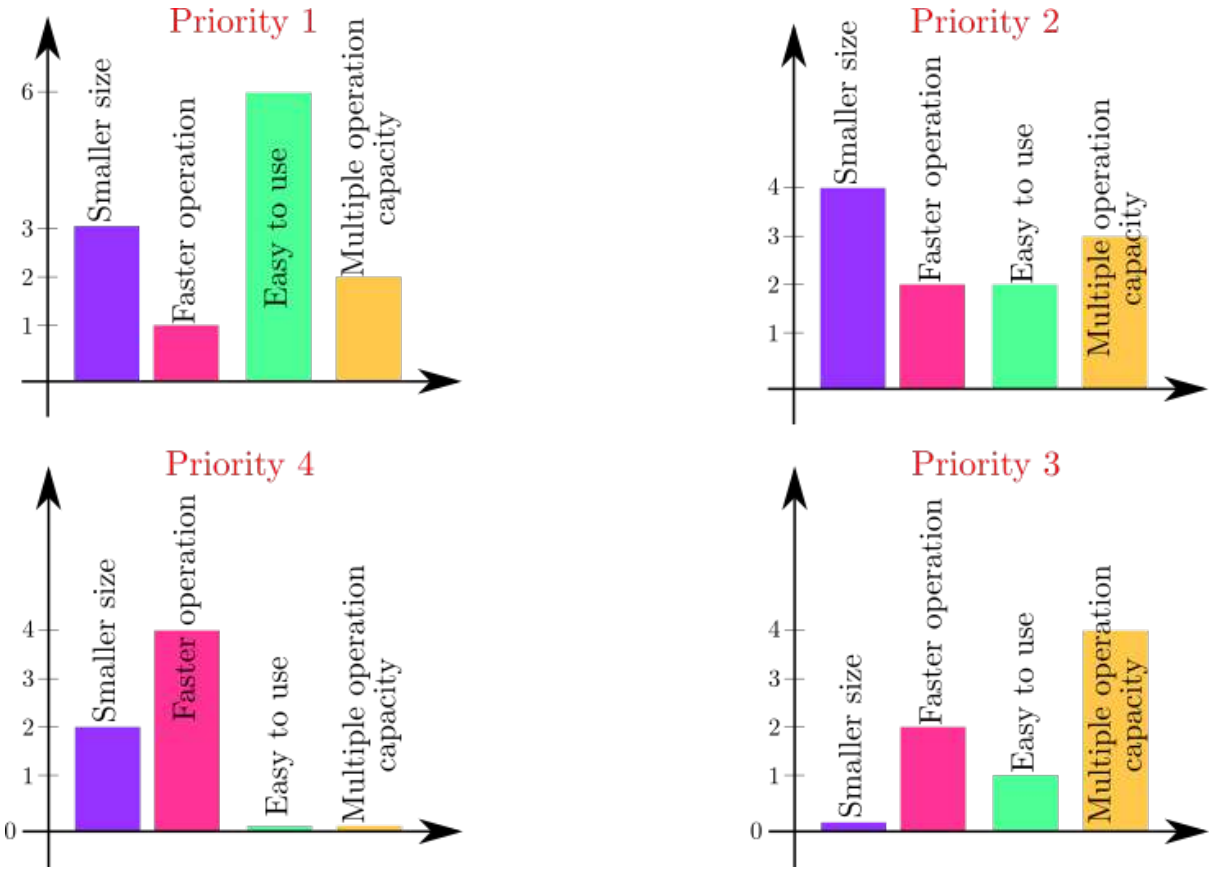

Figure 5.2: The different priorities scored by the surgeons

Fig. 5.2 shows the result of the priorities filled by the surgeons. It was thus concluded that we will be focusing on compact size of the mechanism and choose actuators based

on the speed/size ratio. The low priority of multiple operation capacity also helped us in concentrating on the minimum quality discussed in Section 4.5.3. The reason being that the assembly of the architecture can be different for otological and sinus surgery such that most common positions are the default positions of the mechanism ($\alpha = 0$, $\beta = 0$).

5.2 Results from optimization

In this section, we present the results from the optimization process of the mechanism. The effect of time on the choice of parameters as well as the choice of the objective function is also discussed in the following subsections.

5.2.1 How to read the results

This subsection is aimed at making the reader comfortable with the interpretation of the data presented. When the mechanism was parameterized with 13 parameters for the 2UPS-1U case, the following array was used to define a point in the corresponding optimization space, $\mathcal{O}$ and corresponds to the mechanism shown in Fig. 5.3.

$$[a1, \phi_1, h1, b1, \psi_1, h3, a2, \phi_2, h2, b2, \psi_2, h4, t]$$

The bounds for these parameters are :
$a1, a2 \in [0.25, 1.5]$, $\phi_1, \phi_2, \psi_1, \psi_2 \in [-100^0, 100^0]$, $b1, b2 \in [0.25, 2]$, $h1, h4 \in [-0.1, 0.1]$ and $h2, h3 \in [-0.5, 0.5]$. The optimized point was then visualized with a schematic

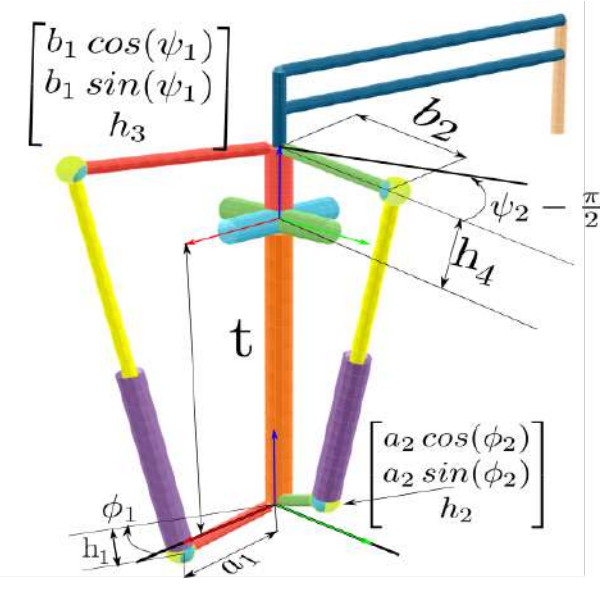

Figure 5.3: 2UPS-1U mechanism corresponding to a single point in the 13 dimension $\mathcal{O}$

diagram. The red dotted line is the actuator of first leg while the black dotted line is the actuator of the second leg. All the schematics are shown in the default position of $\alpha = 0$ and $\beta = 0$. An example plot code with parameters [1, -1, 0, 1, -0.8, 0.5, 0.9, 0.2, 0.5, 1, 1, -0.2, 3.5] is illustrated in Fig. 5.4.

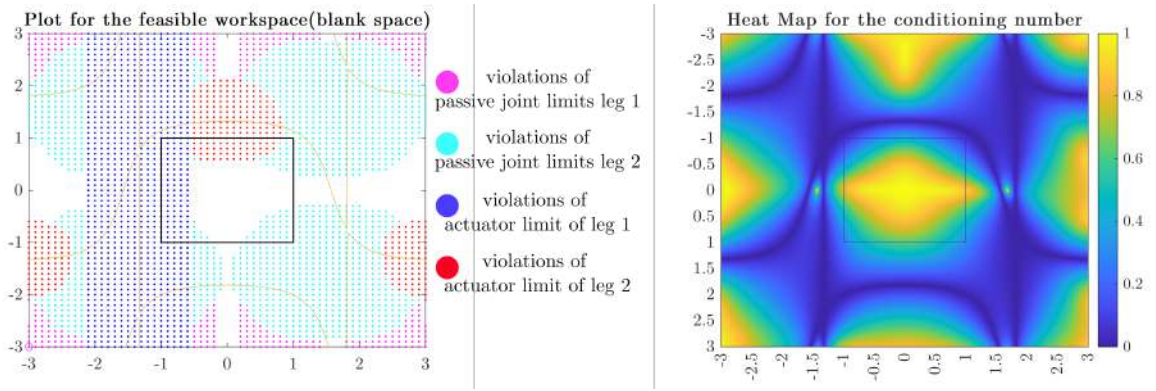

Figure 5.5: An example of the output space with constraints violation (right) and the heat map for the quality index (left)

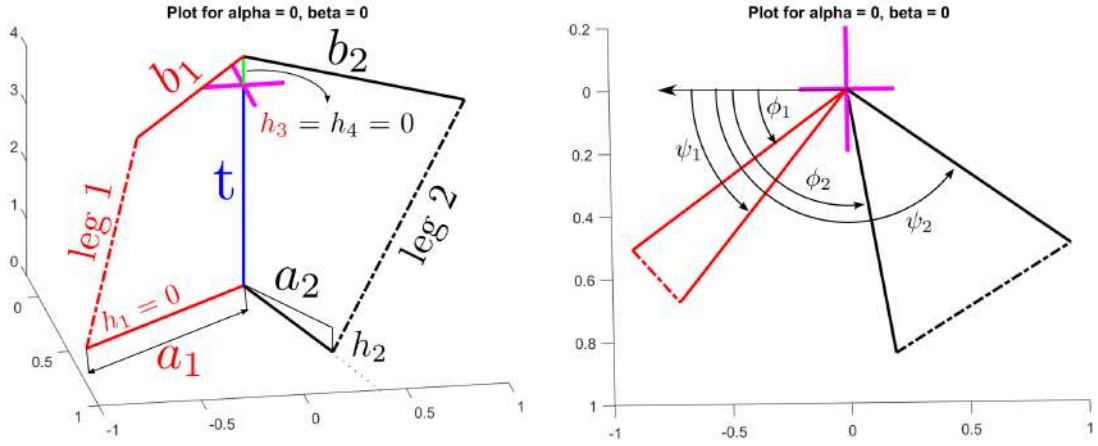

Figure 5.4: An example of a schematic plot of the 2UPS-1U mechanism

The evaluation of these parameters is done by checking for the constraints implemented in the optimization problem. The complete output space is visualized to understand the area of violations and the constraints violated. Along with the constraint violations, it is also helpful to visualize the local quality of the manipulator. It allows us to graphical understand how good the manipulator will behave in the desired (frequently used) workspace. For these reasons, we visualize the local quality as a heat map where the minimum value (darkest) corresponds to the singular regions while the brightest regions correspond to isotropic configuration.

5.2.2 Different objective functions

The two different objective functions used are the global conditioning number and the joint limit norm. Till now, only single objective optimization has been carried out and both the objective functions were implemented individually. The results obtained from the same are very interesting. Fig. 5.6 shows the feasible workspace and the heat map for the quality index for corresponding parameters. Fig. 5.6 is the result of maximizing the conditioning number along with maximizing the feasible workspace. The black box of ± 1 radian is the RDW_d and the white space in the plot is the feasible workspace.

Fig. 5.7 shows the feasible workspace and the heat map for the quality index for the parameters for the results of maximizing the passive joint limit norm along with maximizing the feasible workspace. It is interesting to note that the conditioning number for the optimized result is very poor suggesting that the joint limit norm and the kinematic performance index are contrasting objective functions.

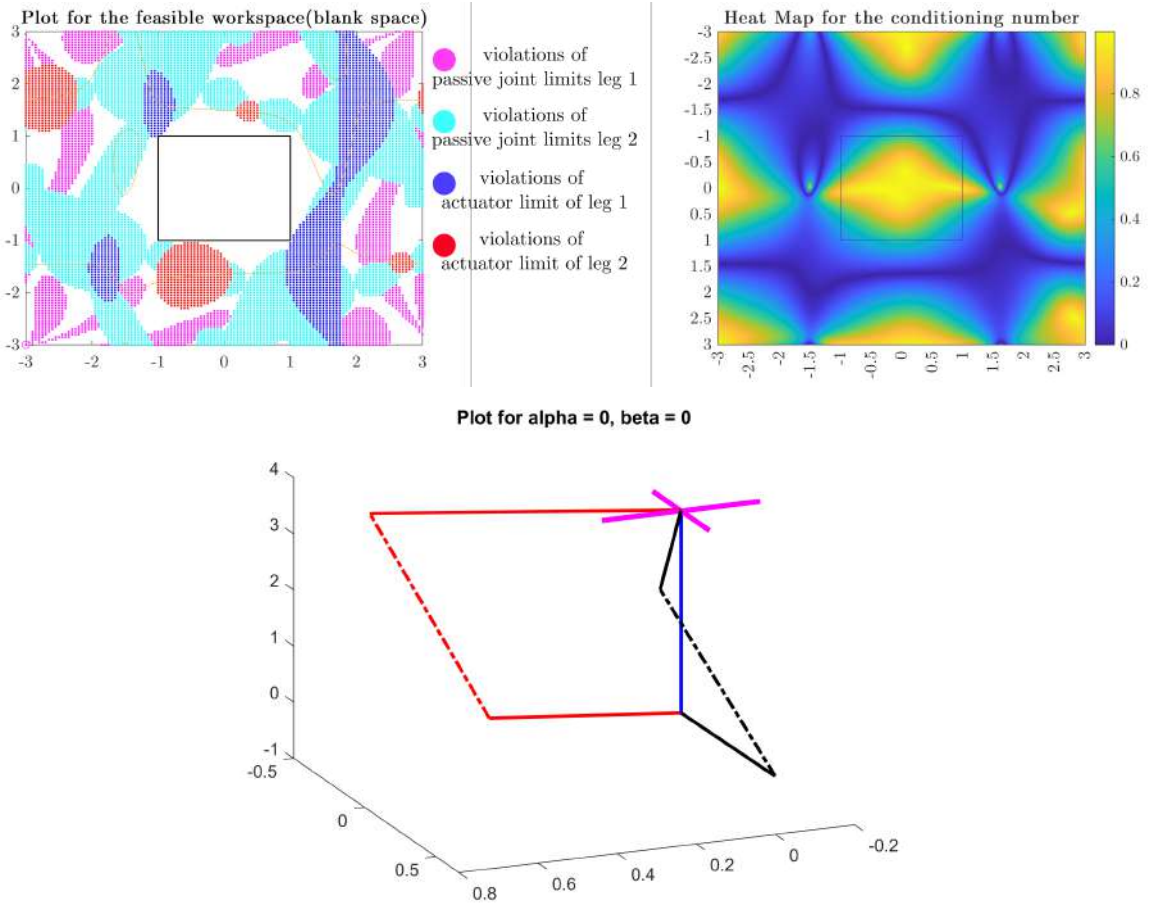

Figure 5.6: Results for one of the best local optima acquired while maximizing the global quality index. Parameters = [0.4584, -0.4439, -0.0846, 0.7423, -0.4097, 0.0183, 0.6314, 1.5885, -0.0307, 0.7247, 1.1574, 0.0124, 3.6], actuator range = [2.9864, 4.3548]

5.2.3 Effect of change of constraints

Best feasible actuator range

The method in which we can implement the Nelder-Mead algorithm allows us to calculate the best actuator range for maximizing the feasible workspace. To illustrate the advantage of the same, we initiate two instances of proposed Nelder-Mead algorithm with identical initial simplex. The results obtained while using the biggest actuator range and the best actuator range are illustrated in Fig. 5.8 and Fig. 5.9 In Fig. 5.8, we implemented a constraint such that the largest possible actuator range is chosen for evaluation. Fig. 5.9 shows the results when the optimized actuator range is chosen for evaluation. This example highlights the fact that the largest actuator range is not always the best actuator range. As both the optimization methods were initiated with identical simplexes, we can

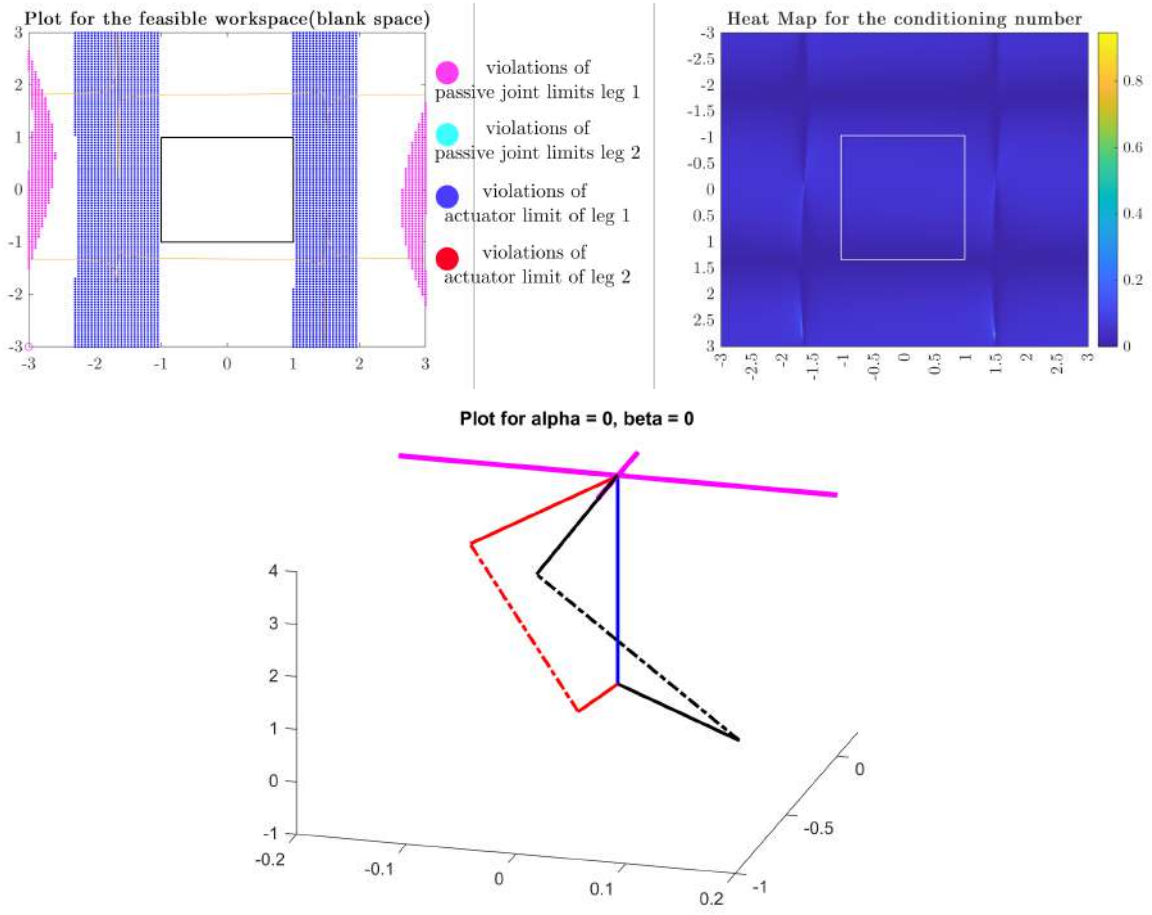

Figure 5.7: Results for one of the best local optima acquired while maximizing the joint limit norm. Even though it has large feasible workspace, it performs kinematically poor, Parameters = [0.281024, -1.606316, 0.080873, 0.644999, -1.687512, -0.011566, 0.380352, -1.183068, -0.022100, 0.843396, -1.565658, 0.011168, 3.971212], actuator range = [3.289266, 4.712601]

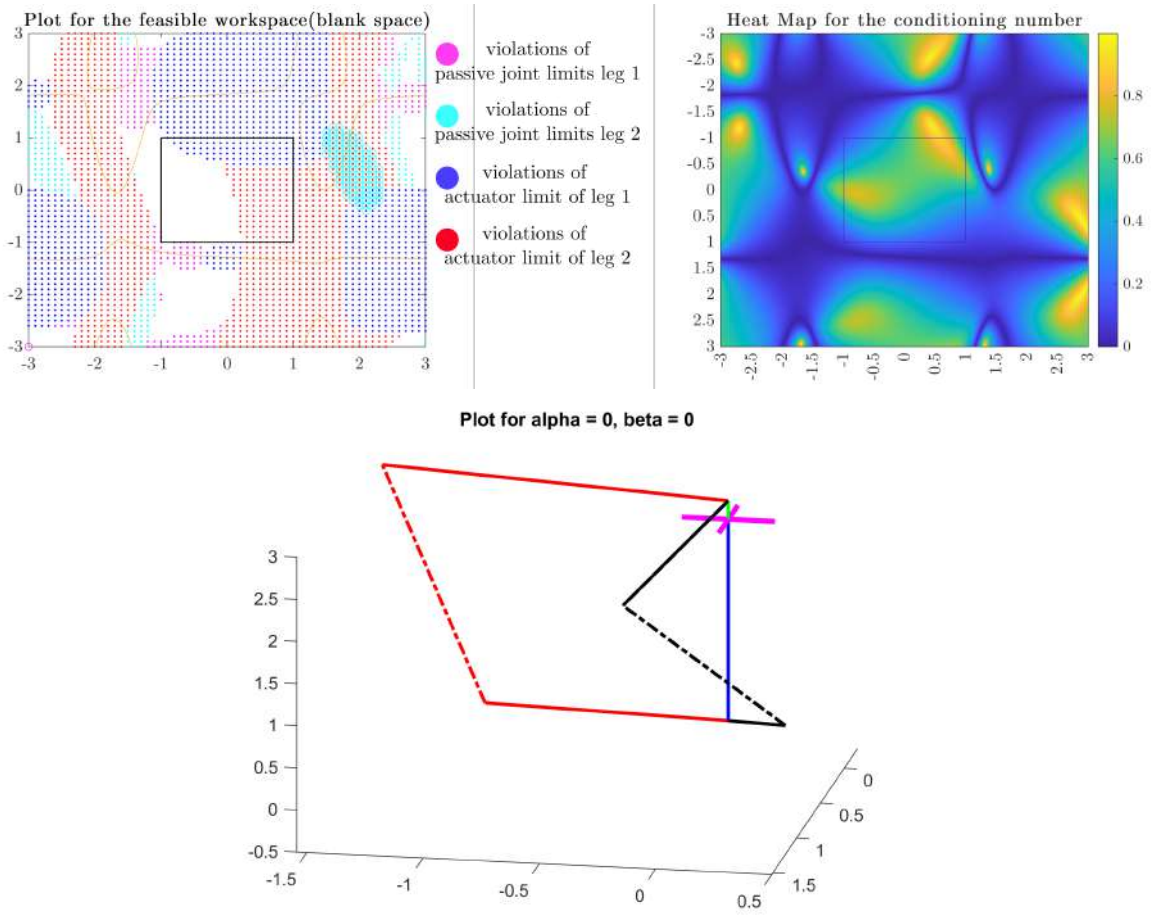

Figure 5.8: Results for the implemented biggest actuator range. Parameters = [1.056069, -1.610967, 0.035785, 1.568429, -1.745329, 0.219276, 0.250000, 1.501642, -0.011370, 1.530870, -0.091670, 0.219896, 2.390018], actuator range = [2.5850, 3.8775]

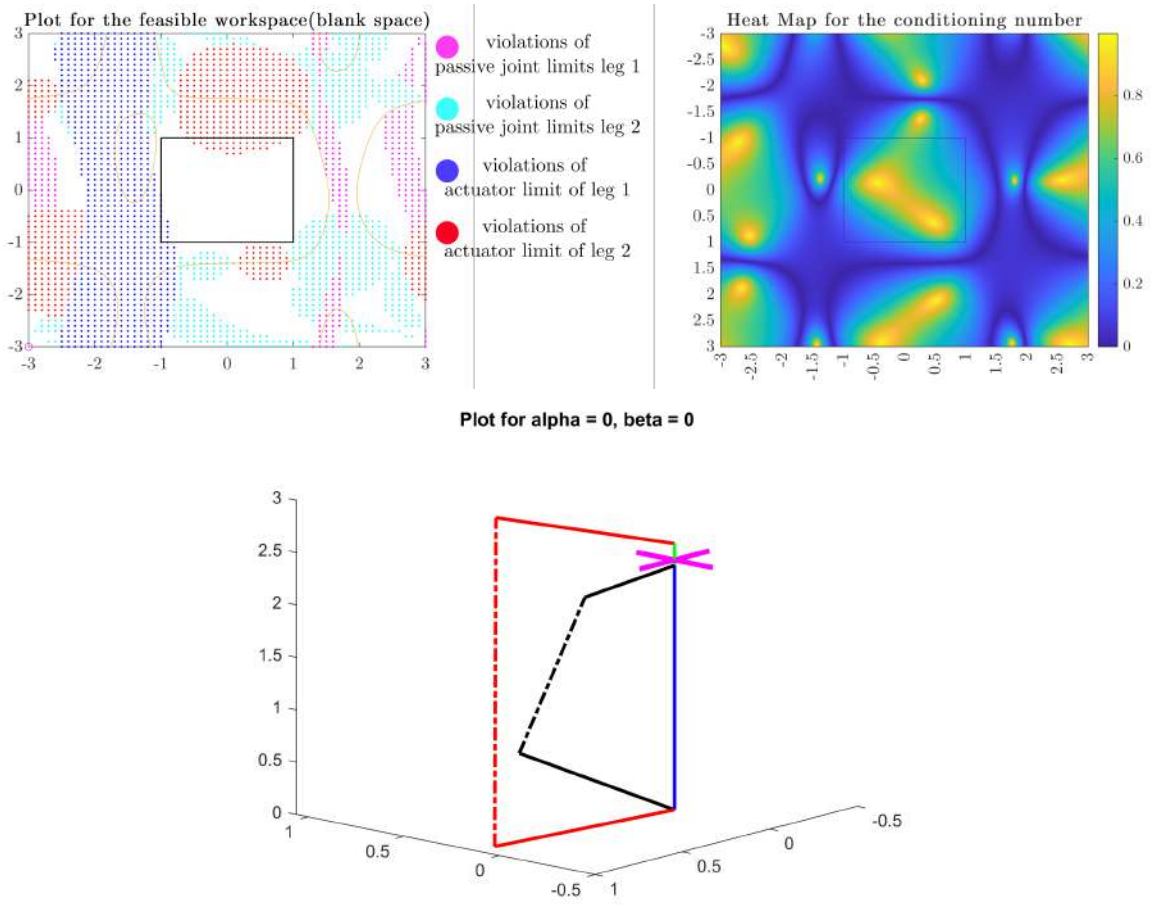

Figure 5.9: Results for the implemented best actuator range. Parameters = [0.994852, 1.540909, 0.071788, 0.829097, 0.151599, 0.156304, 1.096556, -0.251495, 0.030696, 0.624417, 1.725550, -0.052983, 2.383970], actuator range = [2.2087, 3.3131]

also conclude that the way the constraints are implemented have a great impact on the results achieved. The variable actuator range also allows us to choose the mechanism with best kinematic performance too.

Collision constraint

Another important constraint to be considered is the collision constraint. The modeling of the actuator as a cylinder or some other shape contributes majorly to the evaluation of the mechanism. One such curious case was found when we applied a design that was supposed to be valid according to the human intuition. The joint limits were respected for a large workspace and the configuration was suitable for the global kinematic quality too as shown in Fig. 5.10. Still, the algorithm never proposed a solution towards the expected zone.

With manual intervention and forcing the algorithm to go near the zone, it was observed that the actuators were colliding in a small area of the desired workspace. To counter this problem, a tapered shape was implemented as discussed in Section 4.5.3. This improved the result with great success and many such invalid cases were corrected by the same. This is also an example to show that the efficiency of the algorithm highly depends on the modeling of the constraints as well as the rewarding strategies.

5.2.4 Effect of parameterization

As discussed in the Chapter 4, the manipulator can be parameterized with 13 variables for a general geometry or else we can implement a general architecture using human intuition to reduce the dimension. The following results explain how close the human intuition is to the optimized result for particular rewarding strategies. When we were optimizing the mechanism by rewarding the quality of the manipulator inversely proportional to the distance of the point (α, β) from (0, 0), the general parameterization lead to an optimized result with parameters very close the the humanly chosen 4-parameterization.

The optimized results with the 4 parameters is: [0.357173, 0, 0, 0.438437, 0, 0.105441, 0.357173, 1.5708, 0, 0.438437, 1.5708, 0.105441, 3.723585] with actuator range of [3.411769, 4.154748].

The optimized results with the 13 parameters is: [0.4584, -0.4439, -0.0846, 0.7423, -0.4097, 0.0183, 0.6314, 1.5885, -0.0307, 0.7247, 1.1574, 0.0124, 3.6] with actuator range of [2.9864, 4.3548]

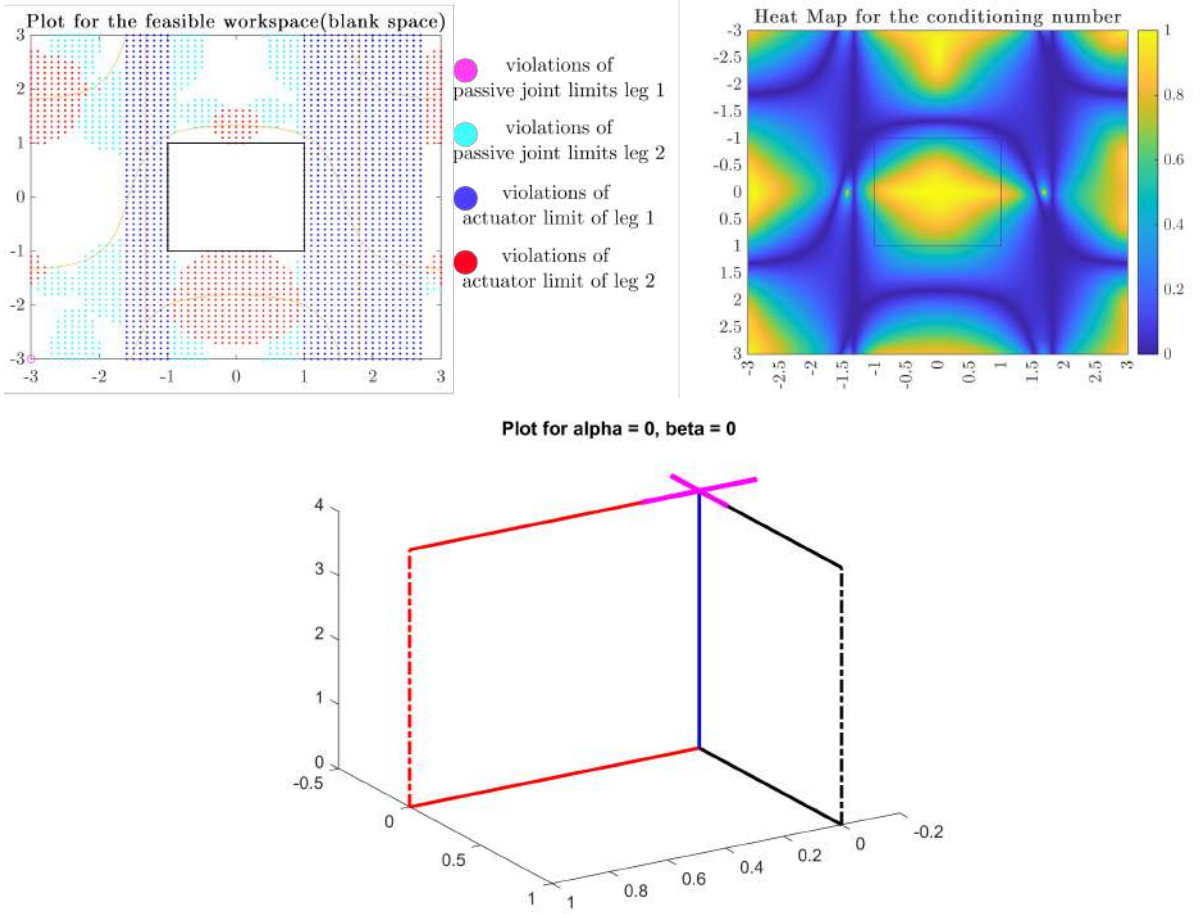

Figure 5.10: Results for the curious case of collision avoidance. The heat map and feasible workspace highlights the high kinematic performance of the manipulator at this particular constraint, Parameters = [1, 0, 0, 1, 0, 0, 1, 1.5708, 0, 1, 1.5708, 0, 4]

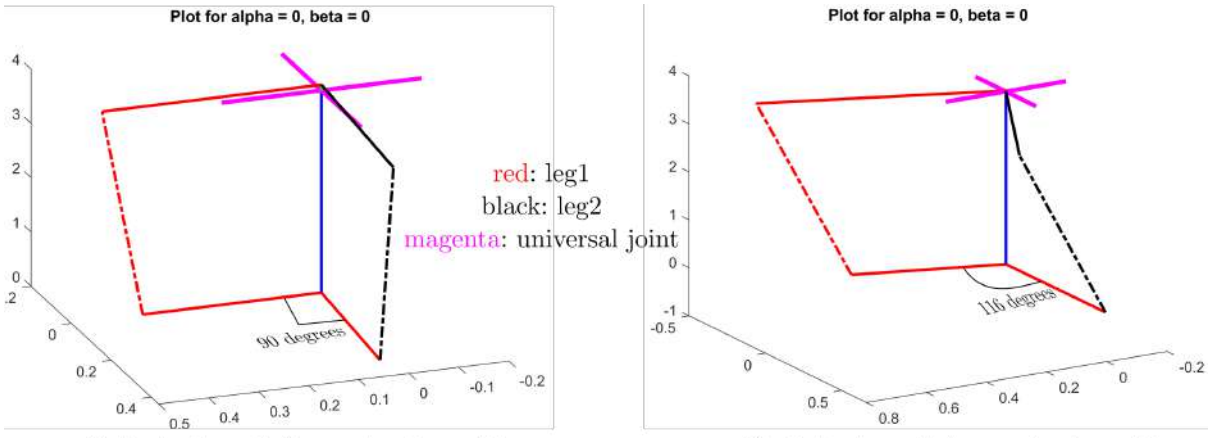

Optimised result for mechanism with 4-parameters

Optimised result for mechanism with 13-parameters

Figure 5.11: Results for the optimized architecture using 4 parameters and 13 parameters

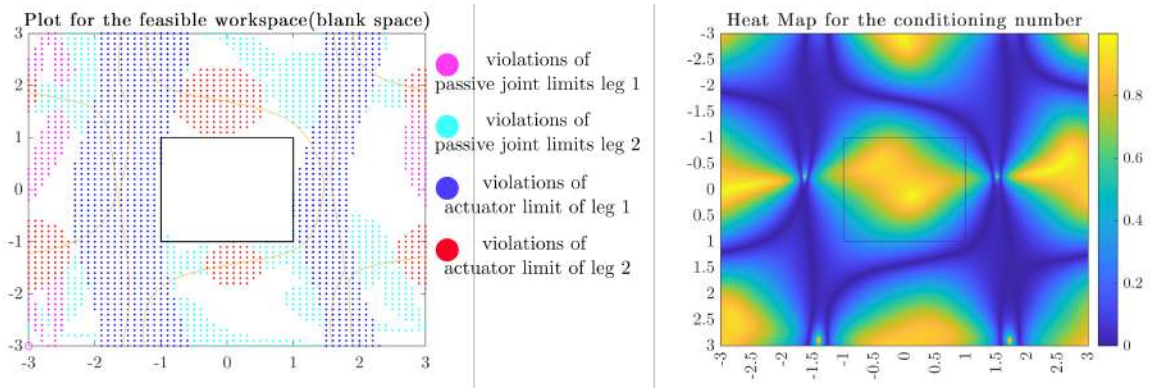

Figure 5.12: The valid feasible space and the heat map for the quality index for optimized mechanism using 4 parameters

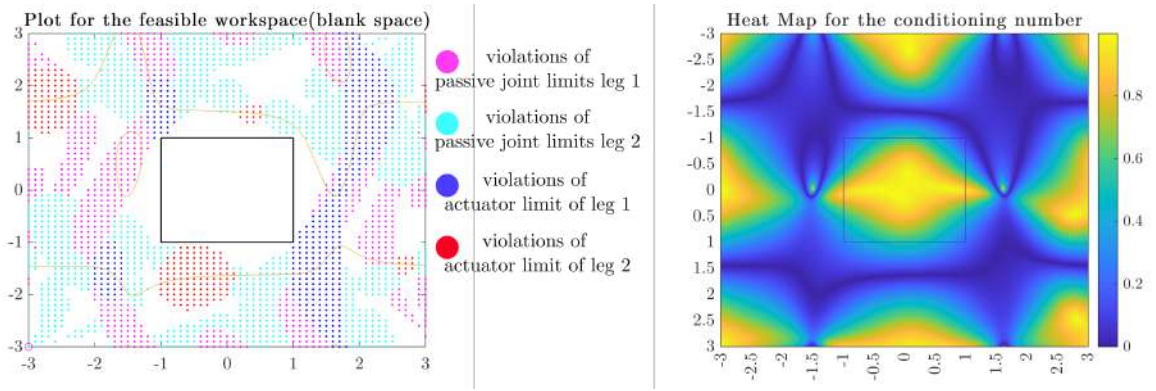

Figure 5.13: The valid feasible space and the heat map for the quality index for optimized mechanism using 13 parameters

5.2.5 Different rewarding strategies

While optimising the mechanism for a particular objective, we implemented various different rewarding strategies. The modeling of the rewarding strategies play an important role in the optimized architecture. Fig. 5.14 shows the evaluation surface only with respect to 2 of the optimizing variables. It is impossible to visualize the complete optimization surface as we have 13 optimizing variables and the following figures are just the tip of the iceberg. But, certain conclusions can be drawn from the same. Especially, how the mechanism is penalized equally, irrespective of the rewarding strategy and also how does the area near the penalty region is affected with change of the rewarding strategy as illustrated in Fig. 5.15.

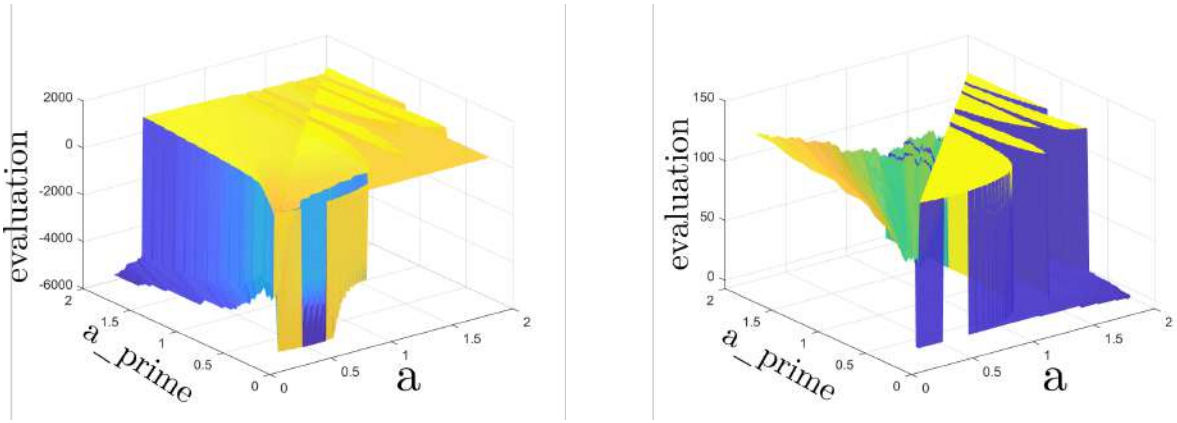

Figure 5.14: The small subset of the evaluation surface while implementing the binary rewarding strategy and biased rewarding strategy

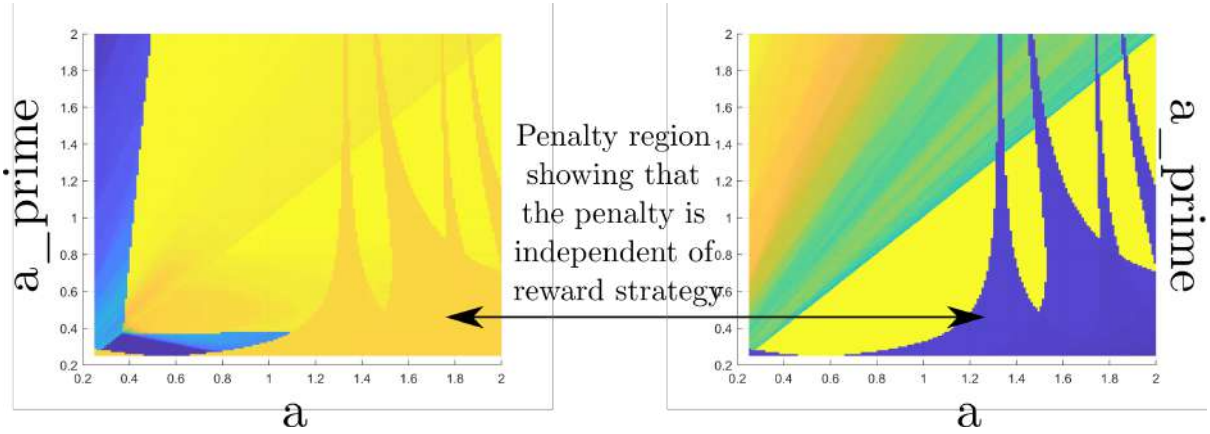

Figure 5.15: The small subset of the evaluation in top view to observe the penalty regions

5.2.6 Coarse and fine search

The proposed strategy of coarse and refined search for a faster and efficient global scan of the optimization space has been explained in Section 4.7. The results of the same for a single example has been shown in Fig. 5.17 to present the clear advantage of the proposed search mechanism.

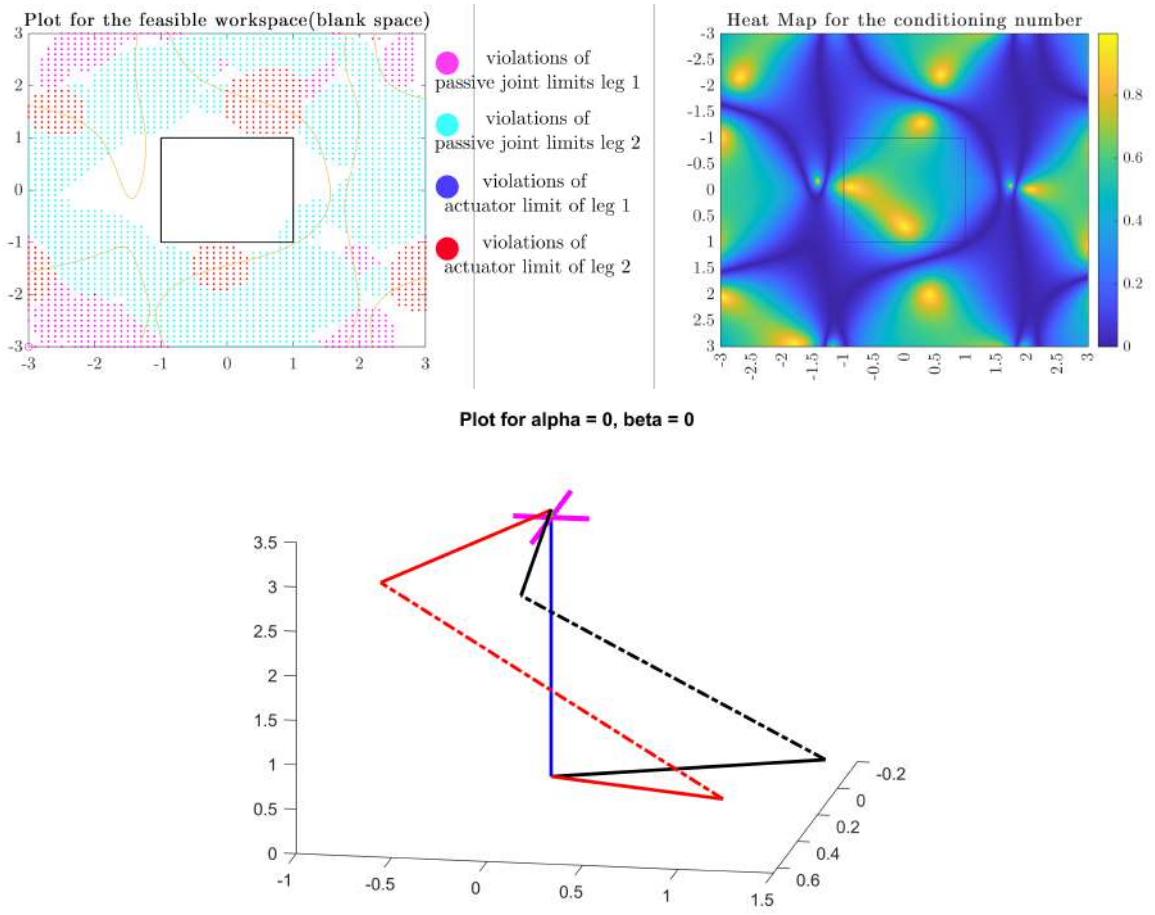

Figure 5.16: Valid feasible space and heat map for the quality index with coarse search. Parameters = [0.824612, 1.911219, 0.082068, 1.061443, -0.323155, 0.010461, 1.136735, 1.911284, 0.039281, 0.667857, 0.805770, 0.217043, 3.265619]

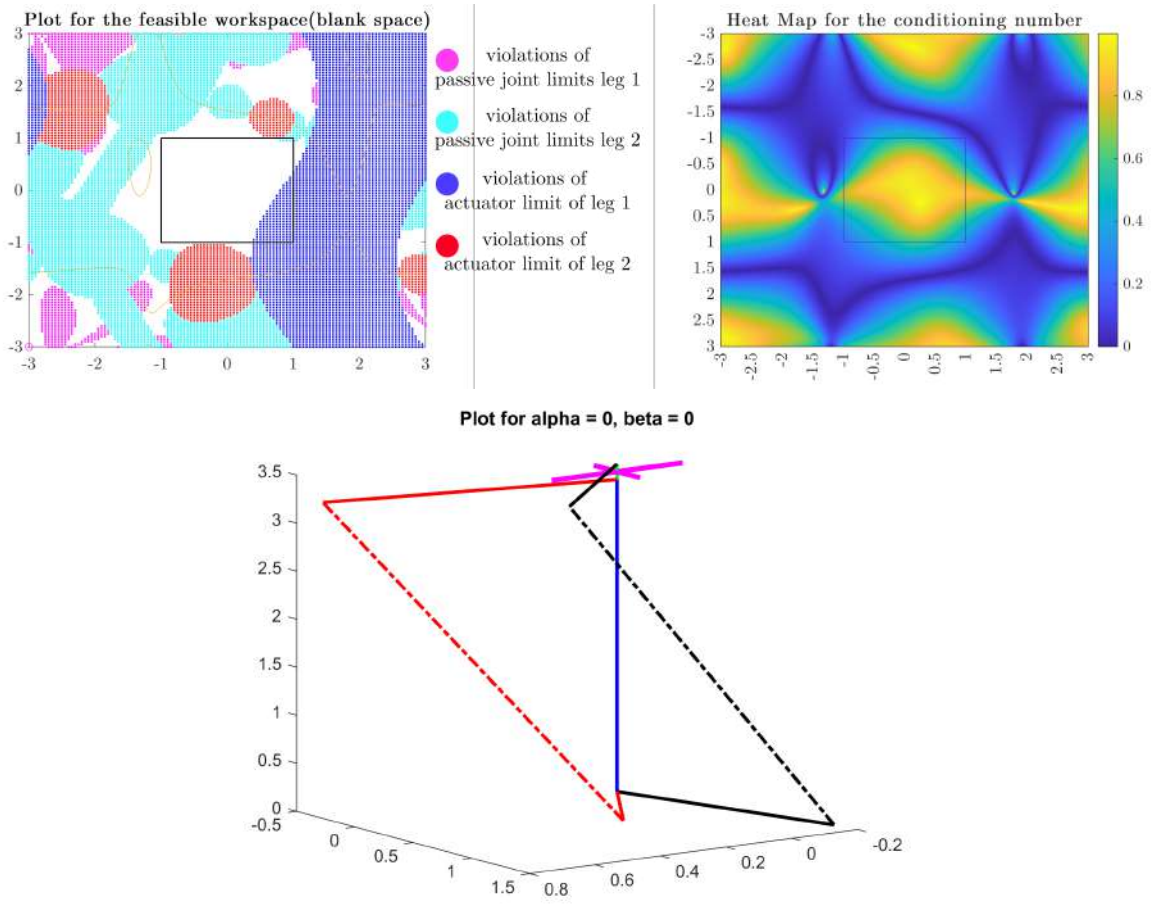

Figure 5.17: Valid feasible space and heat map for the quality index after fine search. The discretization of the workspace is also done with finer intervals, Parameters = [0.802151, 1.251624, 0.060514, 0.849475, -0.438371, -0.083466, 1.367378, 1.702786, 0.009458, 0.878488, 1.072529, 0.079628, 3.328403]

5.2.7 Computational time

This is important in order to understand the importance of reducing the optimization dimension as well as the effect of different constraints on the overall computational time. The following table presents the number of iterations as well as the time for each iteration while optimizing with 4-parameters and 13-parameters. Also, as the discretization as well as the search criteria are stricter in fine search, it was observed that finer searches are computationally very expensive as expected. This corroborates our proposal of a coarse search allowing us to choose few valid simplexes in order to initiate a much deeper search for a better optimum point.

Parameters	type	iterations(min-max)	avg. time (sec/iteration)
4-parameters	coarse	12 - 42	64
4-parameters	fine	25-98	84
13-parameters	coarse	34-138	286
13-parameters	fine	58-152	410

Chapter 6

Conclusions and future works

The thesis work presents a detailed explanation of the current scenario and the existing shortcomings in the use of an endoscope in otological surgeries. The requirements of the surgeons for the same are then translated into technical requirements for better analysis. The report then states the analysis and comparison of possible architectures that can be used for the same. The state of the art on such mechanisms is presented and the novel implemented architecture is detailed. It was observed that adding a motion generator leg in the mechanism helps avoid constraint singularities and thus promise better workspace qualities.

The main objective of the work is to optimize the proposed mechanism. Several objective functions and constraints are highlighted and their effect on the choice of the optimization algorithm is discussed. The global kinematic quality implemented with independent constraints promises a result with physical interpretation allowing us to choose proper actuators for the mechanism. A novel implementation of a fast local search algorithm is presented coupled with a global search mechanism to combine the speed and efficiency of the search of complete optimization space. The algorithm searches for an optimized point in a geometric travel across the optimization space which is very relevant for mechanism design. The simplicity of modeling the algorithm allows one to implement the algorithm for general mechanism design optimization. This algorithm works in two phases, the coarse search and the fine search, and the advantages of such methodology is objectively presented in the report. Later, several rewarding strategies are mentioned which further corroborates the optimized parameters for certain objective functions. The report also touches upon the effect of parameterization of the mechanism and how human intuition can help reduce the optimization time remarkably. In the presented variation of the mechanism, we optimize the mechanism for a general 13 dimensional optimization space and later note that the dimension can be reduced to 4 parameters with human knowledge of the singularities and isotropic configurations of the mechanism.

Several results are shown to highlight the importance of each parameter, constraint and rewarding strategy used. The report also showed the importance of careful modeling of such strategies and their effect on the optimized parameters. A short comparison of computational time has been done to get a relative idea of the optimization with different parameters.

The further work of the thesis is to implement multi-objective optimisation using Pareto front as detailed in [71, 72]. The author also plans to create an open library for the implemented algorithm so that any parallel mechanisms can be optimized using the

presented work.

Human factors is a the study of how humans react and interact with equipment, services and their environment : sometimes bad design is funny but in medicine it can be harmful! To understand how human interacts with the proposed mechanism, we need to make observations, questionnaires and interviews, and also need to test the same on the physical prototype. Even though our questionnaire helped us prevent the big mistakes, it is not enough to prevent smaller mistakes, so we need a prototype that the surgeons can test. So, another important future task would be to develop a prototype for a mock use by surgeons.

A virtual simulator can be produced to visualize the effect of dimension and scaling of the mechanism on the motion of the manipulator.Another aspect in focus is the control of the manipulator. It is important that the control environment is intuitive as well as easy to use. A study on the virtual simulation with the control interface can be done to understand the perspective of the surgeons on the use of the endoscope.

Bibliography

[1] D. Chablat, G. Michel, and B. Philippe, "Dispositif d'aide a la chirugie," 2020 Patent FR1910523 Centre Nationale de Recherche Scientifique - CNRS, CHU de Nantes.

[2] G. Michel, D. Salunkhe, D. Chablat, and P. Bordure, "A new RCM mechanism for an ear and facial surgical application," in *Advances in Service and Industrial Robotics*. Poitiers: Springer International Publishing, 2020, p. 12.

[3] A. Alessandri, C. Cervellera, and M. Sanguineti, "Design of asymptotic estimators: an approach based on neural networks and nonlinear programming," *IEEE Trans. on Neural Networks*, vol. 18, no. 1, pp. 96–96, 2007.

[4] J. G. Meara and J. M. e. a. Andrew, "Global Surgery 2030: evidence and solutions for achieving health, welfare, and economic development," *The Lancet*, vol. 386, no. 9993, pp. 569–624, Aug. 2015.

[5] M. Moran, "Stationary and automated laparoscopically assisted technologies," *Journal of Laparoendoscopic Surgery*, vol. 3, pp. 221–7, 07 1993.

[6] M. Lum, J. Rosen, M. Sinanan, and B. Hannaford, "Optimization of a spherical mechanism for a minimally invasive surgical robot: theoretical and experimental approaches," *IEEE Transactions on Biomedical Engineering*, vol. 53, no. 7, pp. 1440–1445, Jul. 2006.

[7] Y. Yang, K. Kong, J. Li, S. Wang, and J. Li, "Design and evaluation of a dexterous and modular hand-held surgical robot for minimally invasive surgery," *Journal of Medical Devices*, vol. 13, no. 4, Dec. 2019.

[8] B. Dahroug, B. Tamadazte, S. Weber, L. Tavernier, and N. Andreff, "Review on Otological robotic systems: toward microrobot-assisted cholesteatoma surgery," *IEEE Reviews in Biomedical Engineering*, vol. 11, pp. 125–142, 2018.

[9] B. Bell, C. Stieger, N. Gerber, A. Arnold, C. Nauer, V. Hamacher, M. Kompis, L. Nolte, M. Caversaccio, and S. Weber, "A self-developed and constructed robot for minimally invasive cochlear implantation," *Acta Oto-Laryngologica*, vol. 132, no. 4, pp. 355–360, 2012.

[10] M. Miroir, Yann Nguyen, J. Szewczyk, S. Mazalaigue, E. Ferrary, O. Sterkers, and A. B. Grayeli, "RobOtol: from design to evaluation of a robot for middle ear surgery," in *2010 IEEE/RSJ International Conference on Intelligent Robots and Systems*. Taipei: IEEE, Oct. 2010, pp. 850–856.

[11] A. Danilchenko, R. Balachandran, J. L. Toennies, S. Baron, B. Munske, J. M. Fitzpatrick, T. J. Withrow, R. J. Webster, and R. F. Labadie, "Robotic mastoidectomy," *Otology & Neurotology*, vol. 32, no. 1, pp. 11–16, Jan. 2011.

[12] V. Vitiello, Su-Lin Lee, T. P. Cundy, and Guang-Zhong Yang, "Emerging robotic platforms for minimally invasive surgery," *IEEE Reviews in Biomedical Engineering*, vol. 6, pp. 111–126, 2013.

[13] B. M. Haus, N. Kambham, D. Le, F. M. Moll, C. Gourin, and D. J. Terris, "Surgical robotic applications in otolaryngology:," *The Laryngoscope*, vol. 113, no. 7, pp. 1139–1144, Jul. 2003.

[14] S. Vittoria, G. Lahlou, R. Torres, H. Daoudi, I. Mosnier, S. Mazalaigue, E. Ferrary, Y. Nguyen, and O. Sterkers, "Robot-based assistance in middle ear surgery and cochlear implantation: first clinical report," *European Archives of Oto-Rhino-Laryngology*, May 2020.

[15] C. Germain, S. Caro, S. Briot, and P. Wenger, "Optimal design of the IRSBot-2 based on an optimized test trajectory," in *Volume 6A: 37th Mechanisms and Robotics Conference*. Portland, Oregon, USA: American Society of Mechanical Engineers, Aug. 2013, p. V06AT07A056.

[16] S. Kucuk, "A dexterity comparison for 3-DOF planar parallel manipulators with two kinematic chains using genetic algorithms," *Mechatronics*, vol. 19, no. 6, pp. 868–877, Sep. 2009.

[17] S. Caro, D. Chablat, R. Ur-Rehman, and P. Wenger, "Multiobjective design optimization of 3–PRR planar parallel manipulators," in *Global Product Development*, A. Bernard, Ed. Berlin, Heidelberg: Springer Berlin Heidelberg, 2011, pp. 373–383.

[18] S. Ganesh, A. Koteswara Rao, and B. Sarath kumar, "Design optimization of a 3-DOF star triangle manipulator for machining applications," *Materials Today: Proceedings*, vol. 22, pp. 1845–1852, 2020.

[19] Z. Zhang, B. Chang, J. Zhao, Q. Yang, and X. Liu, "Design, optimization, and experiment on a bioinspired jumping robot with a six-bar leg mechanism based on jumping stability," *Mathematical Problems in Engineering*, vol. 2020, pp. 1–23, Jan. 2020.

[20] S. Ha, S. Coros, A. Alspach, J. Kim, and K. Yamane, "Computational co-optimization of design parameters and motion trajectories for robotic systems," *The International Journal of Robotics Research*, vol. 37, no. 13-14, pp. 1521–1536, Dec. 2018.

[21] S. Kumar, A. Nayak, H. Peters, C. Schulz, A. Müller, and F. Kirchner, "Kinematic analysis of a novel parallel 2SPRR+1U ankle mechanism in humanoid robot," in *Advances in Robot Kinematics 2018*, J. Lenarcic and V. Parenti-Castelli, Eds. Cham: Springer International Publishing, 2019, vol. 8, pp. 431–439, series Title: Springer Proceedings in Advanced Robotics.

[22] A. Sharon, N. Hogan, and D. E. Hardt, "The macro/micro manipulator: an improved architecture for robot control," *Robotics and Computer-Integrated Manufacturing*, vol. 10, no. 3, pp. 209–222, Jun. 1993.

[23] C. Gosselin and J. Angeles, "The optimum kinematic design of a spherical three-degree-of-freedom parallel manipulator," *ASME Journal of Mechanisms, Transmissions, and Automation in Design*, vol. 111, pp. 202–207, 06 1989.

[24] D. Chablat and P. Wenger, "Design of a spherical wrist with parallel architecture: application to vertebrae of an eel robot," in *Proceedings of the 2005 IEEE International Conference on Robotics and Automation.* Barcelona, Spain: IEEE, 2005, pp. 3336–3341.

[25] R. Ur-Rehman, S. Caro, D. Chablat, and P. Wenger, "Kinematic and dynamic analysis of the 2-DOF spherical wrist of orthoglide 5-axis," in *Troisième Congrès International. Conception et Modélisation des Systèmes Mécaniques*, Hammamet, Tunisia, Mar. 2009, pp. 1–8.

[26] S. Kumar, B. Bongardt, M. Simnofske, and F. Kirchner, "Design and kinematic analysis of the novel almost spherical parallel mechanism active ankle," *Journal of Intelligent & Robotic Systems*, vol. 94, no. 2, pp. 303–325, May 2018.

[27] F. Caron, "Analyse et conception d'un manipulateur paralléle sphérique à deux degrés de liberté pour l'orientation d'une caméra," *L'Université de Laval*, p. 137, May 1997.

[28] P. Wenger and D. Chablat, "Kinematic analysis of a new parallel machine tool: the Orthoglide," in *Advances in Robot Kinematics*, J. Lenarčič and M. M. Stanišić, Eds. Dordrecht: Springer Netherlands, 2000, pp. 305–314.

[29] C. Gosselin and J. Angeles, "Singularity analysis of closed-loop kinematic chains," *IEEE Transactions on Robotics and Automation*, vol. 6, no. 3, pp. 281–290, Jun. 1990.

[30] C.-H. Kuo and J. S. Dai, "Task-oriented structure synthesis of a class of parallel manipulators using motion constraint generator," *Mechanism and Machine Theory*, vol. 70, pp. 394–406, Dec. 2013.

[31] J. Serracín, L. Puglisi, R. Saltaren, G. Ejarque, J. Sabater-Navarro, and R. Aracil, "Kinematic analysis of a novel 2-d.o.f. orientation device," *Robotics and Autonomous Systems*, vol. 60, no. 6, pp. 852–861, Jun. 2012.

[32] S. Lohmeier, T. Buschmann, H. Ulbrich, and F. Pfeiffer, "Modular joint design for performance enhanced humanoid robot LOLA," in *Proceedings 2006 IEEE International Conference on Robotics and Automation, 2006. ICRA 2006.* Orlando, FL, USA: IEEE, 2006, pp. 88–93.

[33] S. Bartsch, M. Manz, P. Kampmann, A. Dettmann, H. Hanff, M. Langosz, K. v. Szadkowski, J. Hilljegerdes, M. Simnofske, P. Kloss, M. Meder, and F. Kirchner, "Development and control of the multi-legged robot mantis," in *Proceedings of ISR 2016: 47st International Symposium on Robotics*, 2016, pp. 1–8.

[34] M. Hildebrandt, J. Albiez, M. Fritsche, J. Hilljegerdes, P. Kloss, M. Wirtz, and F. Kirchner, "Design of an autonomous under-ice exploration system," *OCEANS - San Diego, San Diego, CA*, p. 6, Aug. 2013.

[35] D. F. Lahr, H. Yi, and D. W. Hong, "Biologically inspired design of a parallel actuated humanoid robot," *Advanced Robotics*, vol. 30, no. 2, pp. 109–118, Jan. 2016.

[36] B. Lee, C. Knabe, V. Orekhov, and D. Hong, "Design of a human-like range of motion hip joint for humanoid robots," in *Volume 5B: 38th Mechanisms and Robotics Conference*. Buffalo, New York, USA: American Society of Mechanical Engineers, Aug. 2014.

[37] N. A. Radford, P. Strawser, K. Hambuchen, J. S. Mehling, W. K. Verdeyen, A. S. Donnan, J. Holley, J. Sanchez, V. Nguyen, L. Bridgwater, R. Berka, R. Ambrose, M. Myles Markee, N. J. Fraser-Chanpong, C. McQuin, J. D. Yamokoski, S. Hart, R. Guo, A. Parsons, B. Wightman, P. Dinh, B. Ames, C. Blakely, C. Edmondson, B. Sommers, R. Rea, C. Tobler, H. Bibby, B. Howard, L. Niu, A. Lee, M. Conover, L. Truong, R. Reed, D. Chesney, R. Platt Jr, G. Johnson, C.-L. Fok, N. Paine, L. Sentis, E. Cousineau, R. Sinnet, J. Lack, M. Powell, B. Morris, A. Ames, and J. Akinyode, "Valkyrie: Nasa's first bipedal humanoid robot," *Journal of Field Robotics*, vol. 32, no. 3, pp. 397–419, 2015.

[38] M. H. Saadatzi, M. T. Masouleh, H. D. Taghirad, C. Gosselin, and M. Teshnehlab, "Multi-objective scale independent optimization of 3-RPR parallel mechanisms," in *13th World Congress in Mechanism and Machine Science, Guanajuato, Mexico*, Guanajuato, Mexico, Jun. 2011, p. 11.

[39] M. Gallant and R. Boudreau, "The synthesis of planar parallel manipulators with prismatic joints for an optimal, singularity-free workspace," *Journal of Robotic Systems*, vol. 19, no. 1, p. 13, Jan. 2002.

[40] A. Hassan and M. Abomoharam, "Modeling and design optimization of a robot gripper mechanism," *Robotics and Computer-Integrated Manufacturing*, vol. 46, pp. 94–103, Aug. 2017.

[41] V. Muralidharan, A. Bose, K. Chatra, and S. Bandyopadhyay, "Methods for dimensional design of parallel manipulators for optimal dynamic performance over a given safe working zone," *Mechanism and Machine Theory*, vol. 147, p. 103721, May 2020.

[42] J.-A. Leal-Naranjo, J.-A. Soria-Alcaraz, C.-R. Torres-San Miguel, J.-C. Paredes-Rojas, A. Espinal, and H. Rostro-González, "Comparison of metaheuristic optimization algorithms for dimensional synthesis of a spherical parallel manipulator," *Mechanism and Machine Theory*, vol. 140, pp. 586–600, Oct. 2019.

[43] N. Durand and J.-M. Alliot, "A combined nelder-mead simplex and genetic algorithm," in *GECCO 1999, Genetic and Evolutionary Computation Conference*, Orlando, FL, USA, Jul. 1999, p. 8.

[44] A. Koscianski and M. Luersen, "Globalization and parallelization of Nelder-Mead and Powell optimization methods," in *Innovations and Advanced Techniques in Systems, Computing Sciences and Software Engineering*, K. Elleithy, Ed. Dordrecht: Springer Netherlands, 2008, pp. 93–98.

[45] M. A. Luersen and R. Le Riche, "Globalized Nelder–Mead method for engineering optimization," *Computers & Structures*, vol. 82, no. 23-26, pp. 2251–2260, Sep. 2004.

[46] P. Niegodajew, M. Marek, W. Elsner, and Ł. Kowalczyk, "Power plant optimisation—effective use of the Nelder-Mead approach," *Processes*, vol. 8, no. 3, p. 357, Mar. 2020.

[47] A. Dutta, D. H. Salunkhe, S. Kumar, A. D. Udai, and S. V. Shah, "Sensorless full body active compliance in a 6 DOF parallel manipulator," *Robotics and Computer-Integrated Manufacturing*, vol. 59, pp. 278–290, Oct. 2019.

[48] I. A. Bonev, D. Zlatanov, and C. Gosselin, "Advantages of the modified Euler angles in the design and control of PKMs," *Verlag Wissenschaftliche Scripten*, pp. 171–188, 2002.

[49] J. Brooke, "Sus - a quick and dirty usability scale," in *P.W.Jordan, B. Thomas, B.A. Weerdmeester, and I.L. McClelland (Eds.) Usability Evaluation in Industry.* London: Taylor and Francis, 2006.

[50] R. A. Srivatsan and S. Bandyopadhyay, "Determination of the safe working zone of a parallel manipulator," in *Computational Kinematics*, F. Thomas and A. Perez Gracia, Eds. Dordrecht: Springer Netherlands, 2014, pp. 201–208.

[51] S. Chiu, "Kinematic characterization of manipulators: an approach to defining optimality," in *Proceedings. 1988 IEEE International Conference on Robotics and Automation.* Philadelphia, PA, USA: IEEE Comput. Soc. Press, 1988, pp. 828–833.

[52] C. Gosselin and J. Angeles, "A global performance index for the kinematic optimization of robotic manipulators," *Journal of Mechanical Design*, vol. 113, no. 3, pp. 220–226, Sep. 1991.

[53] D. Chablat, P. Wenger, and J. Angeles, "Conception isotropique d'une morphologie parallèle : Application à l'usinage," *CoRR*, vol. abs/0707.2034, 2007.

[54] K. H. Hunt, "Review: don't cross-thread the screw!" *Journal of Robotic Systems*, vol. 20, no. 7, pp. 317–339, Jul. 2003.

[55] D. Chablat, P. Wenger, and F. Majou, "The Optimal Design of Three Degree-of-Freedom Parallel Mechanisms for Machining Applications," in *In the Proceedings of 11th International Conference on Advanced Robotics, 2003.* Coimbra, Portugal: IEEE, 2003, pp. 1–6. [Online]. Available: https://hal.archives-ouvertes.fr/hal-00145366

[56] J. P. Merlet, "Jacobian, Manipulability, Condition Number, and Accuracy of Parallel Robots," *Journal of Mechanical Design*, vol. 128, no. 1, pp. 199–206, 06 2005.

[57] P. Borrel and A. Liegeois, "A study of multiple manipulator inverse kinematic solutions with applications to trajectory planning and workspace determination," in *Proceedings. 1986 IEEE International Conference on Robotics and Automation*, vol. 3. San Francisco, CA, USA: Institute of Electrical and Electronics Engineers, 1986, pp. 1180–1185.

[58] J. A. Nelder and R. Mead, "A simplex method for function minimization," *The Computer Journal*, vol. 7, no. 4, pp. 308–313, Jan. 1965. [Online]. Available: https://academic.oup.com/comjnl/article-lookup/doi/10.1093/comjnl/7.4.308

[59] J. C. Lagarias, J. A. Reeds, M. H. Wright, and P. E. Wright, "Convergence properties of the Nelder–Mead simplex method in low dimensions," *SIAM Journal on Optimization*, vol. 9, p. 7, Dec. 1998.

[60] K. I. M. McKinnon, "Convergence of the Nelder–Mead simplex method to a nonstationary point," *SIAM Journal on Optimization*, vol. 9, no. 1, pp. 148–158, Jan. 1998.

[61] P. C. Wang and T. E. Shoup, "Parameter sensitivity study of the Nelder–Mead Simplex Method," *Advances in Engineering Software*, vol. 42, no. 7, pp. 529–533, Jul. 2011.

[62] D. Byatt, "Convergent variants of the Nelder-Mead algorithm.pdf," Ph.D. dissertation, University of Canterburry, England, 2000.

[63] S. Zapotecas Martínez and C. A. Coello Coello, "A proposal to hybridize multiobjective evolutionary algorithms with non-gradient mathematical programming techniques," in *Parallel Problem Solving from Nature – PPSN X*, G. Rudolph, T. Jansen, N. Beume, S. Lucas, and C. Poloni, Eds. Berlin, Heidelberg: Springer Berlin Heidelberg, 2008, vol. 5199, pp. 837–846, series Title: Lecture Notes in Computer Science.

[64] J. M. Hammersley and D. C. Handscomb, *Monte Carlo Methods*. London: Methuen, 1964.

[65] K.-T. Fang and Y. Wang, *Number-Theoretic Methods in Statistics*. London: Chapman & Hall, 1994.

[66] A. Alessandri, C. Cervellera, D. Macciò, and S. M, "Optimization based on quasi-Monte Carlo sampling to design state estimators for nonlinear systems," *Optimization*, vol. 59, pp. 963–984, 2010.

[67] A. Alessandri, C. Cervellera, and M. Sanguineti, "Functional optimal estimation problems and their solution by nonlinear approximation schemes," *Journal of Optimization Theory and Applications*, vol. 134, no. 3, pp. 445–466, 2007.

[68] R. Zoppoli, M. Sanguineti, G. Gnecco, and P. T, *Neural Approximations for Optimal Control and Decision*. Springer, 2000.

[69] H. Niederreiter, *Random Number Generation and Quasi-Monte Carlo Methods*. Philadelphia: SIAM, 1992.

[70] I. M. Sobol', "The distribution of points in a cube and the approximate evaluation of integrals," *Zh. Vychisl. Mat. i Mat. Fiz.*, vol. 7, pp. 784–802, 1967.

[71] H. Ghiasi, D. Pasini, and L. Lessard, "Pareto frontier for simultaneous structural and manufacturing optimization of a composite part," *Structural and Multidisciplinary Optimization*, vol. 40, no. 1-6, pp. 497–511, Jan. 2010.

[72] A. Messac, A. Ismail-Yahaya, and C. Mattson, "The normalized normal constraint method for generating the Pareto frontier," *Structural and Multidisciplinary Optimization*, vol. 25, no. 2, pp. 86–98, Jul. 2003.